University of Dundee

DOCTOR OF PHILOSOPHY

Targeting the Rho1 GTPase signalling pathway in Aspergillus fumigatus

Wei, Wenfan

Award date:
2017

Link to publication

General rights
Copyright and moral rights for the publications made accessible in the public portal are retained by the authors and/or other copyright owners and it is a condition of accessing publications that users recognise and abide by the legal requirements associated with these rights.

- Users may download and print one copy of any publication from the public portal for the purpose of private study or research.
- You may not further distribute the material or use it for any profit-making activity or commercial gain
- You may freely distribute the URL identifying the publication in the public portal

Take down policy
If you believe that this document breaches copyright please contact us providing details, and we will remove access to the work immediately and investigate your claim.

Download date: 06. Feb. 2023

Ph.D. Thesis

Targeting the Rho1 GTPase signalling pathway in *Aspergillus fumigatus*

Wenfan Wei

Supervisor: Prof. Daan van Aalten

University of Dundee

August 2017

Table of Contents

Table of Contents II
List of figures IV
List of tables VI
Abbreviations VII
Acknowledgements XI
Declaration XIII
Abstract XIV
Chapter 1 : Introduction 1
1.1 Fungal infections and antifungals 1
1.1.1 Fungi as human pathogens 1
1.1.2 *Aspergillus fumigatus* and aspergillosis 2
1.1.3 Current antifungal treatments 6
1.2 The fungal cell wall as a source of antifungal targets 10
1.2.1 The unique features of the fungal cell wall in *Aspergillus fumigatus* 11
1.2.2 Glucan synthase as a target in *A. fumigatus* 12
1.3 Rho GTPase signalling regulates the fungal cell wall synthesis 14
1.3.1 Rho1 as a regulatory subunit of glucan synthase 14
1.3.2 Rho1 plays a pivotal role in the fungal CWI pathway 16
1.3.3 The GEFs are the activators of Rho GTPases 18
1.3.4 *Af*Rom2 is a GEF protein of *Af*Rho1, and an essential cell wall target 20
1.3.5 *Af*Rom2 possesses a C-terminal CNH domain with unknown functions 20
1.4 Targeting Rho GTPases 23
1.4.1 The Rho GTPases as anti-cancer targets in mammalian cells 23
1.4.2 Rho inhibitor development through multiple approaches 24
1.4.3 Fragment-based drug discovery (FBDD): state of the art 27
1.5 Aims and objectives 30
Chapter 2 : Structural and fragment-based ligand design of Rho1 GTPase in *Aspergillus fumigatus* 31
2.1 Introduction 32
2.2 Materials and Methods 35
2.2.1 Protein expression and purification 35
2.2.3 Structure determination 37
2.2.4 Fragment screening by biolayer interferometry (BLI) 37
2.2.5 Testing the protein-protein interaction between *Af*Rho1/*Hs*RhoA with their corresponding GEFs using BLI 38
2.2.6 Testing GEF-mediated *Af*Rho1/*Hs*RhoA activation using mant-GDP 39
2.3 Results 40
2.3.1 *Af*Rho1 structure reveals potential exploitable differences with its human orthologue 40
2.3.3 A complex structure of *Af*Rho1 with fragment DDD01511162 reveals the binding mode at the atomic level 49
2.3.4 The fragment binding pocket is conserved in *Hs*RhoA and located at the Rho/Rho GEF interaction interface 54
2.3.5 Fragment DDD01511162 inhibits the GEF mediated *Af*Rho1/ *Hs*RhoA nucleotide exchange 60
2.3.6 The fragment-based ligand design 61

2.4 Discussion **65**

Chapter 3 : Genetic and molecular characterization of Rom2 CNH domain in *Aspergillus fumigatus* **70**

3.1 Introduction **71**

3.2 Materials and Methods **73**

3.2.1 Construction of *rom2Δcnh* mutant 73

3.2.2 Analysis of the *rom2Δcnh* mutant 75

3.2.3 Construction of *gfp-cnh* mutant 76

3.2.4 Protein extraction and GFP-Trap® affinity purification 77

3.2.5 Mass spectrometry and data analysis 78

3.2.6 Protein expression and purification of the *Af*Rom2 CNH domain 78

3.2.7 *In vitro* interaction assay 80

3.2.8 Crystallization, data collection and structure determination of *Af*Rom2 CNH domain 80

3.3 Results **82**

3.3.1 *Af*Rom2 possesses a C-terminal CNH domain of unknown function 82

3.3.2 The *Af*Rom2 CNH domain is required for cell growth and cell wall integrity 84

3.3.3 The CNH domain is required for cell wall synthesis and ultrastructure 88

3.3.4 The *Af*Rom2 CNH domain bound to the major cell wall synthesizing protein *Af*Rho1 91

3.3.5 The *Af*Rom2 CNH structure adopts a seven bladed WD40 fold 95

3.3.6 An interaction mode of *Af*Rom2 CNH domain with *Af*Rho1 GTPase suggested by the transducin complex 101

3.4 Discussion **107**

Chapter 4: Conclusions ..... Error! Bookmark not defined.

4.1 Fragment based inhibitor discovery of *Af*Rho1 ..... **111**

4.2 The potential of using *Af*Rom2 CNH domain as a selective anti-fungal target **114**

List of References: **117**

List of figures

Figure 1.1: The typical sexual and asexual life cycle of *Aspergillus* spp., represented by *Aspergillus nidulans* 3
Figure 1.2: Conidiophore architecture of *Aspergillus fumigatus*. 4
Figure 1.3: Saprophytic and pathogenic cycles of *A. fumigatus*. 6
Figure 1.4: Chemical structures of antifungal classes. 7
Figure 1.5: Mode of actions of different antifungals. 9
Figure 1.6: Scheme of *Aspergillus fumigatus* cell wall. 11
Figure 1.7: The molecular mechanism of echinocandin drugs and their mode of action. 13
Figure 1.8: Schematic representation of Rho1p regulation of glucan synthase activity. 16
Figure 1.9: CWI signalling pathway in *S. cerevisiae*. 18
Figure 1.10: Rho GTPase activation/ deactivation cycle. 19
Figure 1.11: Domain presentation of *Af*Rom2 and Rho GEF proteins from other organisms. 22
Figure 1.12: A fragment screen pipeline. 28
Figure 1.13: The workflow to do a fragment screen in Daan van Aalten's lab 29
Figure 2.1: Purification and crystallization of *Af*Rho1 full length 40
Figure 2.2: Purification and crystallization of *Af*Rho1 (C-terminal truncation) 41
Figure 2.3: General structure of *Af*Rho1*GDP. 44
Figure 2.4: Sequence and structural differences between *Af*Rho1 and *Hs*RhoA. 46
Figure 2.5: Primary screen hits of *Af*Rho1 using BLI. 48
Figure 2.6: Chemical structure of the fragment hit DDD01511162 and the complex structure it bound to *Af*Rho1 52
Figure 2.7: Biolayer interferometry (BLI) to test binding of the fragment DDD01511162 to *Af*Rho1 and W58A, E40A mutants. 54
Figure 2.8: Surface comparison between *Af*Rho1 and *Hs*RhoA, and the BLI binding graphs of *Hs*RhoA to the fragment hit DDD01511162 56
Figure 2.9: Structures of *Hs*RhoA in complex with LARG and superimposed with the fragment DDD01511162 59
Figure 2.10: mant-GDP assays to measure the nucleotide exchange of *Af*Rho1/HsRhoA in the presence of their corresponding GEF proteins (LARG and Rom2), and in the presence of the fragment hit DDD01511162 61
Figure 2.11: Strategies for the fragment optimization based on the complex structure. 63
Figure 2.12: BLI binding graphs of the fragment hit DDD01511162 and derivatives compounds to *Af*Rho1. 64
Figure 3.1: Sequence conservation of Rom2 CNH domain from fungal organisms and to citron kinases CNH domain from *Drosophila* and Human 84
Figure 3.2: Generation of *rom2Δcnh* mutant 86
Figure 3.3: Sensitivity of the *rom2Δcnh* mutant to chemical reagents 88
Figure 3.4: Cell wall analysis of the *rom2Δcnh* mutant 90
Figure 3.5: Generation of gfp-cnh mutant 91
Figure 3.6: Pull down of *Af*Rom2 CNH interacting proteins by GFP-CNH . 93

Figure 3.7: *In vitro* binding analysis of Rom2 CNH domain and *Af*Rho1 ... 95
Figure 3.8: Overall structure of AfRom2 CNH and comparison with bovine β-transducin ... 99
Figure 3.9*:* The sequence alignment of CNH domain containing proteins based on the AfRom2 CNH domain structure ... 101
Figure 3.10: Binding surface comparison of *Af*Rom2 CNH domain with the bovine transducin complex ... 104
Figure 3.11: *In vitro* binding analysis of Rom2 CNH domain to *Af*Rho1, and to the *Af*Rho1 switch II helix mutant ... 106

List of tables

Table 2.1: The primers used to clone the *Af*Rho1 and AfRom2 CNH domain expression construct. 35
Table 2.2: X-ray crystallographic data collection and refinement statistics of *Af*Rho1 and the fragment complex 42
Table 2.3: Compound structures from the fragment screening..... 49
Table 3.1: Primers used to generate and verify the rom2Δcnh and gfp-cnh mutants 74
Table 3.2: Protein hits from the GFP pull down experiment that are involved in cell wall synthesis 94
Table 3.3: X-ray crystallographic data collection and refinement statistics of *Af*Rom2 CNH domain..... 97

Abbreviations

Å Ångström (10^{-10}metres)

A. fumigatus Aspergillus fumigatus

ABPA Allergic bronchopulmonary aspergillosis

Af Aspergillus fumigatus

Amp Ampicillin

BLI Bio-layer interferometry

BSA Bovine serum albumin

C-terminus Carboxyl-terminus

C. albicans Candida albicans

CCP4 Collaborative Computational Project, Number 4 in protein crystallography

CIT-K Citron kinase

CNH Citron homology domain

CR Congo red

Da Dalton

DH Dbl homology

DMSO Dimethyl sulfoxide

DNA Deoxyribonucleic acid

DTT Dithiothreitol

DVA Daan van Aalten

E. coli Escherichia coli

EDTA Ethylene diamine tetraacetic acid

ESRF European Synchrotron Radiation Facility

FBDD Fragment based drug discovery

FDA Food and Drug Administration (U.S)

g gram

GST Glutathione-S-transferase

GTP Guanosine-5'-triphosphate

GDP Guanosine-5'-diphosphate

GTPase GTP hydrolyzing enzymes

GEF Guanine nucleotide exchange factors

GFP Green fluorescent protein

GAP GTPase activation proteins

GDI Guanosine nucleotide dissociation inhibitor

h hours

H. sapiens Homo sapiens

Hs Homo sapiens

HEPES 2-[4-(2-hydroxyethyl)piperazin-1-yl]ethanesulfonic acid

IA Invasive aspergillosis

IC_{50} Half-maximal inhibitory concentration

IMAC Immobilised metal ion affinity chromatography

IPTG Isopropyl β-D-1-thiogalactopyranoside

ITC Isothermal titration calorimetry

K_d Equilibrium dissociation constant

kDa kilo Dalton

K_i Inhibition constant

L litre

LB Lysogeny broth

LB+Amp Lysogeny broth supplemented with 50 µg/ml ampicillin

LE ligand efficiency

M molar

m milli (10^{-3})

MIC minimum inhibitory concentration

Min minutes(s)

Milli-Q Ultrapure water of Type I

MM minimal medium

MRC Medical Research Council

MS Mass spectrometry

n nano (10^{-9})

NMR Nuclear magnetic resonance

N-terminus Amino-terminal

°C Degrees Celsius

OD Optical density

PAGE Polyacrylamide gel electrophoresis

PBS Phosphate buffered saline

PCR Polymerase chain reaction

PDB Protein data bank

PDB ID Protein databank identifier

PEG Polyethylene glycol

PH domain Pleckstrin homology domain

PP Prescission protease

PVDF Polyvinylidene fluoride

R^2 Coefficient of determination

RFU Relative fluorescent units

RMSD Root mean square deviation

RNA Ribonucleic acid

Rpm Revolutions per minute

s **seconds**

S. cerevisiae ***Saccharomyces cerevisiae***

Sc ***Saccharomyces cerevisiae***

SD **Standard deviation**

SDS **Sodium dodecyl sulphate**

SEC **Size-exclusion chromatography**

SEM **Standard error of the mean**

SPR **Surface electron microscopy**

TBS **Tris-buffered saline**

TBST **Tris-buffered saline Tween 20**

TEM **Transmission electron microscopy**

Tris **Tris (hydroxymethyl) aminomethane**

UDP **Uridine diphosphate**

UK **United Kingdom**

v/v **Volume per volume**

w/v **weight per volume**

λem **Emission wavelength**

λex **Excitation wavelength**

μ **micro (10^{-6})**

α **alpha**

β **beta**

γ **gamma**

Δ **delta (deletion)**

Acknowledgements

I would like to first thank my supervisor Professor Daan van Aalten for giving me this precious opportunity to do research in his lab, and giving me guidance for my research training. I would also like to thank members in his lab and in the School of Life Science, University of Dundee, for assisting some part of my research. Their contributions to this thesis are listed below:

Daan van Aalten lab

- Dr. Andrew Ferenbach provided technical advice on all aspects of molecular cloning in my research. He constructed the *A. fumigatus Af*Rho1, *Af*Rom2 CNH domain overexpression plasmid, and also the *Afrom2Δcnh* domain deletion, *gpd-gfp-cnh* plasmids
- Dr. Wenxia Fang supervised all genetic manipulations in *A. fumigatus*.
- Dr. Olawale Raimi assisted with the *Af*Rho1 fragment screen and subsequent data analysis
- Dr. Deborah Lockhart for proof reading the genetics part of my thesis
- Dr. Marianne Schimpl and Mr. Karim Rafie provided technical advice on X-ray crystallography and structural biology

  Dr. Matthews Stanley for providing chemical support for the synthesis of the fragment derived compounds

Dundee Imaging Facility

- Mr. Martin Kierans processed *A. fumigatus* hyphae for electron microscopy

Dundee FingerPrints Proteomics facility

- Miss Samantha Kosto for assisting the Mass spectrometry experiment and the subsequent data analysis

Declaration

I declare that the following thesis is on the results of investigations conducted by myself, and that is of my own composition. Work other than my own is clearly indicated in the text by reference to the relevant researchers or to their publications. This dissertation has not in whole or in part been previously submitted for a higher degree.

Signature:

Mr. Wenfan Wei

Abstract

For individuals with compromised immune systems, *Aspergillus fumigatus* has emerged as one of the most common airborne fungal pathogens in recent decades. In immunosuppressed patients, inhalation of *A. fumigatus* spores can initiate life-threatening invasive aspergillosis (IA) with mortality rates up to 90%. The high mortality is largely due to a limited arsenal of antifungal drugs and emerging resistance and also the poor diagnosis. At present, the treatment for this fungal infection is dominated by three antifungal classes. Polyenes and azoles target the fungal cell membrane, and echinocandins target β-glucan synthesis in the fungal cell wall. However, they all have significant drawbacks in terms of toxicity, drug-drug interactions and/or efficacy.

The current efforts are to structurally and chemically validate new targets that are genetically proven as essential in *A. fumigatus.* One such protein *Af*Rho1 is a Rho GTPase, plays essential roles in fungal physiology and cell wall organization. In this research, I combined X-ray crystallography and fragment-based small molecule screening by BLI (Biolayer interferometry) to investigate the ligandability of *Af*Rho1. Using X-ray crystallography, the structure of *Af*Rho1 was solved and a complex structure with one of the hit fragments was obtained. The complex structure showed that this fragment molecule bound to *Af*Rho1 in a 2:1 molar ratio, and the fragment binding pocket is conserved with the human orthologue protein *Hs*RhoA. Structure analysis shows that the pocket is located at the previously validated interaction interface between Rho GTPases and the upstream activation GEF (Guanine nucleotide exchange factor) proteins. Therefore, in this research I have identified a lead molecule that could be used to develop inhibitors against *Af*Rho1 and *Hs*RhoA by inhibiting the corresponding GEF proteins mediated nucleotide exchange.

Rom2, a Rho1 GTPase guanine nucleotide exchange factor (GEF), plays an essential role in the fungal cell wall integrity pathway and possesses a unique C-terminal CNH (Citron homology) domain. Using genetic and molecular approaches I characterised the functions of the Rom2 CNH domain in the pathogenic fungus *Aspergillus fumigatus*. Cell wall analysis including TEM and chemical analysis suggest that this domain is important for both β-glucan and chitin synthesis. GFP pull-down mass spectrometry and *in vitro* binding assays suggest that the CNH domain is a Rho1 GTPase binding protein. The protein structure of *Af*Rom2 CNH domain was solved by X-ray crystallography. This revealed that the structure of *Af*Rom2 CNH domain is a seven bladed WD40 protein that shares structural similarities to the GTPase binding protein β-transducin. From structure comparison of the *Af*Rom2 CNH domain and *Af*Rho1 to the heterotrimeric transducin complex, I discovered that the top surface of the CNH domain and an α-helix in the switch II region of *Af*Rho1 may form the potential interaction surface. My work provides both genetic evidence and the molecular basis that the *A. fumigatus* Rom2 CNH domain regulates cell wall synthesis, therefore validate it as a potential antifungal target.

Chapter 1 : Introduction

Infections caused by opportunistic fungal pathogens have become a significant clinical problem, due of the increasing number of immuno-compromised patients, and a lack of efficient therapies (Bains and Judson, 2012; Denning et al., 2013). Among these pathogens, *Aspergillus fumigatus* is the cause of one of the major fungal infection diseases called aspergillosis, which affects millions of patients globally. The current antifungal therapies suffer from significant drawbacks such as lack of efficacy, or the presence of drug–drug interaction. This is partly due to limited number of characterised protein targets for drug development. The *A. fumigatus* fungal cell wall is a complex and multi- layered structure that is essential for growth (Bowman and Free, 2006; Free, 2013; Latge, 2007, 2010). Therefore, understanding of the molecular mechanisms of fungal cell wall biosynthesis in *A. fumigatus* will help to identify new antifungal drug targets. The Rho GTPase signalling pathway has been shown to play important roles in regulating cell wall synthesis in *Aspergillus fumigatus* and other fungi (Arellano et al., 1996; Bickle et al., 1998; Dichtl et al., 2012).

1.1 Fungal infections and antifungals

1.1.1 Fungi as human pathogens

The kingdom of fungi is a group of eukaryotic organisms, distinct from animals and plants, that includes microorganisms such as yeasts, moulds and mushrooms. Fungi are ubiquitous in nature and play important ecological and economic roles in human society. Of approximately 1.5 million described species of fungi, a little more than 400 are pathogenic and may cause diseases in humans or other organisms (Wakefield et al., 1992).

The majority of human pathogenic fungi are naturally soil-inhabiting species where they live as saprophytes. However, when given the opportunity, they will

attack mammals with a compromised immune system or an open wound. Therefore, most of the fungal pathogens are opportunistic.

There are three main classes of fungal diseases according to the types of infections they cause:

1) Superficial infections are caused by fungal infection of the hair, nail, and skin, such as: ring worm, athlete's foot, jock itch and piedra. These fungal pathogens are therefore called dermatophytes, and include species from the genera *Epidermophyton*, *Microsporum* and *Trichophyton* (Al-Shboul et al., 2014).

2) Systemic infections are caused by pathogens that primarily infect the lungs and then disseminate to other organs. The most common species that lead to fungal systemic infections are: *Candida albicans*, *Aspergillus fumigatus* and *Cryptococcus neoformans*, as well as other fungal pathogens such as *Histoplasma capsulatum, Coccidiodes immitis* and *Fusarium* (Fernandez-Garcia et al., 2017).

3) Intermediate infections are fungal infections occurring below the skin but remaining localized. These fungal infections will not disseminate but often extend to a considerable depth within the infected tissue.

1.1.2 *Aspergillus fumigatus* and aspergillosis

Aspergillus fumigatus is a saprophytic filamentous fungus from the phylum Ascomycota, which means it can reproduce both sexually and asexually (Fig. 1.1). Although the sexual stage of *A. fumigatus* has only been reported recently, the asexual stage has been very well studied (O'Gorman et al., 2009).

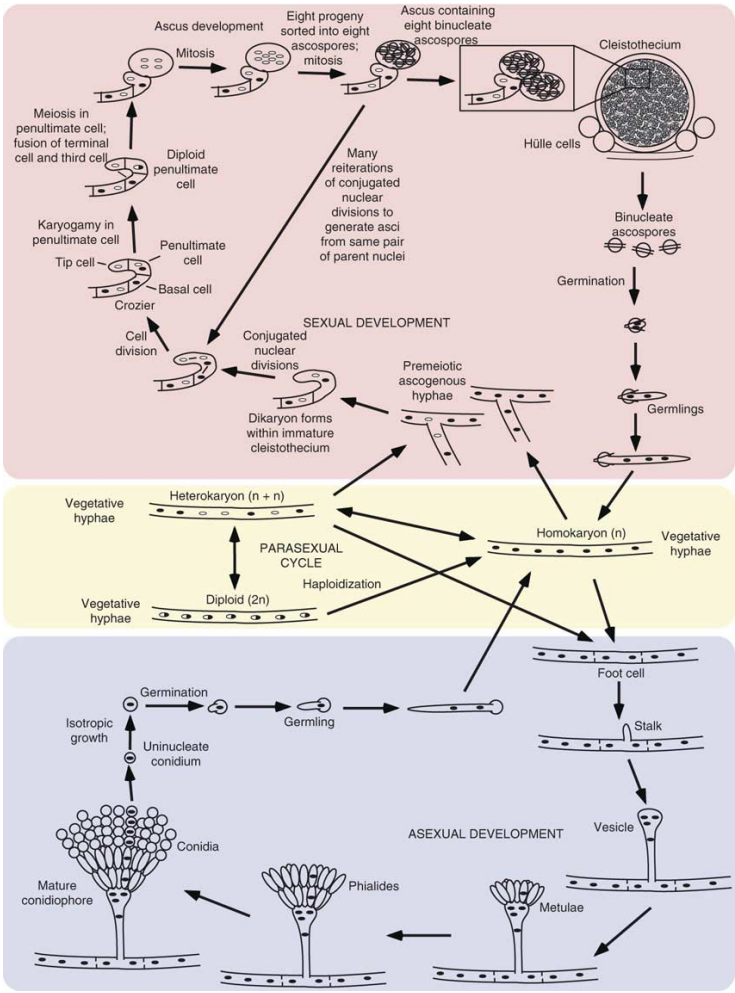

Figure 1.1: The typical sexual and asexual life cycle of *Aspergillus spp*., represented by *Aspergillus nidulans*

Vegetative hyphae (highlighted in yellow) differentiate to asexual development by producing spores on structures called conidiophores (highlighted in grey). For sexual development (highlighted in pink), ascospores are produced in sexual fruiting bodies (cleistothecia). Image adapted from (Todd et al., 2007)

During the asexual development cycle, *A. fumigatus* will differentiate haploid hyphae to foot cells, after which it will form asexual spore-bearing structures on top of the foot cells. These resemble the structure of an aspergillum (holy water sprinkler in Latin) (Fig. 1.2), and hence the name of the genus (Bennett, 2010). *A. fumigatus* is very abundant in nature and is usually found in soil or decaying material. The airborne asexual spores produced by *A. fumigatus* are extremely

small (only 2–3 μm in diameter), so are very easily inhaled into human lungs (Fig 1.3). As a matter of fact, every human being inhales hundreds of *A. fumigatus* spores during the day, however these spores usually do not cause illness in people with healthy immune systems.

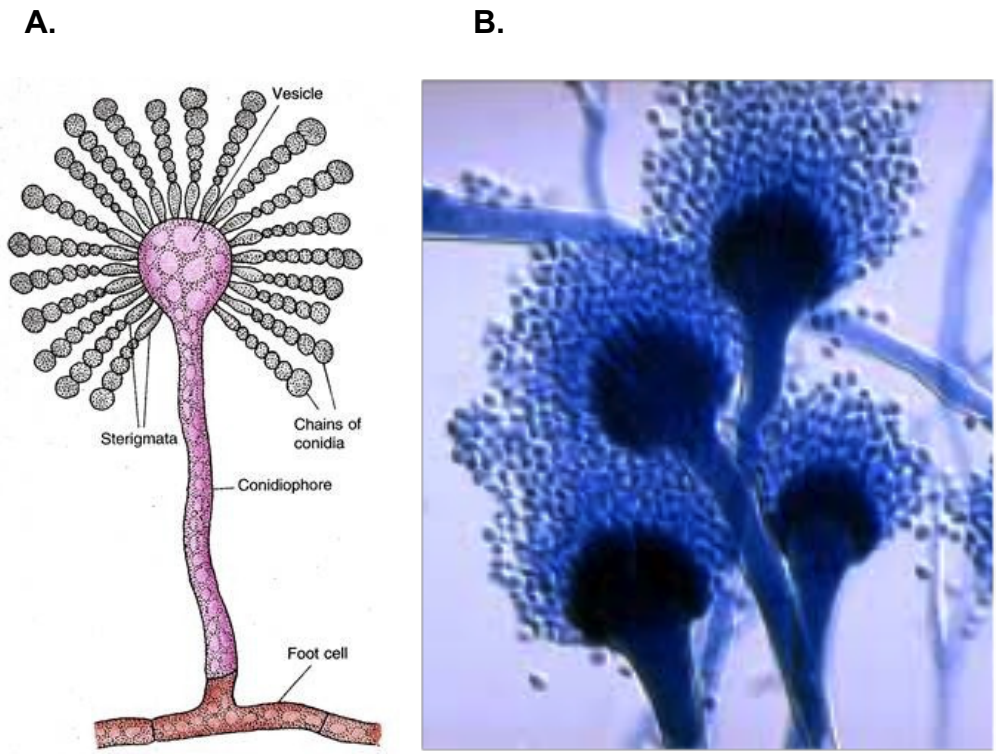

Figure 1.2: Conidiophore architecture of *Aspergillus fumigatus*.

(A) Schematic representation of the spore-forming structure (conidiophore) of the *Aspergillus* species. (Image adapted from biologydiscussion.com). (B) Light microscopy image of *Aspergillus fumigatus* stained with lactophenol cotton blue. (Image adapted from Mycology Practical MLS, Monmouth University)

However, for individuals with a compromised immune system, infections with *A. fumigatus* can cause aspergillosis, a deadly fungal disease that claims hundreds of thousands people's lives annually world-wide (Denning et al., 2013). According to the localisation of the disease within the respiratory tract and the extent of mycelial colonization or invasion, aspergillosis can be classified into three major classes: allergic bronchopulmonary (ABPA), aspergilloma, and invasive

aspergillosis (IA) (Latge, 1999). ABPA is a hypersensitive allergic reaction to fungal components in patients suffering from cystic fibrosis and asthma. Without careful treatment, ABPA will eventually lead to pulmonary fibrosis and respiratory failure (Latge, 1999). Aspergilloma, which is also known as “fungal ball’, is caused by fungal hyphal mass embedded into pre-existing pulmonary cavities caused by tuberculosis, sarcoidosis, or other lung disorders (Agarwal et al., 2013; Latge, 1999). Finally, invasive aspergillosis (IA), the most fatal form of aspergillosis, mainly infects immune-compromised patients such as those with cancer, AIDS or organ transplant recipients. The stages of an IA infection start from an invasion of the blood stream, then to its dissemination into the endothelium at other sites, which will lead to a haemotogenously disseminated disease (Dagenais and Keller, 2009) .

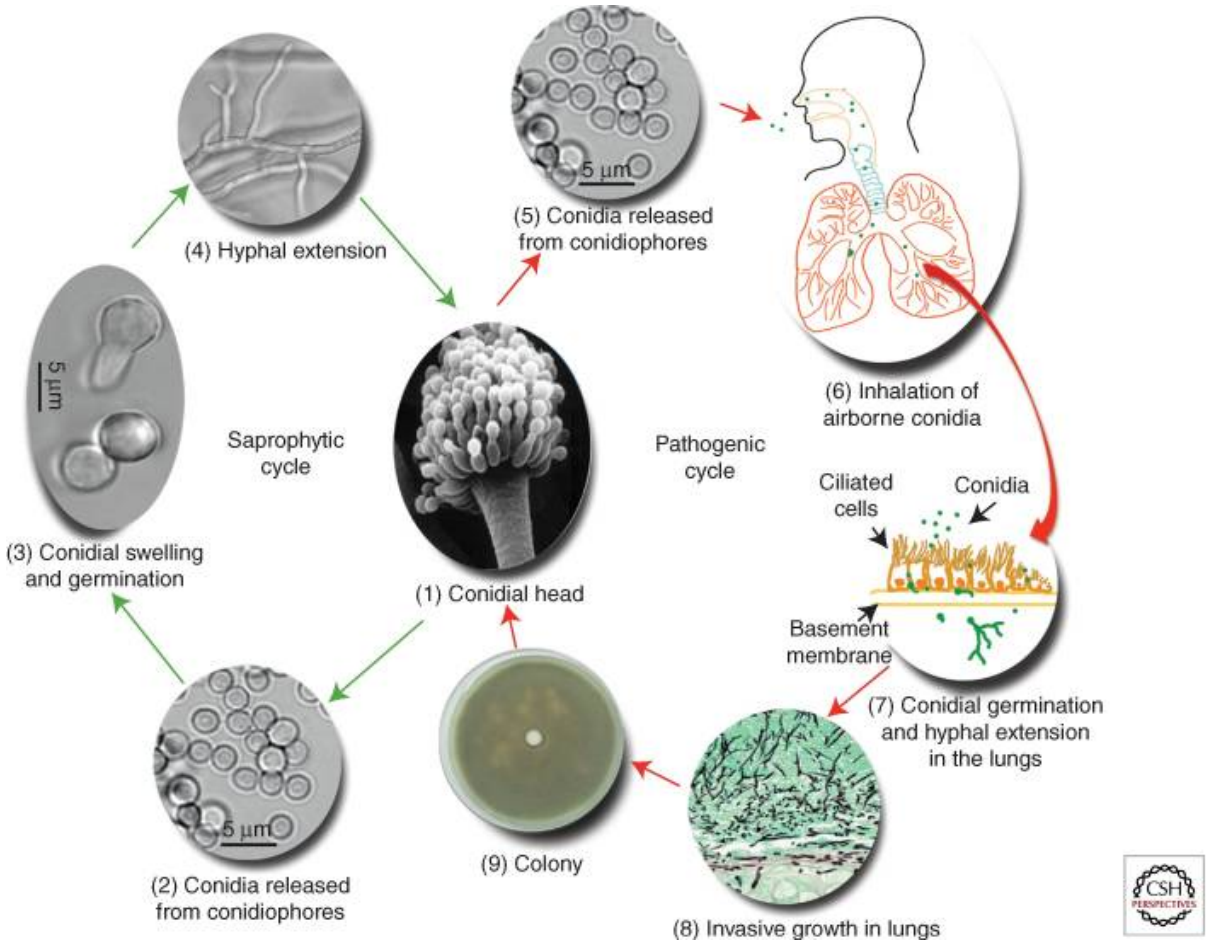

Figure 1.3: Saprophytic and pathogenic cycles of *A. fumigatus*.

(1)–(4) Saprophytic cycle of *Aspergillus fumigatus* from asexual spores to extended hyphae and finally conidial head. (5)–(8) Pathogenic cycle of *A. fumigatus* infection of immuno-compromised patients. (5) (6) (7) Airborne *Aspergillus fumigatus* spores inhaled and grow in the human lungs (8) Invasive growth of *A. fumigatus* hyphal filaments in human lungs (9) Colony growth of *A. fumigatus* under laboratory conditions. Image adapted from (Losada et al., 2015)

1.1.3 Current antifungal treatments

Humans (hosts) and fungi both belong to the eukarya domain, thus most essential proteins are conserved among them. Therefore, for target-based antifungal drug development, the challenge is to consider minimising the toxicity to the human host while still eliminating the fungal pathogens. Currently, there are only three major classes of antifungals in clinical use: polyenes, azoles, and echinocandins, and they target fungal organisms via different molecular mechanisms (Fig 1.4).

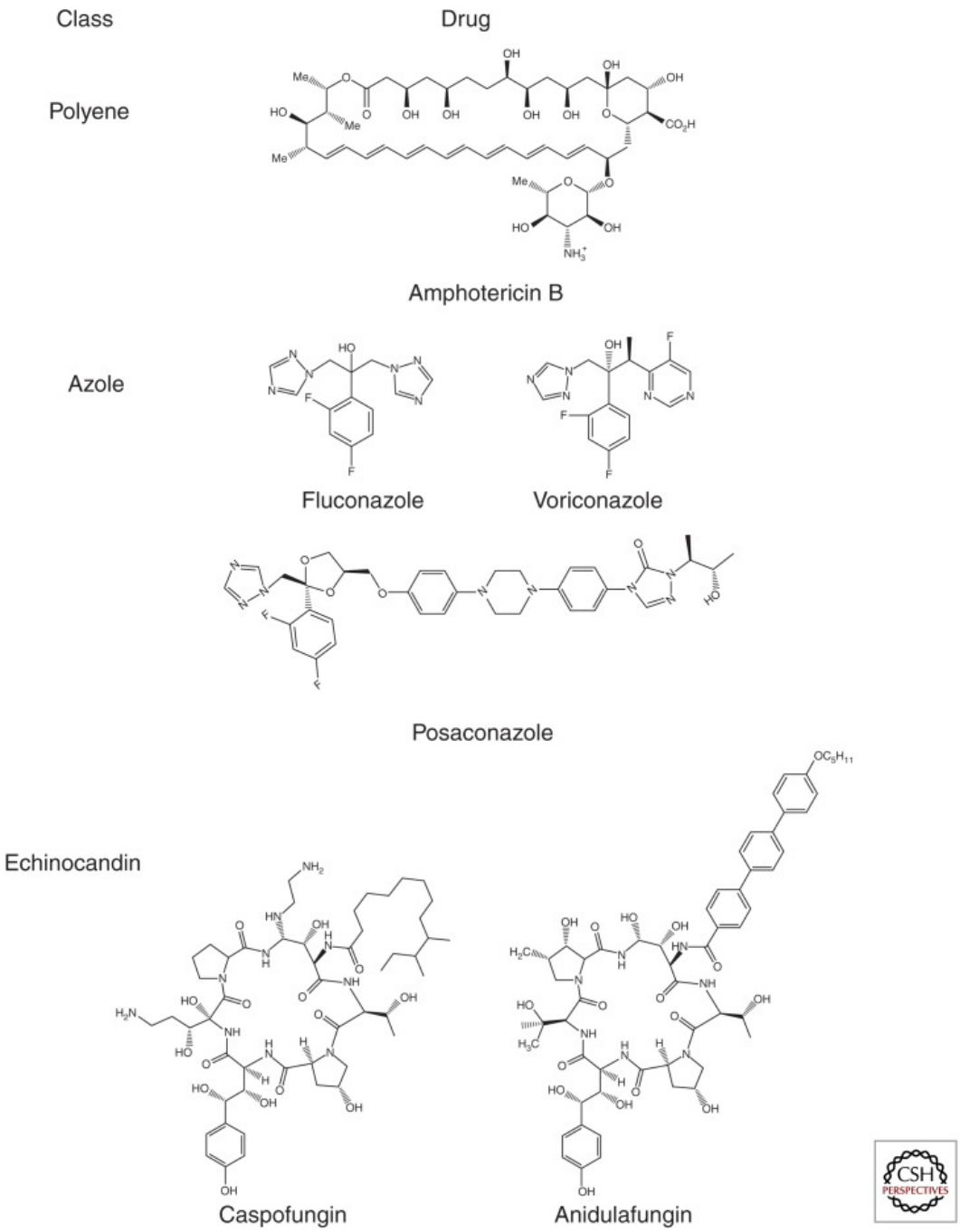

Figure 1.4: Chemical structures of antifungal classes.

Chemical structures of antifungals represented of Polyenes, Azoles and Echinocandins. Images adapted from (Roemer and Krysan, 2014)

Polyenes, which are natural compounds derived from the bacterium *Streptomyces*, are the earliest class of antifungal introduced for treatment of life-threatening fungal infections e.g. amphotericin B (AmB) introduced in 1959

(Newcomer et al., 1959). Polyenes such as AmB bind to ergosterol, which is the main sterol present in the fungal membrane (and is absent in human cells), causing pore formation and membrane permeabilization (Fig 1.5) (Balakrishnan and Easwaran, 1993; Palacios et al., 2011). AmB was discontinued for clinical use due to its affinity for the cholesterol in mammalian membranes (Joly et al., 1992). The toxic side effects include cellular injury and organ dysfunction of the kidney (Lane et al., 2008). However, new formulations of AmB, such as liposomal AmB, which can be administered intravenously with minimal side effects, are now part of the second-line treatment for invasive aspergillosis (Dotis et al., 2008).

Azoles are synthetic organic compounds containing at least one triazole ring attached to an isobutyl core (voriconazole) or asymmetric carbon atom with a lipophilic complex (itraconazole and voriconazole) (Fig 1.4). The azoles target the fungal ergosterol biosynthesis pathway by inhibiting the fungal cytochrome P450-dependent enzyme lanosterol 14-α-demethylase (Fig 1.5). The inhibition of this enzyme is fungicidal or fungistatic, due to the accumulation of the precursor methylsterols within the cell membrane (Mohr et al., 2008). Although triazoles such as voriconazole are now the recommended first line treatment options for invasive aspergillosis (Mohr et al., 2008), azole drugs suffer from drawbacks such as drug–drug interactions and the recent appearance of azole resistant fungal strains (Walsh et al., 2008) (van der Linden et al., 2013).

Echinocandins are semisynthetic amphiphilic lipopeptides that include caspofungin, micafungin and anidulafungin (Fig 1.4). These compounds inhibit the enzyme glucan synthase that catalyses the synthesis of the major cell wall component β-1,3-glucan from the substrate UDP-glucose (Fig 1.5). β-1,3-glucan is an important cell wall component that contributes to the shape and scaffolding of the fungal cell wall, and inhibition of the glucan synthase will lead to cell wall

destabilization, which then results in cell death (Douglas, 2001; Free, 2013). However, in contrast to azoles and polyenes, echinocandins have only fungistatic activity against *Aspergillus spp,* and recent genetic studies suggest that the gene encoding for the glucan synthase, *fks1*, is not essential in *A. fumigatus* (Dichtl et al., 2015).

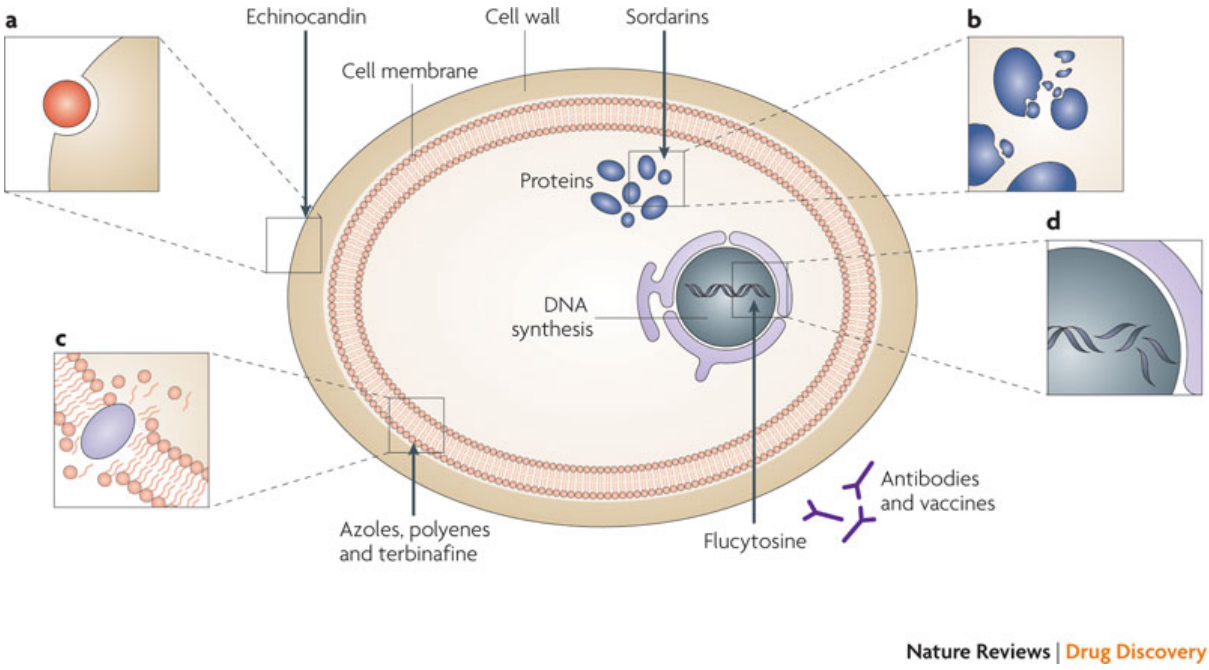

Figure 1.5: Mode of actions of different antifungals.

(a) The echinocandins target the cell wall synthesis by inhibiting glucan synthase (b) Sordarins inhibit the protein translation process (c) Azoles and polyenes target the cell membrane component ergosterol (d) Flucytosine targets DNA synthesis. Image adapted from (Ostrosky-Zeichner et al., 2010).

Invasive aspergillosis affects approximately 3–5 million patients globally, in particular those suffering from cystic fibrosis or asthma (Agarwal et al., 2013; Brown et al., 2012), with a mortality rate up to 90% (Zmeili and Soubani, 2007). This very high mortality rate accurately reflects the fact that on the one hand there are lack of good diagnostics, and on the other hand the current clinically

antifungal treatment options (polyenes, azoles and echinocandins) are limited against these types of fungal infections. None of the clinically used antifungals, represented by the first line therapy voriconazole, are without significant drawbacks such as toxicity, drug–drug interactions and/or lack of efficacy (Agarwal et al., 2013). Therefore, new antifungal targets and new antifungal precursors are urgently needed for drug development.

1.2 The fungal cell wall as a source of antifungal targets

The fungal cell wall is a unique and essential structure for fungal organisms: unique because it is a highly ordered carbohydrate structure that is absent from mammalian cells; and essential because the cell wall is important for growth, survival and morphogenesis of fungal cells. Polysaccharides account for over 90% of the cell wall, making up the alkali-insoluble and alkali-soluble fractions. The alkali-insoluble fraction is formed by the β-glucan central core cross-linked to chitin (Fig 1.6). The alkali-soluble fraction is covalently bound to the glucan–chitin complex and in *A. fumigatus* is known to be composed of galactomannan and α-glucan (Fig 1.6) (Latge, 2007). The importance of the fungal cell wall is not only for providing protection against hostile environments such as temperature changes, pH, oxidative stress, nutrient limitations, but also other mechanical stresses (Bowman and Free, 2006). For the pathogenic fungi, such as *A. fumigatus*, the fungal cell wall also functions as an essential intermediate for the colonization and invasion of host tissues as well as biofilm formation (Free, 2013). The cell wall is constantly subject to synthesis, degradation and remodelling by a large arsenal of enzymes whose activities are precisely regulated, and this makes them a source of potential antifungal targets.

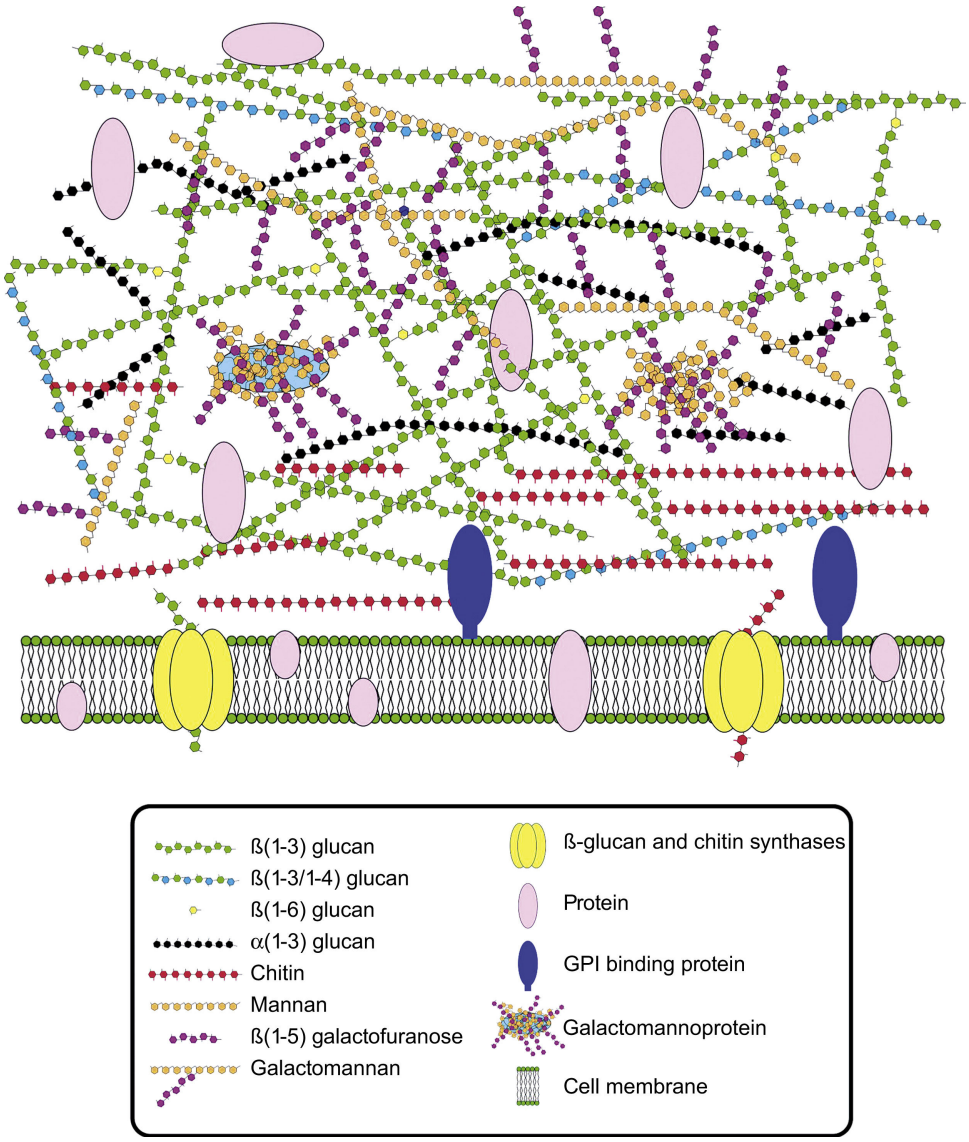

Figure 1.6: Scheme of *Aspergillus fumigatus* cell wall. Image adapted from (Abad et al., 2010)

1.2.1 The unique features of the fungal cell wall in *Aspergillus fumigatus*

The general organisation and architecture of fungal cell walls are conserved among fungal phyla. However, *A. fumigatus* also has some unique characteristics. The major components of *A. fumigatus* cell wall are β-1,3-glucans, α-glucan, chitin, galactomannan and a mixed β-1,3-/β-1,4-glucan layer (Latge, 2007). The levels of the chitin component are much higher than other characterized fungal organisms (Latge, 2007). The mixed β-1,3-/β-1,4-glucan layer is a unique feature of *A. fumigatus*, whereas in *Candida albicans* it is β-1,6-glucan (Fontaine et al.,

2000; Latge, 2010). Moreover, the core mannan structure of the cell wall in *A. fumigatus* is also found to be different from that in other fungal organisms. Instead of having an α-1,6-mannan core, the galactomannan in *A. fumigatus* has been reported to have a repeating tetramannose core that contains both α-1,2- and α-1,6-mannose linkages (Fontaine et al., 2000).

1.2.2 Glucan synthase as a target in *A. fumigatus*

β-1,3-glucan is a major constituent of the fungal cell wall, making up 20% to 35% of the cell wall mass in *A. fumigatus*, and it functions as the major cell wall building block. The β-1,3-glucans are synthesized by a plasma membrane-bound glucan synthase complex, encoded by the *fks1* gene, which converts the substrate UDP-glucose to linear chains of β-1,3-glucans, and a putative regulatory subunit, which is most likely encoded by *rho1* (Fig 1.7) (Beauvais et al., 2001; Beauvais et al., 1993; Douglas, 2001). Given the importance of glucan synthase to cell wall biogenesis, it has been considered as a prime target for the development of antifungals. The recently developed echinocandin family of drugs e.g. caspofungin, micafungin and anidulafungin, are inhibitors of the regulatory subunit of glucan synthase Fks1 (Fig 1.7). However, the echinocandins are only fungistatic rather than fungicidal against *A. fumigatus*, and therefore used as a salvage therapy for aspergillosis. This is partly caused by the recent discovery that *fks1,* which encodes the catalytic subunit of glucan synthase, is not essential in *A. fumigatus (Dichtl et al., 2015)*. Deletion of *fks1* in A. *fumigatus* will result in a cell wall devoid of β-1,3-glucan, but it is accompanied by a compensatory increase of chitin and galactosaminogalactan (Fig 1.7) (Dichtl et al., 2015). Fks1 is a large transmembrane protein with a molecular weight over 200 kDa containing 16 predicted transmembrane helices. Further rational improvement of echinocandin drugs is therefore limited by the inability to produce this large

membrane protein in an over-expression system. However, the regulatory subunit of glucan synthase Rho1 is a small cytosolic protein, and is essential for *A. fumigatus* survival (Dichtl et al., 2012). The essentiality of Rho1 in *A. fumigauts* is because Rho1 is also a master regulator of the CWI (cell wall integrity) pathway, which is a savage pathway to stimulate cell wall synthesis when in stressed conditions (Dichtl et al., 2012). Therefore, the *A. fumigatus* Rho1 GTPase may be considered as a potential target against which to develop chemical inhibitors.

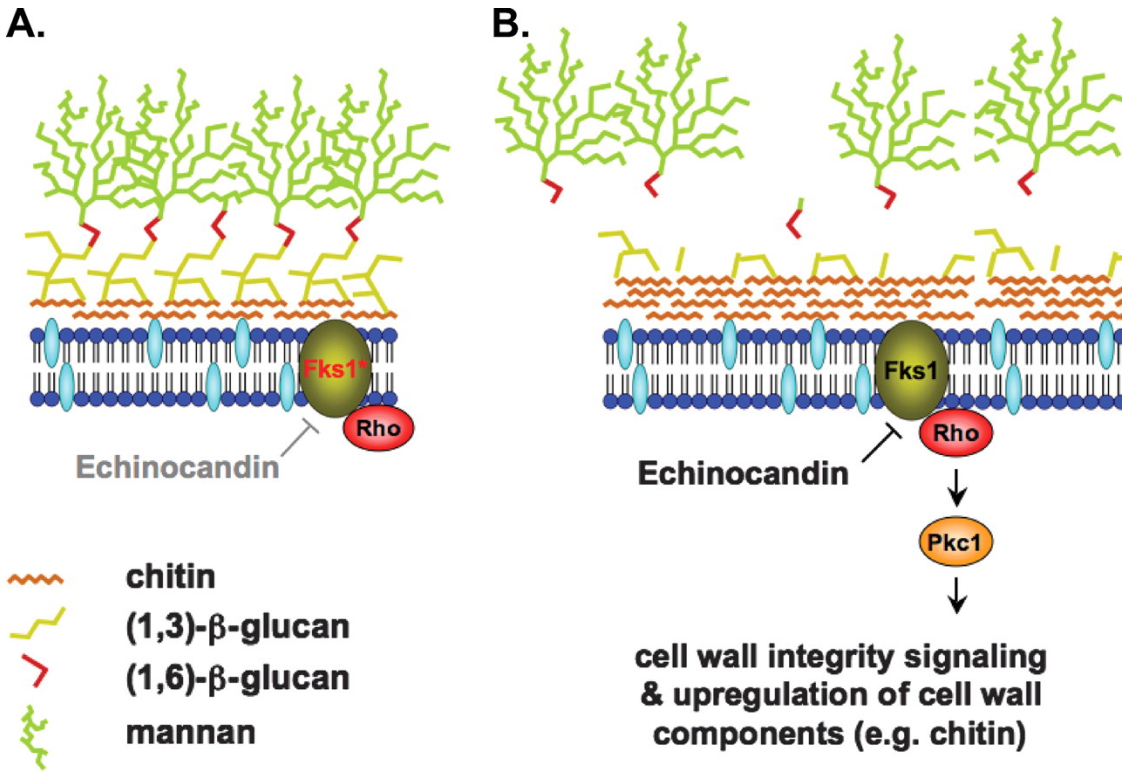

Figure 1.7: The molecular mechanism of echinocandin drugs and their mode of action. Image adapted from (Cowen, 2008).

(A) The echinocandin drugs target Fks1, catalytic subunit of glucan synthase of *A. fumigatus*,

(B) Inhibition of Fks1 will result in cell wall with compromised β-1,3-glucan, which is compensated for by an increase in chitin and other cell wall components.

1.3 Rho GTPase signalling regulates the fungal cell wall synthesis

1.3.1 Rho1 as a regulatory subunit of glucan synthase

The identification of Rho1 GTPase as the regulatory subunit of β-1,3-glucan synthase was first made in the budding yeast *Saccharomyces cerevisiae* (Drgonova et al., 1996). Mutants in *rho1* were found to be defective in the GTP stimulation of glucan synthase activity, and this defect could be rescued by addition of purified or recombinant Rho1 protein (Kondoh et al., 1997). Rho1 in *S. cerevisiae* was found to co-localise with actin patches at the site of bud emergence, which is also a cell wall synthesis locus (Drgonova et al., 1996). A cellular model of the Rho1 GTPase regulatory mechanism of glucan synthase in *S. cerevisiae* was therefore established, based on the above research results (Fig 1.8). In this model, the small cytosolic protein Rho1 GTPase trans-localizes from cytosol to actin patches at the cell membrane, where it changes its binding conformation from the inactive GDP bound form to the activated GTP bound form. In the latter form, the Rho1 GTPase will activate the inactive glucan synthase by changing its conformation, exposing its active site. This allows the substrate UDP-glucose to bind into the active site and be synthesized into β-1,3-glucan (Fig 1.8). This model was confirmed in other fungal organisms. In the pathogenic fungus *C. albicans*, for example, recombinant Rho1 protein was able to reactivate β-1,3-glucan synthase in *C. albicans* membranes (Kondoh et al., 1997). *C. albicans* Rho1 was also found co-purified with the β-1,3-glucan synthase putative catalytic subunit in a product entrapment experiment, which suggests potential protein–protein interactions (Kondoh et al., 1997). In *A. fumigatus*, the Rho1 orthologue protein *Af*Rho1 was cloned and purified, and was shown to co-purify with the glucan synthase complex in a product entrapment experiment (Beauvais et al., 2001). The biological function of *Af*Rho1 was further investigated by genetic

approaches. A GFP-tagged *Af*Rho1 mutant was shown to be predominantly localised at the hyphal tips in *A. fumigatus*, sharing a similar localization pattern with glucan synthase (Beauvais et al., 2001; Dichtl et al., 2010). A conditional knockdown mutant of *Af*Rho1 was generated to show that *Af*Rho1 is essential in *A. fumigatus*, and mutants lacking *Af*Rho1 showed a cytoplasmic leakage phenotype (Dichtl et al., 2012). The above evidence clearly suggests that *Af*Rho1 in *A. fumigatus* shares a conserved function with that in yeast in regulating glucan synthase, and could potentially be a novel cell wall target for development of inhibitors.

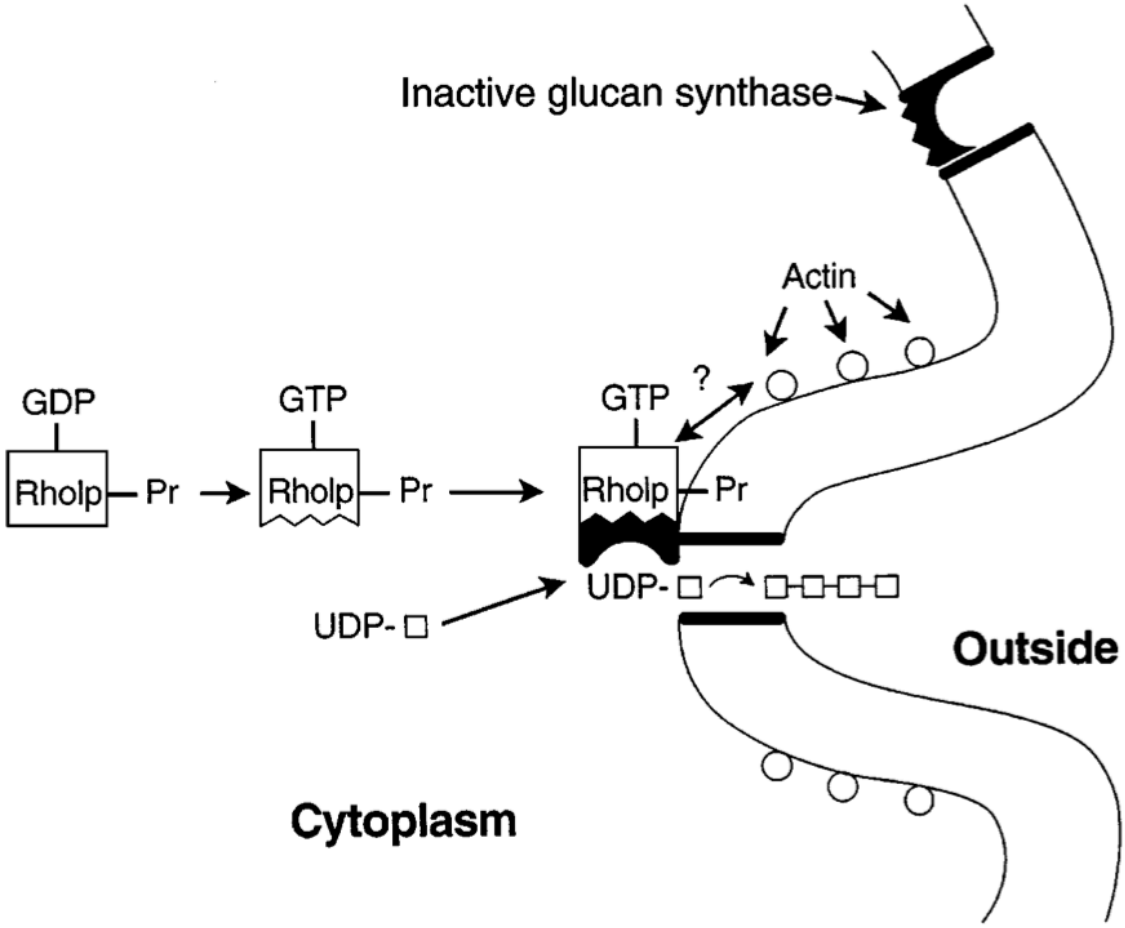

Figure 1.8: Schematic representation of Rho1p regulation of glucan synthase activity. Rho1p translocates from cytoplasm to the cell membrane, and changes from the GDP bound inactive state to the GTP bound active state. In the GTP bound state, Rho1p activates the in active glucan synthase, to enable the biosynthesis of β-1,3-glucan from UDP-glucose. The small squares attached to UDP represent glucosyl units. Pr, Prenyl group. Image adapted from (Drgonova et al., 1996)

1.3.2 Rho1 plays a pivotal role in the fungal CWI pathway

Fungal cells employ a so-called cell wall integrity pathway (CWI) that orchestrates changes in the cell wall composition to deal with extracellular stresses, such as high temperature, drastic changes in pH and osmotic shock during growth and

morphogenesis. The CWI pathway was first discovered and characterised in the budding yeast *S. cerevisiae* (Levin, 2005, 2011). The CWI pathway is a well-organised cell signalling pathway that comprises transmembrane sensor proteins (*Sc*Wsc1-3), guanine nucleotide exchange factors (GEFs) (*Sc*Rom1/2), Rho1 GTPase, protein kinase C (*Sc*Pkc1) and a mitogen-activated protein (MAP) kinase module (Fig 1.9). The CWI pathway is activated by extracellular stresses sensed by the transmembrane sensors such as Wsc1, Wsc2, Wsc3, Mid2 and Mlt1, which then stimulate the downstream GEF proteins. These in turn activate the Rho1 GTPase. The activated Rho1 GTPase can either activate the glucan synthase directly or further activate Pkc and the downstream MAP kinases to finally trigger the transcription of genes through the transcription factors such as Swi4/6 and Rlm1 to regulate cell wall biogenesis (Fig. 1.9). *Sc*Rho1 as a central regulator of the CWI pathway was shown to be essential in *S. cerevisiae* (Madaule et al., 1987). The CWI pathway was recently found to be conserved in *A. fumigatus*, in which *Af*Rho1 also functions as a central player (Dichtl et al., 2012; Samantaray et al., 2013). Investigation of the CWI pathway not only further emphasized the importance of the Rho1 GTPase in regulating fungal cell wall synthesis, but also helped to identify the potential upstream regulators of Rho1.

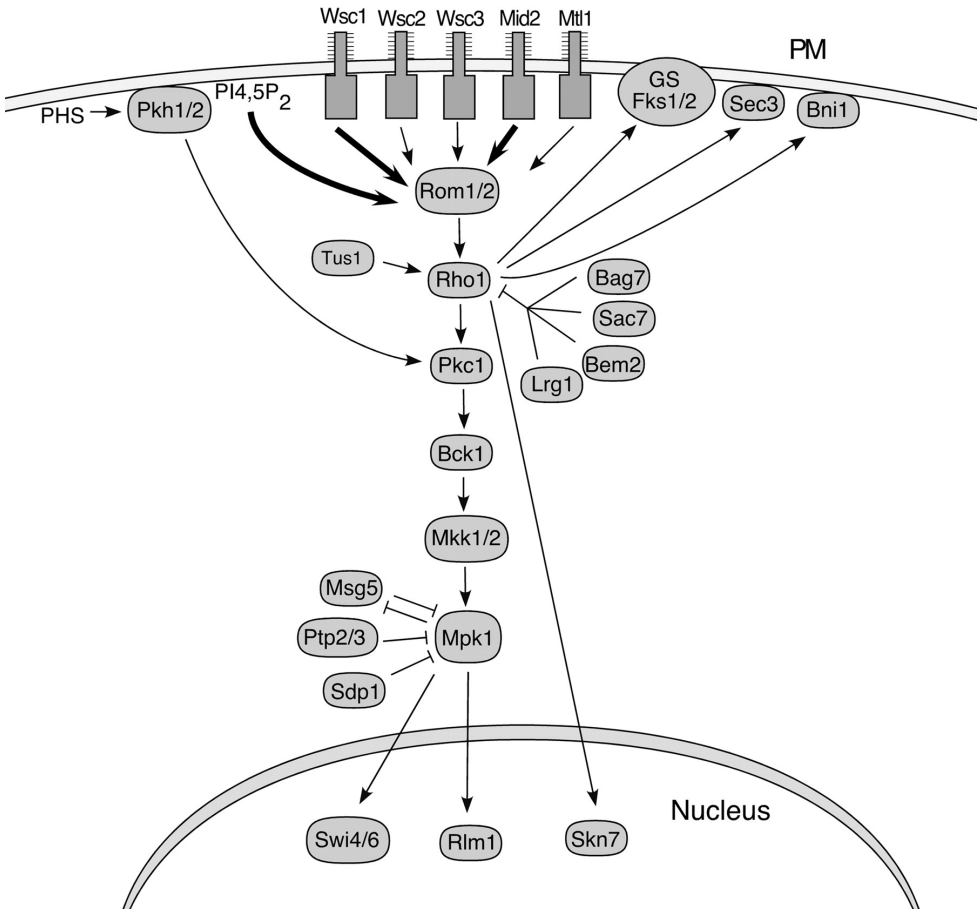

Figure 1.9: CWI signalling pathway in *S. cerevisiae*.

The sensors transduce signals through GEFs Rom1/2 to the central Rho1 GTPase, which then either activates glucan synthase complex or activates the Pkc1-dependent MAPK cascade to stimulate transcription. Image adapted from (Levin, 2005).

1.3.3 The GEFs are the activators of Rho GTPases

Rho GTPases as molecular switches usually have two different conformational states: the GDP bound inactive state and the GTP bound active state (Rossman et al., 2005). In the GTP bound active state, Rho GTPases associate with the plasma membrane and activate different kinds of downstream effectors to regulate an array of cellular events such as organization of actin cytoskeleton, cell cycle progression and expression of various genes (Rossman et al., 2005). Cycling of Rho GTPases between these two states is primarily regulated by two classes of molecule: the guanine nucleotide exchange factors (GEFs) and the

GTPase activating proteins (GAPs). The GEFs catalyse the exchange of GDP to GTP, therefore are positive regulators of Rho GTPases. The GAPs, on the contrary, stimulate the intrinsic GTPase activity of Rho proteins, to transform Rho GTPases from the GTP to the GDP bound conformation, thereby acting as down-regulators (Fig 1.10). There is also a third group of regulatory protein called guanine nucleotide dissociation inhibitors (GDIs), which inhibit Rho GTPase activation by maintaining them in the cytoplasm in the inactive GDP bound form (Dransart et al., 2005) .

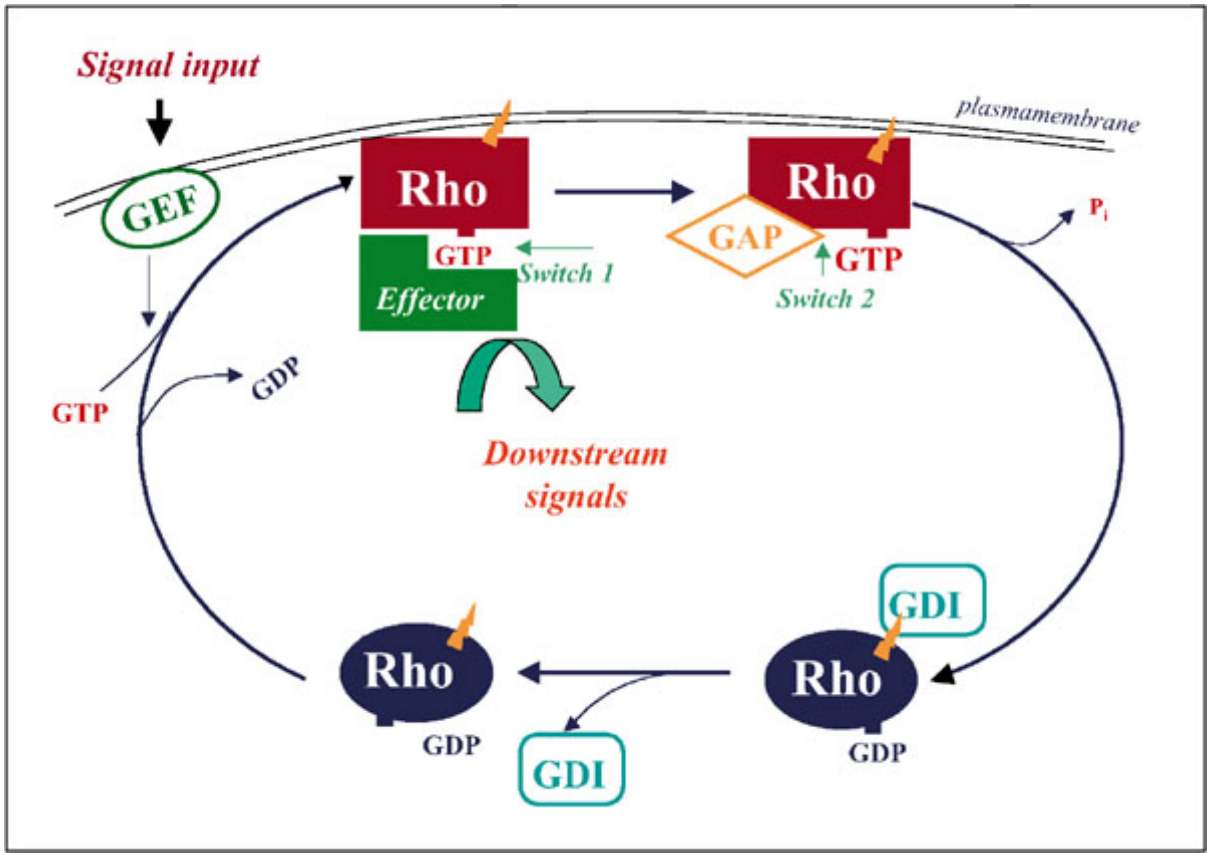

Figure 1.10: Rho GTPase activation/ deactivation cycle.

Rho GTPases are molecular switches that cycle between an inactive GDP bound state and an activated GTP bound state. In the GTP bound state, Rho GTPases will activate downstream effector proteins. The guanine nucleotide exchange factors (GEFs) catalyse the release of GDP and binding of GTP. The GTPase activating proteins (GAPs) transform the Rho GTPases from the GTP to GDP bound state by stimulating intrinsic GTPase activity. The guanine dissociation inhibitor (GDI) maintains Rho in the cytoplasm in its inactive GDP bound form. Image adapted from (Kawano et al., 2014) .

1.3.4 *Af*Rom2 is a GEF protein of *Af*Rho1, and an essential cell wall target

In the *S. cerevisiae* CWI pathway, *Sc*Rho1 is regulated by two GEF proteins: *Sc*Rom1 and *Sc*Rom2. The *rom1* and *rom2* (*rho1* multi copy suppressors) homologous genes were identified as multi-copy suppressors of a temperature sensitive *rho1* mutant in *S. cerevisiae* (Bickle et al., 1998). *Sc*Rom1 and *Sc*Rom2 share overlapping functions, in that a double mutant that deletes both of them is lethal. Whereas deletion of *Sc*Rom1 resulted in no detectable phenotypes, *Sc*Rom2 deletion resulted in temperature-sensitive growth that was partially rescued by osmotic stabilization (Vilella et al., 2005). In *A. fumigatus,* an orthologous protein of *Sc*Rom1/*Sc*Rom2 was identified as *Af*Rom2 (Samantaray et al., 2013). A conditional knockdown mutant of *Afrom2* shows severe growth defects under repressive conditions (Samantaray et al., 2013). The down-regulation of *Afrom2* shows sensitivity to cell wall stress agents such as Congo red, calcofluor white and echinocandins, which suggests a compromised cell wall (Samantaray et al., 2013). *Af*Rom2 was also shown to have protein–protein interactions with *Af*Rho1 in a co-immunoprecipitation (Co-IP) experiment (Samantaray et al., 2013), and *Af*Rom2-GFP localized to the hyphal tips, in agreement with the reported *Af*Rho1 localization pattern (Beauvais et al., 2001; Samantaray et al., 2013). Therefore, *Af*Rom2 is likely to be the *Af*Rho1 GEF protein and may itself also be a potential cell wall target in *A. fumigatus*.

1.3.5 *Af*Rom2 possesses a C-terminal CNH domain with unknown functions

Rho GEF proteins usually harbour a conserved Dbl homology (DH) domain (~200 residues), and an adjacent Pleckstrin homology (PH) domain (~100 residues) (Kristelly et al., 2004). The DH and PH domains are the catalytic domains of Rho

GEFs, which is responsible for the exchange of GDP to GTP by binding to the switch regions of Rho GTPases, altering the conformation of the nucleotide-binding pocket (Kristelly et al., 2004). The PH domain also helps to localise the GEF proteins to the cell membrane by binding to phosphoinositide (Rossman et al., 2005). However, *Af*Rom2 was found to have a C terminal citron homology (CNH) domain in addition to the canonical GEF domains (DH–PH) (Samantaray et al., 2013). Secondary structure comparison also shows that the CNH domain is only found in *Af*Rom2 and is not present in all the vertebrate Rho GEF proteins, which suggests that the *Af*Rom2 CNH domain may have some unique cellular functions in *A. fumigatus* (Fig 1.11*).*

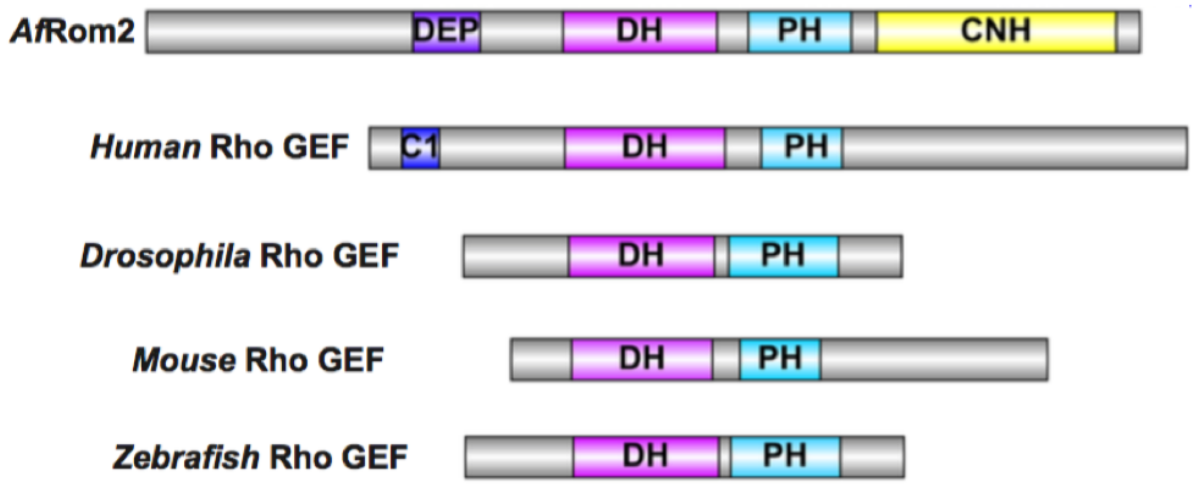

Figure 1.11: Domain presentation of *Af*Rom2 and Rho GEF proteins from other organisms. The domain architectures of the protein were based on the Uniprot protein domain annotation and displayed using IBS 1.0.1- Illustrator for Biological Sequences (Liu et al., 2015). DEP: Dishevelled, Egl-10 and Pleckstrin domain. DH: Dbl homology domain. PH: Pleckstrin homology domain. CNH: Citron homology domain. C1: phorbol esters/diacylglycerol binding domain.

The CNH domain is also the signature C-terminal domain of citron kinases (CIT-Ks), which are a group of kinases that have been shown to play important roles in regulating cytokinesis in mammalian cells and *Drosophila melanogaster* (Bassi et al., 2011; Gai et al., 2011). The CIT-Ks have important functions in mid-body organization and are required for the proper RhoA localization in the late stages of cytokinesis (Dean and Spudich, 2006). However, the exact function of CNH domain in CIT-K is not clear. In *Drosophila melanogaster*, the CNH domain of the CIT-K, Sticky, was shown to interact with recombinant Rho1 in both its GTP- (active) and GDP- (inactive) bound forms, but it is not required for the correct cellular localization of Rho1 (Bassi et al., 2011). A Sticky construct lacking the CNH domain could not fully rescue the cytokinesis defects caused by a Sticky knockdown, suggesting that the CNH domain is necessary for at least some functions of Sticky (Bassi et al., 2011). In a recent screen to characterize the CIT-

K interactome in human cells, the CNH domain was found to interact predominantly with the key chromosomal passenger complex (CPC) components Aurora B and INCENP (McKenzie et al., 2016). These data suggested that the CNH domain in CIT-K might function as a protein–protein interaction platform to mediate the protein complex structure formation around RhoA and other important cytokinesis-related scaffold proteins.

It is not yet clear what the role of the *Af*Rom2 CNH domain is and one of the aims of this thesis is to study its molecular functions and protein structure. The aim was to explore the *Af*Rom2 CNH domain as a novel selective antifungal target, but also use it as a template to provide insights into the function of CNH domains in mammalian CIT-K proteins.

1.4 Targeting Rho GTPases

1.4.1 The Rho GTPases as anti-cancer targets in mammalian cells

Rho GTPases are small Ras-like GTPases with a molecular weight ~20 kDa. In mammalian cells, there are over 20 Rho family proteins which include the most thoroughly characterised RhoA, Cdc42 and Rac1 (Ridley, 2006). They are important intracellular molecular switches in mammalian cells, Rho GTPases can relay signals from integrins (Renshaw et al., 1996), growth factor receptors (Nobes et al., 1995), ion channels (Pochynyuk et al., 2007) and G-protein coupled receptors (Sah et al., 2000) by transition from the GTP-bound active state to the GDP-bound inactive state. Rho GTPases regulate a number of important cellular events that include gene transcription (Marinissen et al., 2001), cell proliferation (Provenzano and Keely, 2011), migration (Ridley, 2015) and cell division (Chircop, 2014). The Rho proteins have over 60 identified downstream effector proteins in

mammalian cells, and the most common result of Rho GTPase activation is reorganisation of the actin cytoskeleton.

Through the regulation of the actin cytoskeleton, the Rho GTPase pathway is involved in the regulation of a wide variety of cellular processes such as cell morphology, survival, proliferation and adhesion (Ridley, 2006). These cellular events are important for cancer transformation. Over the past decades, many clinical research investigations have reported the links between Rho protein over-activation and cancer (Gomez del Pulgar et al., 2005). In a study of breast cancer, overexpression of RhoA, Rac1 and Cdc42 was found in 100% of all diagnosed patients' tumours, compared to their control tissues (Fritz et al., 2002). In testicular tumours, the overexpression of RhoA, Rac1, Cdc42 and the downstream Rho kinases are indicative of cancer progression (Kamai et al., 2004). Moreover, many other cancer types such as lung (Touge et al., 2007), ovarian (McGrail et al., 2014), gastric liver (Pan et al., 2004) and bladder (Kamai et al., 2003) cancers are all associated with overexpression of Rho GTPases. Therefore, down-regulation of Rho GTPase through therapeutic interventions is widely thought to be a viable anti-cancer strategy and has been pursued over the past decades.

1.4.2 Rho inhibitor development through multiple approaches

The most obvious and direct way to target Rho GTPases would be to develop a substrate competitive inhibitor. However, this approach has been found to be impractical and very difficult to achieve. This is because the binding affinity between Rho GTPases and the substrate GDP/GTP is in the picomolar range, and it is extremely difficult to develop an inhibitor that has a higher binding affinity (Smithers and Overduin, 2016). Furthermore, there are hundreds of GTP/GDP binding proteins in cells, and therefore a simple GDP/GTP analogue inhibitor

would not be able to achieve the desired selectivity. Alternative approaches are to target the regulatory proteins of Rho GTPases.

1.4.2.1 Carboxyl terminal prenylation inhibitors

Carboxyl terminal prenylation of Rho GTPases is a necessary step for the proper membrane localization and activation of the protein (Mondal et al., 2000). The statin drugs have been recently shown to decrease Rho activity, which inhibits the progression of different types of cancer development (Tang et al., 2008). The mechanisms of statin activity is by the inhibition of farnesyl pyrophosphate and geranylgeranyl pyrophosphate synthesis, which are responsible for Rho prenylation (Mondal et al., 2000). Cerivastatin, for example, was found to reduce RhoA activity in breast cancer cells (Denoyelle, Vasse et al., 2001), atorvastatin has been shown to inhibit metastasis of human melanoma cells by inhibiting Rho geranylgeranylation (Collisson, Kleer et al., 2003), and lovastatin was found to reduce tumour cell adhesion by inhibiting Rho mediated expression of E-selectin (Nubel et al., 2004). However, the biggest limitation of the statin drugs is that they are not specific to Rho GTPases, so the exact molecular mechanisms of the effect are difficult to interpret.

1.4.2.2 Rho kinase inhibitors

The Rho interacting kinases (ROCKs), as the downstream effectors of Rho GTPases, are appealing therapeutic targets. The RhoA specific ROCK kinase was shown to play roles in cancer progression and neoangiogenesis (Somlyo and Somlyo, 2003). Two ROCK inhibitors (Fasudil and Y-2762) have been developed for the treatment of ROCK-related diseases. The ATP binding pocket of ROCK can accommodate the binding of fasudil or Y-27632, which leads to effective inhibition of its kinase activity (Guilluy et al., 2005). Y-27632 was shown to effectively treat hypoxia induced pulmonary hypertension (Guilluy et al., 2005)

and fasudil was found to effectively attenuate aneurism in a mouse model (Wang et al., 2005). However, there are over 60 known downstream effector proteins of Rho GTPases, and thus to target a single Rho effector protein will not be as effective as targeting the Rho proteins themselves.

1.4.2.3 Rho–RhoGEF interaction inhibitors

Rho activity is promoted by guanine nucleotide exchange factors (GEFs) that catalyse the transition of Rho GTPases from the inactive GDP bound state to the activated GTP bound state. Therefore, targeting GEF-mediated Rho activation has become a very attractive approach to inhibit Rho GTPase signalling. There are several ways of achieving this, among them targeting the GEF–Rho GTPase interactive interface essential for the guanine nucleotide exchange reaction has been successful in the discovery of several Rho family inhibitors. The Rac1 inhibitor NSSC23766, that specifically binds to the surface groove of Rac1 involved in GEF interaction, effectively inhibits the Rac1 activity in diverse physiological and pathological systems (Gao et al., 2004). The RhoA specific inhibitor Rhosin was discovered from a virtual screen and inhibits the GEF-catalysed RhoA activity in cells (Shang et al., 2012). The compound A13 was found to bind to the Rho GEF protein AKAP13 (Lbc), which acts as an inhibitor of Lbc–RhoA interaction *in cellulo* (Diviani et al., 2016). By interacting with the DH domain, the compound inhibits the catalytic activity of Lbc, and reverses prostate cancer cell phenotypes (Diviani et al., 2016). However, none of these inhibitors have entered into clinical trials at the moment, due to their low binding affinity (μM range), and without detailed structural information further optimisation of these compounds is limited.

1.4.3 Fragment-based drug discovery (FBDD): state of the art

Fragment-based drug discovery (FBDD) has now emerged as one of the most frequently used drug discovery approach in the pharmaceutical industry and academic institutions (Erlanson et al., 2016). The key principle of fragment screen is that by using small molecular weight compounds it is possible to fully explore the potential chemical binding hot spots of the entire protein surface (Scott et al., 2012). A fragment screen library uses chemical compounds that conform to the rule of three: (1) molecular mass < 300 Da, (2) up to three hydrogen bond donors and up to three hydrogen bond acceptors, (3) a calculated log P (clogP) ≤ 3 (The log P value of a compound is the logarithm of its partition coefficient between concentration dissolved in partition solvent and the concentration dissolved in water, which is the measurement of the compound's hydrophilicity) (Congreve et al., 2003). A fragment library with the size of a few thousand compounds will contain enough chemical diversity to ensure a good chance of identifying chemical binders to the target of interest. Compared to high throughput screens, the hit molecules found from FBDD usually have a low binding affinity (~1 mM), however the ligand efficiency (LE) (LE measures the binding energy per atom of a ligand to its binding partner) will be significantly higher (Kuntz et al., 1999). Therefore, hits identified from a fragment screen are subjected to a fragment elaboration cycle that includes iterative rounds of synthetic/medicinal chemistry and structural biology (macromolecular X-ray crystallography, NMR) to develop the initial fragments into inhibitors with drug-like chemical properties (Fig1 .12) (Scott et al., 2012). FBDD has provided a starting point to develop a number of chemical inhibitors for difficult targets like Bcl2 and H-Ras that were considered to be "undruggable" (Ostrem et al., 2013; Petros et al., 2014). A landmark event of the FBDD was achieved in 2011 when the first fragment-derived drug, Zelboraf

(vemurafenib), a BRAF inhibitor for treatment of skin cancers, was approved by FDA. So far, more than 30 drugs derived from FBDD have entered into clinical trials.

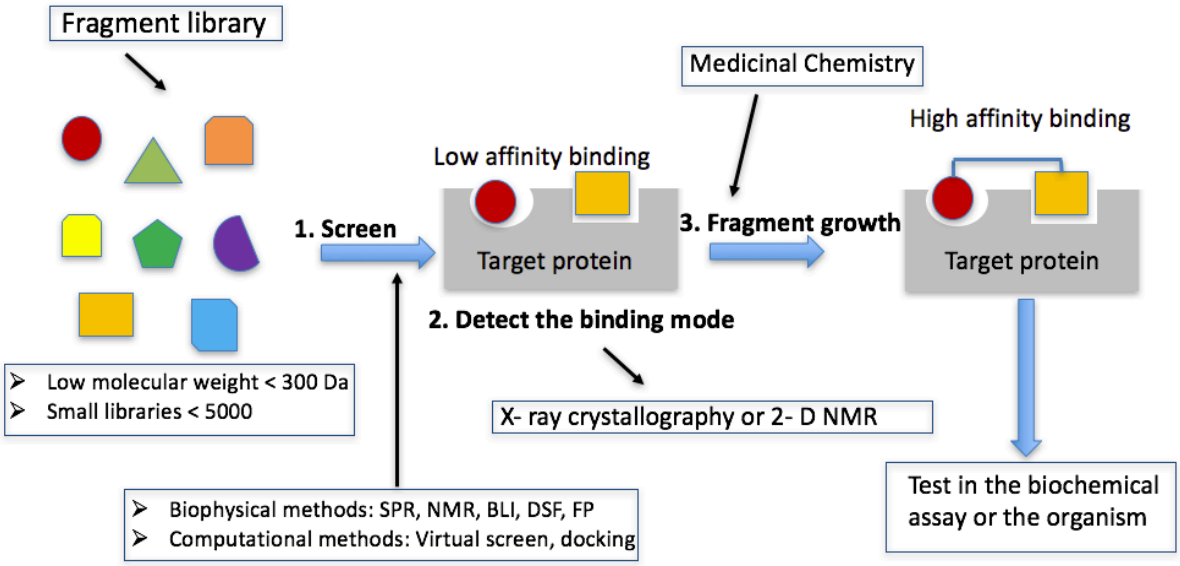

Figure 1.12: A fragment screen pipeline.

A fragment screen starts to build a fragment library that contains small molecule fragments. The initial screening methods are biophysical methods such as SPR, NMR, BLI, etc., and computational methods such as virtual screen and docking. The binding mode of the identified screen hits is determined by X-ray crystallography or protein observed NMR. The information of the binding mode is used to guide the medicinal chemistry, to further synthesize the initial fragment hits into high binding affinity inhibitors. The synthesized inhibitors will then need to be tested either in a biochemical assay or at the cellular level.

In Daan van Aalten's lab, we have established a workflow to do fragment screen by using BLI (BioLayer Interferometry) (Fig. 1.13). To do a fragment screen, the target protein was need to be biotinylated and immobilized to a streptavidin sensor. BLI measures biomolecule interactions by analysing the interference pattern of white light reflected from sensor surfaces, when the target protein binds to the fragment, the interference pattern will be changed and gives the signal. For the primary screen, single concentration (50 μM) of fragment compounds were

used to test binding to the target protein by BLI. And the for the secondary screen, the serial dilutions of the primary binding hits were used to test binding to the target protein, to confirm the binding and also determine the binding affinity. After two rounds of BLI screen, the confirmed binding hits were used to do X-ray crystallography, binding affinity assay and enzymatic assay to determine the binding mode and guide the next step molecular design and the next step chemical synthesis. The synthesized compound will be tested again to determine the binding affinity and binding mode, and finally at the cellular model.

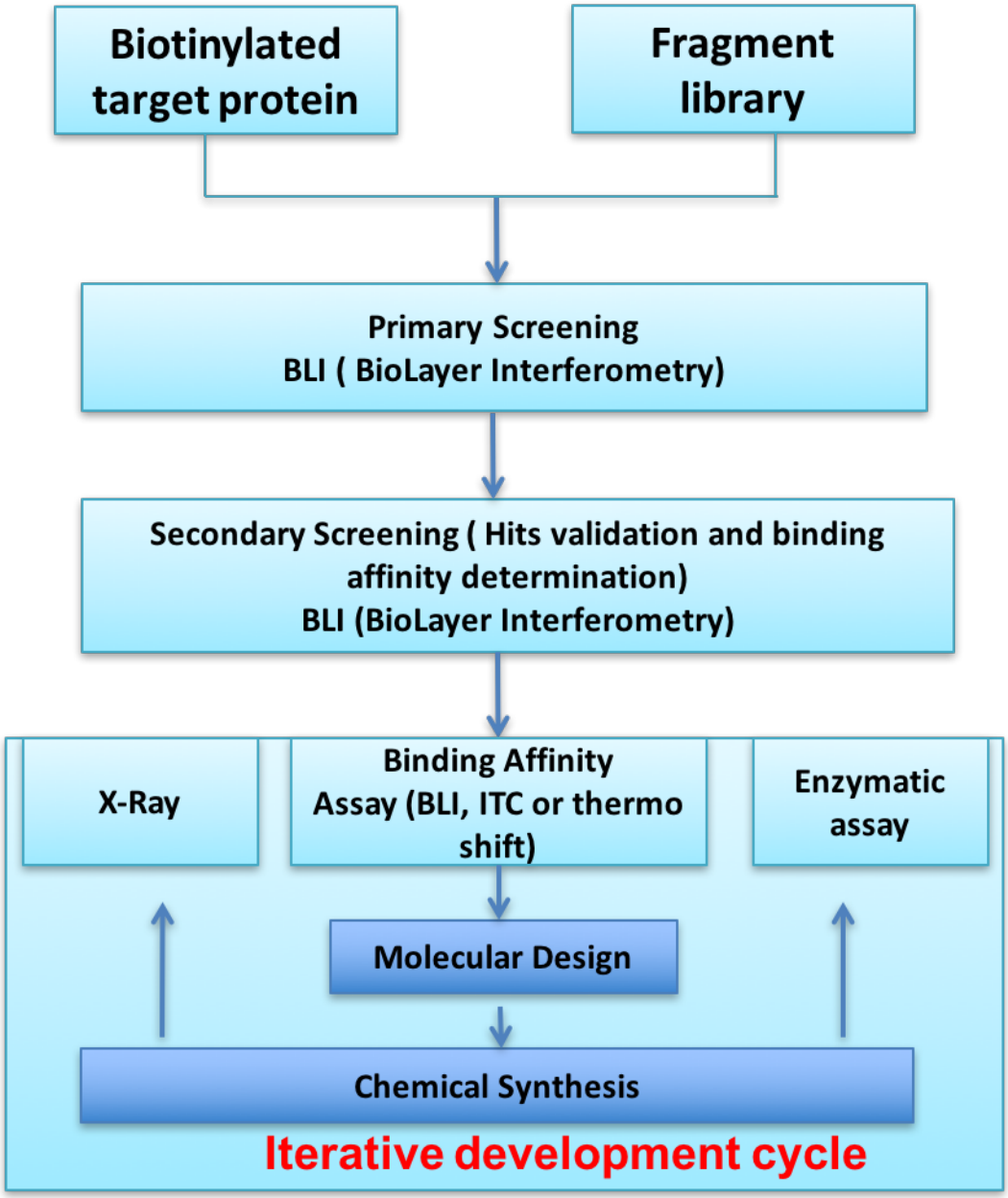

Figure 1.13: The workflow to do a fragment screen in Daan van Aalten's lab

1.5 Aims and objectives

For my PhD research, my aims were

a) Using X-ray crystallography to solve the structure of *Af*Rho1 from *Aspergillus fumigatus*, and compare to the known structure of *Hs*RhoA, to explore the structural differences

b) Applying the fragment screen techniques, to identify chemical binders to *Af*Rho1, then based on that to develop fragment derived inhibitors.

c) Genetically validate the Rom2 CNH domain in *A. fumigatus* as a potential fungal cell wall target.

d) Using X-ray crystallography to solve the structure of CNH domain in Rom2 from *A. fumigatus*, which will be the first structure of this domain family and will provide new insights into how this kind of domain functions at the atomic level.

Chapter 2 : Structural and fragment-based ligand design of Rho1 GTPase in *Aspergillus fumigatus*

2.1 Introduction

Therapeutic targets against pathogenic fungal infections include enzymes that are involved in synthesizing the fungal cell wall, which is essential for fungal growth (Cabib et al., 2001; Douglas, 2001; Munro et al., 2001). Polysaccharides account for over 90% of the fungal cell wall, containing chitin, glucan and galactomannan (Gastebois et al., 2009). One of the most abundant polysaccharides in *A. fumigatus*' cell wall is β-(1,3)-glucan, accounting for 20-35% of the total polysaccharides (Cabib et al., 2001; Latge, 2007). β-(1,3)-glucan is synthesized by a glucan synthase complex, which first has been characterized biochemically in the budding yeast *S. cerevisiae.* The glucan synthase complex is usually composed of two proteins. The catalytic subunit Fks1p, which is a large molecular size (>200 kDa) protein and contains 16 transmembrane domains (Douglas et al., 1994; Mazur et al., 1995). A regulatory subunit, Rho1p, belongs to the small Rho GTPases family and stimulates β-(1,3)-glucan synthase activity in its GTP binding form (Kondoh et al., 1997; Mazur and Baginsky, 1996; Qadota et al., 1996). The fact that Fks1p and Rho1p have been shown to be essential in yeast and many other fungal organisms (Douglas, 2001) suggests that the function of this protein complex is of vital importance for fungal survival, which makes these two proteins potential anti-fungal drug targets. Among them, Fks homologue proteins are the direct targets of the clinical used echinocandin drugs (Tkacz and DiDomenico, 2001). Unfortunately, further drug discovery and indeed molecular understanding of the Fks protein is severely limited by the inability to produce this large membrane protein in an overexpression system.

In *A. fumigatus,* the glucan synthase complex has also been investigated, the putative *Af*Fks1p and *Af*Rho1 were shown to co-localize with newly synthesized β-(1,3)-glucans (Beauvais et al., 2001). Furthermore, these two proteins are co-

purified by product entrapment purification (Beauvais et al., 2001). However, recent construction of an *fks1* gene knockout mutant suggests that in *A. fumigatus fks1* is not essential (Dichtl et al., 2015). This could also explain the only fungistatic rather than fungicidal effects of echinocandins drugs on *A. fumigatus* (Chen et al., 2011). Intriguingly, *Af*Rho1 does appear to be essential in *A. fumigatus,* as upon knockdown of this gene the *A. fumigatus* cells will display a cell lysis and subsequent death phenotype (Dichtl et al., 2012). Thus, inhibitors of this enzyme could have therapeutic potential.

*Af*Rho1 belongs to the Rho GTPases family, which are intracellular signalling molecules that regulate many cellular events in eukaryotic organisms, including gene transcription (Marinissen et al., 2001), cell proliferation (Provenzano and Keely, 2011), migration (Ridley, 2015) and cell division (Chircop, 2014). Due to the link between abnormal Rho GTPases activities and human cancers, there has been considerable interest in identifying good Rho GTPases inhibitors. However, Rho GTPases are considered difficult to target due to the globular structure and with limited druggable hydrophobic pockets (Hopkins and Groom, 2002, 2003; Verdine and Walensky, 2007). To target challenging proteins, fragment-based drug discovery has been used to effectively identify hits that can be developed into potent inhibitors by structure-based ligand design (Hajduk et al., 1997; Harner et al., 2013).

In this research, I aimed to apply X-ray crystallography and fragment-based small molecule screening by BLI (Biolayer interferometry) to investigate the ligandability of *Af*Rho1. Using X-ray crystallography, the structure of *Af*Rho1 was solved and a complex structure with one of the hit fragments was obtained. The complex structure showed that this fragment molecule bound to *Af*Rho1 in a 2:1 ratio, and the fragment binding pocket is conserved with the human orthologue

protein *Hs*RhoA. Structure analysis shows that the pocket is located at the previously validated interaction interface between *Hs*RhoA and its GEF (Guanine nucleotide exchange factor) protein LARG. The hit fragment was found to interrupt the protein-protein interactions of *Hs*RhoA and *Af*Rho1 to their corresponding GEF proteins. Therefore, I have identified a lead molecule that could be used to develop inhibitors against *Af*Rho1 and *Hs*RhoA by inhibiting the corresponding GEF proteins mediated nucleotide exchanges.

2.2 Materials and Methods

2.2.1 Protein expression and purification

The C-terminal eight amino acids truncated *Af*Rho1 (residues 1- 181) was cloned into the expression vector pGEX6P1 (GE Healthcare) using restriction enzyme BamI and NotI, and primers *Af*Rho1_fwd and *Af*Rho1_rev (Table 2.1).

Table 2.1: The primers used to clone the *Af*Rho1 and *Af*Rom2 CNH domain expression construct.

Primer	Sequence (5' to 3')
*Af*Rho1_fwd	*CTGGGATCCATGGCTGAATCCGCCGCAAGC*
*Af*Rho1_rev	*GATGCGGCCGCTCATCAGTGGGTCTTGGTCAAGAGAGCAG*
Hm2CT1_F	*CAGTCTGGATTTCTGGAACAAAGTAACAACAACAACAATGAGCGGCC*
Hm2CT1_R	GGCCGCTCATTGTTGTTGTTGTTACTTGTTCCAGAAATCCAGACTG

A F25N mutation was introduced for protein stability as described previously (Rose et al., 2005; Yamashita et al., 2010). The molecular cloning of the expression plasmid was done by Dr. Andrew Ferenbach from the DVA lab. The expression construct was transformed into *E. coli* BL21 (non DE3) cells. When cells grew to an OD_{600} of 0.8 at 37 °C, 250 μM IPTG is added for induction at 25 °C for 16 h. Cells were harvested by centrifugation at 4000 rpm at 4 °C for 30 min in a J6-MI centrifuge (Beckman Coulter), and suspended in TBD buffer with 0.5 mM TCEP, 5 mM $MgCl_2$,50 μM GDP plus a protease inhibitor cocktail (1 mM benzamidine, 0.2 mM PMSF, 5 μM leupeptin). Cells were lysed using pressure homogenization with an Emulsiflex (15,000 kilopascals Avestin; Ottawa, Canada). Supernatant and inclusion body were separated by centrifugation at 16,000 rpm for 1 h using an Avanti J26S centrifuge (Beckman Coulter). The soluble fraction was filtered before exposing to 2 ml of glutathione-Sepharose beads 4B (GE healthcare) for 2 h at 4 °C. The GST tag was cleaved from the beads by

incubating with 200 µg of PreScission protease at 4 °C overnight. *Af*Rho1 was concentrated to 2 ml and loaded onto a size-exclusion column (Superdex-75 GE healthcare) using an AKTA prime FPLC system (GE healthcare). Fractions were collected and purity was checked by SDS/PAGE. Pure protein was concentrated to 2 ml before snap freezing and storing at -80 °C. *Hs*RhoA was expressed and purified according to the previous publications (Wei et al., 1997). The DH-PH domains of *Af*Rom2 (residues 483- 858) was cloned into the expression vector pGEX6P1 (GE Healthcare). The expression construct was transformed into *E. coli* BL21 (non DE3) cells. When cells grew to an OD_{600} of 0.8 at 37 °C, 250 µM IPTG is added for induction at 25 °C for 16 h. Cells were harvested by centrifugation and suspended in TBD buffer with 0.5 mM TCEP. Cells were lysed using pressure homogenization with an Emulsiflex (15,000 kilopascals Avestin; Ottawa, Canada). Supernatant and inclusion body were separated by centrifugation at 42,000 g for 1 h using an Avanti J26S centrifuge (Beckman Coulter). The soluble fraction was filtered before exposing to 2 ml of glutathione-Sepharose beads 4B (GE healthcare) for 2 h at 4 °C. The GST tag was cleaved from the beads by incubating with 200 µg of PreScission protease at 4 °C overnight. The *Af*Rom2 DH-PH domain was concentrated to 2 ml and loaded onto a size-exclusion column (Superdex-75 GE healthcare) using and AKTA prime FPLC system (GE healthcare). Fractions were collected and purity was checked by SDS/PAGE. Pure protein was concentrated to 0.5 ml before snap freezing and storing at -80 °C. The DH-PH domain of LARG was expressed and purified according to the previous publication (Kristelly, 2004).

2.2.2 *Af*Rho1 Crystallization and date collection

The purified *Af*Rho1 protein was concentrated to 20 mg/ml using a 10 kD cut-off concentrator (Millipore). A mosquito crystal liquid handling robot (TTP Labtech)

was used to set up sitting drop crystal screens by combining 0.2 µl protein solutions with 0.2 µl commercially available crystallization buffer in 96 well MRC plates. Separate rod crystals of approximately 0.4 × 0.4 × 0.8 mm in size were obtained at 12 °C in a condition containing 37.1% w/v PEG 5000 MME, 150 mM Tris pH 8.0, 40 mM magnesium sulfate. Crystals were flash-frozen directly in the liquid nitrogen before data collection. X-ray diffraction data were collected on beamline i04-1 at the Diamond Synchrotron, Oxford, UK (Table 2.2). Data were auto processed in Diamond using xia2 (Winter et al., 2013). The crystals belonged to the space group $P4_3$ with unit-cell parameters of a = 53.8 Å, b = 53.8 Å, c = 62.7 Å, α = β = γ = 90°, with one molecule in the asymmetric unit. For soaking the crystal with the fragment hits, the selected fragments were dissolved into the crystallization condition with 50 mM concentration to make the soaking solution. Individual *Af*Rho1 crystals were picked and soaked into the soaking solution overnight and flash-frozen directly in the liquid nitrogen before data collection.

2.2.3 Structure determination

The structure was solved by molecular replacement using MOLREP (2008; Cowtan et al., 2011) with the *Hs*RhoA*GDP structure (PDB ID 1FTN) (Wei et al., 1997) as the search model. The Molecular replacement was followed by iterative cycles of manual model building in COOT (Emsley and Cowtan, 2004) and structure refinement by REFMAC5 (Murshudov et al., 2011; Nicholls et al., 2012). Unless otherwise noted, figures were generated using Pymol (DeLano, 2004). The refined model statistics are shown in Table 2.2.

2.2.4 Fragment screening by biolayer interferometry (BLI)

*Af*Rho1 was biotinylated by incubation with NHS-PEG4-biotin (Thermo) in a 1:1 molar ratio for 30 min at room temperature. Excess biotin was removed by

passing through a 2 ml Zeba desalt spin column (Thermo). Biolayer interferometry (BLI) measurements were carried out on an Octet RED 384 instrument (ForteBio). *Af*Rho1 was immobilized onto superstreptavidin (SSA) biosensors by incubation for 900 s at 50 µg ml^{-1}, then free streptavidin sites were blocked by a 60 s dip into 10 µg ml^{-1} biocytin (Tocris). A Maybridge RO3 fragment library composed of 1000 molecules was used for the screen, at a concentration of 200 µM. For hits confirmation, a control set of (SSA) biosensors was prepared in parallel by blocking the surface with biocytin. A five-point concentration series was prepared for each fragment in threefold dilution steps from a top concentration of 500 µM. For each set of biosensors, a 60 s association step and a 60 s dissociation step was used. Data were processed and analysed and K_d values were determined using the global fitting procedures as implemented in ForteBio Data Analysis Software v.7.0.1.5.

2.2.5 Testing the protein-protein interaction between *Af*Rho1/*Hs*RhoA with their corresponding GEFs using BLI

*Af*Rho1 and *Hs*RhoA were biotinylated by incubation with NHS-PEG4-biotin (Thermo) in a 1:1 molar ratio for 30 min at room temperature. Excess biotin was removed by passing through a 2 ml Zeba desalt spin column (Thermo). Biolayer interferometry (BLI) measurements were carried out on an Octet RED 384 instrument (ForteBio). *Af*Rho1 and *Hs*RhoA were immobilized onto superstreptavidin (SSA) biosensors by incubation for 900 s at 50 µg ml^{-1}, then free streptavidin sites were blocked by a 60 s dip into 10 µg ml^{-1} biocytin (Tocris). The DH-PH domains of the *Af*Rho1 GEF protein *Af*Rom2 and the human RhoA GEF protein LARG were tested for the binding at five-point concentration series in threefold dilution steps from a top concentration of 25 µM. A control set of (SSA) biosensors was prepared in parallel by blocking the surface with biocytin. For

each set of biosensors, a 60 s association step and a 60 s dissociation step. For testing the inhibition of the fragment hit compound DDD01511162, 1 mM compound was pre-incubated with *Af*Rho1/*Hs*RhoA before the binding test for 1 h in the room temperature. Data were processed and analysed and K_d values were determined using the global fitting procedures as implemented in ForteBio Data Analysis *Software* v.7.0.1.5.

2.2.6 Testing GEF-mediated *Af*Rho1/*Hs*RhoA activation using mant-GDP

Mant-GDP and GDP were purchased from Jena Biosciences. The measurements were carried out on a SpectraMax i3x spectrometer from Molecular Devices at 37 °C. The nucleotide exchange of *Af*Rho1/*Hs*RhoA was measured over time as the increase in fluorescence intensity at (λ_{ex} 360 nm; λ_{em} 444 nm) of mant-GDP. Mant-GDP (1 μM) was incubated with *Af*Rho1/*Hs*RhoA (0.5 μM) in buffer containing 25 mM HEPES, pH 7.5, 150 mM NaCl, and 25 mM $MgCl_2$. The samples were measured in a cycle of 1 min for 1 s, for an in total time period 40 min. Exponential fitting of the RFU to the time period was done with PRISM 6. To test the GEF activity, *Af*Rho1/*Hs*RhoA (0.5 μM) were pre-incubated with mant-GDP (1 μM) and with or without the hit fragment DDD01511162 at 37 °C in the reaction buffer for 30 min. Then the DH-PH domains of *Af*Rom2 and LARG were added respectively to a final concentration of 200 nM, and GDP 100 μM, then incubated for the indicated time periods. The samples were measured in a cycle of 1 min for 1 s, for an in total time period 40 min. Exponential fitting of the RFU to the time period was done with PRISM 6. Each experiment was repeated three times.

2.3 Results

2.3.1 *Af*Rho1 structure reveals potential exploitable differences with its human orthologue

To crystallize and solve the structure of *Af*Rho1, I first tried to express and purified the full length *Af*Rho1 protein. Recombinant full length *Af*Rho1 protein was expressed and purified by using the affinity tag GST and gel filtration chromatography (Fig 2.1A). The purified protein was concentrated to 10 mg/ml and used to set up crystallization trials in the presence of 2 mM Mg^{2+} and 1 mM GDP. After 2 days, there crystals appeared from conditions which contain 5 mM phosphate (Fig 2.1B). The crystals were sent for X-ray diffraction which showed as salt diffraction pattern, the spots are sporadic and mostly at the high resolution level (Fig 2.1C).

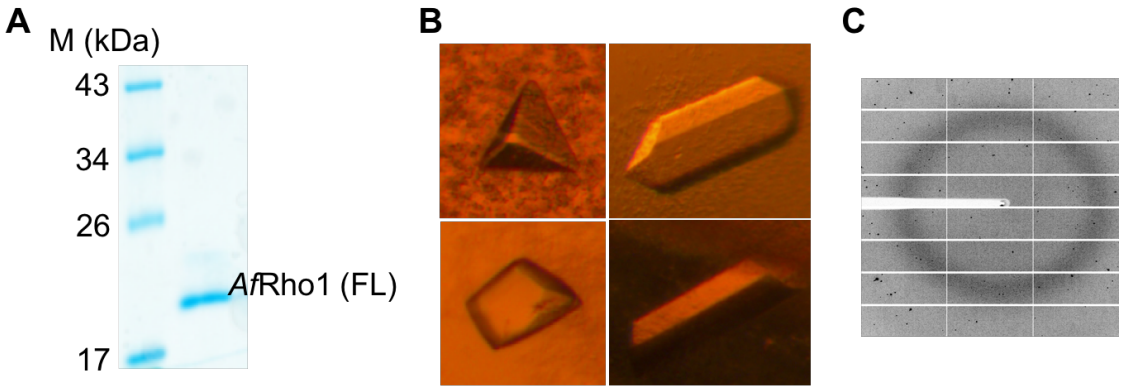

Figure 2.1: Purification and crystallization of *Af*Rho1 full length

(A) SDS-PAGE gel of purified *Af*Rho1 protein. The left lane contains molecular-mass markers. (B) Crystals appeared from crystallization conditions that include 5 mM phosphate. (C) X-ray diffraction pattern the crystal.

In order to crystallize *Af*Rho1, I made truncations of the C-terminal flexible loop region according to the structure of the human orthologue protein *Hs*RhoA (PDB: 1FTN). *Af*Rho1 protein (residues 1-181) with a F25N mutation to increase stability (Yamashita et al., 2010), was successfully overexpressed and purified from

Escherichia coli (Fig. 2.2AB). The concentrated *Af*Rho1 protein was used to set up crystallization trays in the presence of the cofactor magnesium and GDP (Fig. 2.2C). The *Af*Rho1 protein crystals were obtained with diffraction data extending to 1.42 Å resolution (Fig. 2.2D) (Structural statistics are listed in Table 2.2).

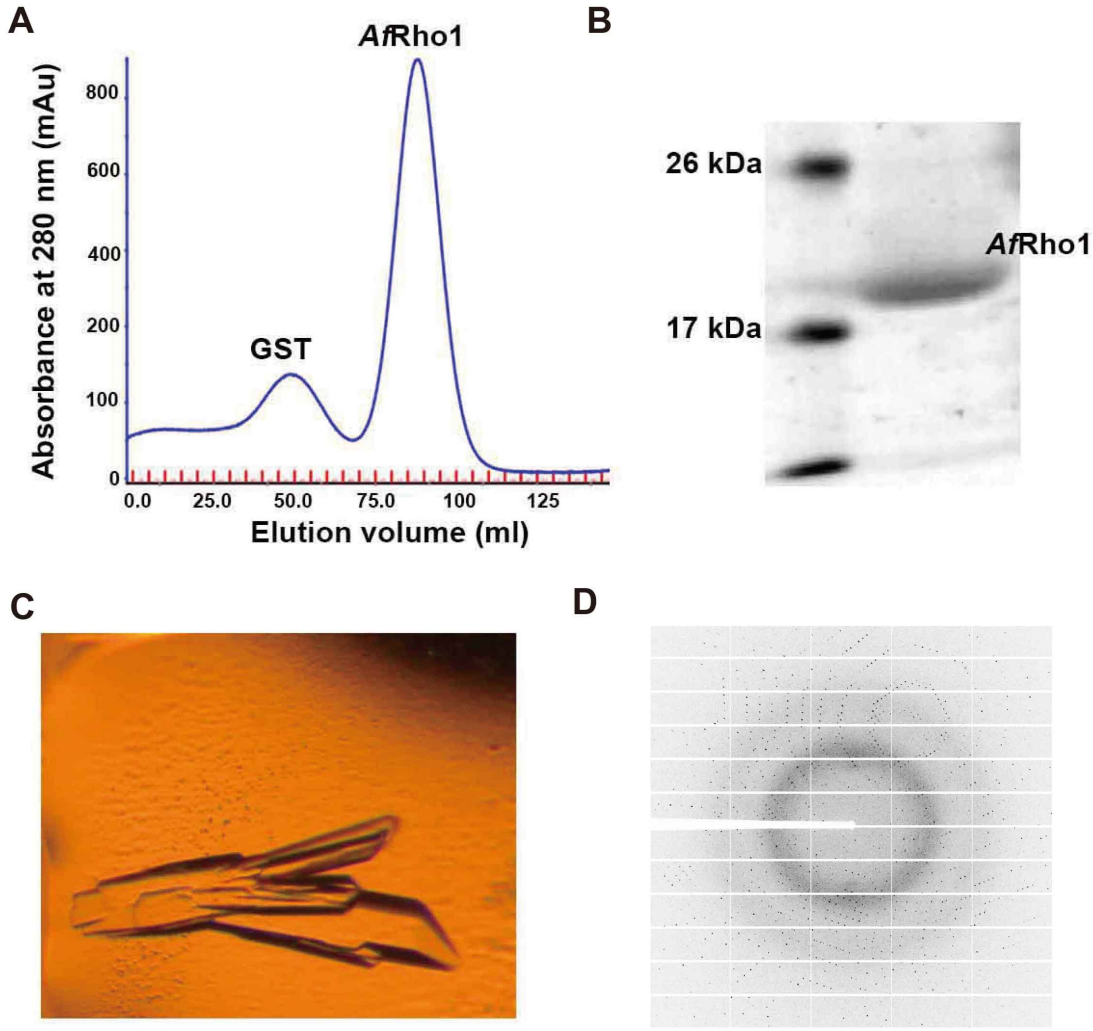

Figure 2.2: Purification and crystallization of *Af*Rho1 (C-terminal truncation)

(A) Superdex 75 gel-filtration column chromatogram showing a peak at an apparent molecular mass of ~20 kDa, corresponding to the molecular mass of *Af*Rho1 (21 kDa). (B) SDS-PAGE gel of purified AfRho1 protein. The left lane contains molecular-mass markers. (C) Protein crystals of AfRho1 appeared in sitting drop tray contains 37.1% PEG5000 MME, 150 Mm TRIS, pH 8.0 and 40 mM magnesium sulphate. (D) X-ray diffraction pattern of *Af*Rho1 crystal, the image was collected from the Diamond synchrotron, resolution range set to 1.4 Å.

Table 2.2: X-ray crystallographic data collection and refinement statistics of *Af*Rho1 and the fragment complex

Data	Rho1(GDP)	Rho1(GDP, DDD01511162)
Resolution range (Å)*	100- 1.42	100- 1.37
Space group	$P4_3$	$P4_3$
Unit cell (Å)	53.8 53.8 62.7	55.2 55.2 60.5
	90 90 90	90 90 90
Observed reflections	140126 (7474)	131577 (5366)
Completeness (%)	99.0 (96.8)	97.8 (84.6)
Multiplicity	4.1 (2.2)	3.5(1.9)
Mean I/σ(I)	18.8 (1.6)	16.1 (1.7)
R-merge (%)	3.6 (50.5)	4.2 (52.8)
Refinement		
R-factor	0.17	0.16
R-free (5%)	0.19	0.19
Protein residues	177	177
Solvent molecules	113	149
RMSD (bonds, Å)	0.02	0.02
RMSD (angles, °)	2.30	2.56
Ramachandran favoured (%)	96.02	96.07
Ramachandran allowed (%)	3.98	3.93
Ramachandran disallowed (%)	0	0

Phases were determined by molecular replacement using the crystal structure model of *Hs*RhoA (PDB ID: 1FTN) (Wei et al., 1997). The overall structure of *Af*Rho1 has a typical Rho GTPase fold, which consists of six core β-sheets and surrounded by α-helices (Fig. 2.3A). Similar to the solved structure of *Hs*RhoA, the *Af*Rho1 structure is consisting of the Rho GTPases conserved switch I (residues 28-39), switch II (residues 59-78) regions and the three-turn insertion helix (residues 124-134) (Fig. 2.3A). The switch I and switch II regions will undergo large conformational changes when Rho GTPase changes from the GDP to GTP binding state and that will lead to Rho GTPase having different protein binding properties (Wei et al., 1997). The insertion helix is another characteristic structure feature of Rho family GTPases, it has no conformational changes when compared the GDP and GTP binding state (Wei et al., 1997). However, there is report about the involvement of this insertion helix region in *Hs*RhoA for interaction and activation of the RhoA downstream kinases (Zong et al., 2001). GDP and the cofactor magnesium were clearly visible in the unbiased F_o-F_c electron density maps calculated from the molecular replacement solution (Fig. 2.3B). The GDP molecule sits in a positively charged pocket, which contains charged residues Lys18, Asp120 and Arg162 which are interacting with β phosphate and nucleotide ribose from GDP. The co-factor magnesium is stabilized by interacting with polar residues Thr19 and Thr60 (Fig. 2.3B).

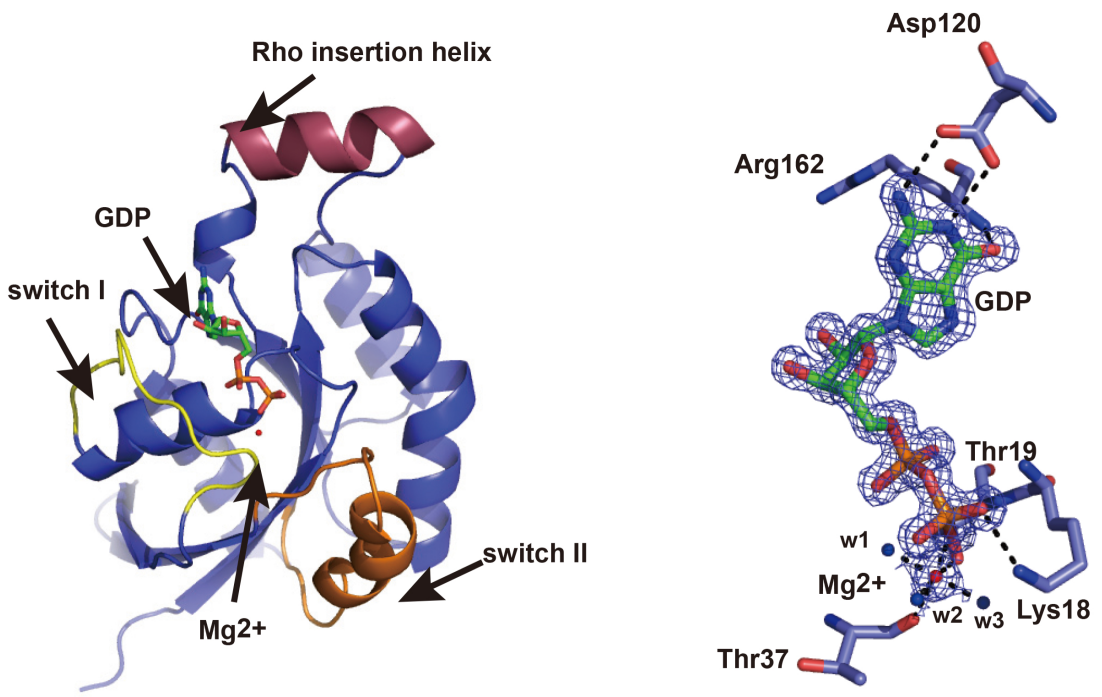

Figure 2.3: General structure of *Af*Rho1*GDP.

(A) Cartoon diagram of *Af*Rho1 crystal structure bound with GDP and the co factor Mg^{2+}. The signature domains are highlighted with different colours (Switch I yellow; Switch II gold; insertion helix yellow). (B) Electron density of GDP and Mg^{2+} and their interactions with related molecules. The F_o-F_c map is contoured at 1.5 σ.

The *Af*Rho1 and *Hs*RhoA have very high sequence identity which is 75% (Fig. 2.4A). The switch I and switch II regions are highly identical in these two proteins (Fig. 2.4A). However, the insertion helix region is shown to be not conserved. (Fig. 2.3A). In *Hs*RhoA, the insertion helix contains several positively charged residues, including Arg128, Arg129, Lys133 and Lys135 (Fig. 2.4A) which might mediate association to the cell membrane or bind to specific effector proteins. Instead, those residues are Ile128, Glu129, Lys133 and Ser135 in *Af*Rho1, suggesting different binding properties. The structural differences between these two orthologue proteins are also investigated. The *Af*Rho1 structure superimposes

well with *Hs*RhoA (GDP bound) (PDB ID: 1FTN) with an overall R.M.S.D. of 0.31 Å (Fig. 2.4B). However, two loop regions in *Af*Rho1 have significant shifts when superimposed with *Hs*RhoA. Loop 1 (47-51) links *β* sheets *β*2 and *β*3 (R.M.S.D =1.2 Å), and loop 2 (62-64) is part of the switch II region (R.M.S.D. =2.4 Å) (Fig. 2.4B). The structural differences between *Af*Rho1 and *Hs*RhoA in these two loop regions maybe enough to cause these two proteins to have different binding properties. The active site of Rho GTPase which is the GDP/GTP binding pocket, was also compared between *Af*Rho1 and *Hs*RhoA. From the investigation of surface conservation, I found the GDP binding active site is also highly conserved between *Af*Rho1 and *Hs*RhoA (Fig 2.4C). The above observations further confirmed that the GTP/GDP binding pocket is very conserved among Rho GTPase family proteins, and to develop a selective substrate analogue inhibitor would be very difficult to achieve.

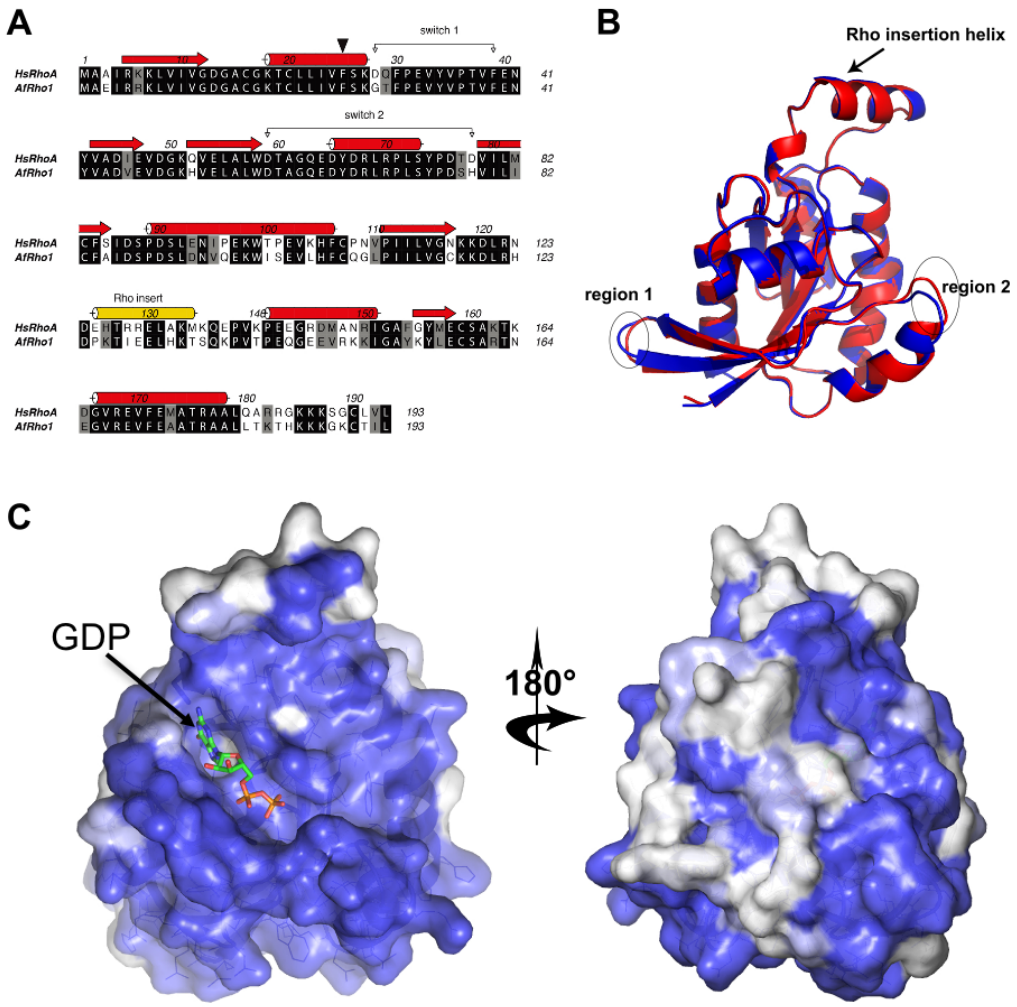

Figure 2.4: Sequence and structural differences between *Af*Rho1 *and Hs*RhoA.

(A) Sequence alignment of *Af*Rho1 and *Hs*RhoA. (B) Superimposed cartoon structure of *Af*Rho1 (Red) and *Hs*RhoA (Blue). (C) Surface conservation between *Af*Rho1 and *Hs*RhoA. Deep blue as identical, light blue as conserved, grey as non-conserved.

2.3.2 Fragment screening identifies potential micromolar *Af*Rho1 binders

Fragment screen has provided a starting point to develop a number of chemical inhibitors for difficult targets like Bcl2 and H-Ras that were considered as "undruggable" in the past (Ostrem et al., 2013; Petros et al., 2014). It also provides an excellent strategy for identifying and exploiting allosteric binding

pockets and inhibitors (Scott et al., 2012). Here, I have applied FBDD strategy in order to investigate the ligandability of *Af*Rho1. A Maybridge RO3 fragment library consisting of in total 1,000 fragment compounds was used to screen against *Af*Rho1 by using BLI (Biolayer interferometry). Initial data analysis suggested that 44 compounds demonstrated responses to *Af*Rho1 (Fig 2.5), but only four of them were confirmed by three folds dilutions with top concentrations from 500 μM, and the calculated K_d is around the micromolar range (Table 2.3). Interestingly, three out of the four hit molecules I found possessed a similar five membered ring core structure, which suggests these three molecules may be bound to *Af*Rho1 at the same pocket (Table 2.3). Thus, by using fragment screening, I have identified several potential fragment ligands to *Af*Rho1 with the binding affinity in the micromolar range.

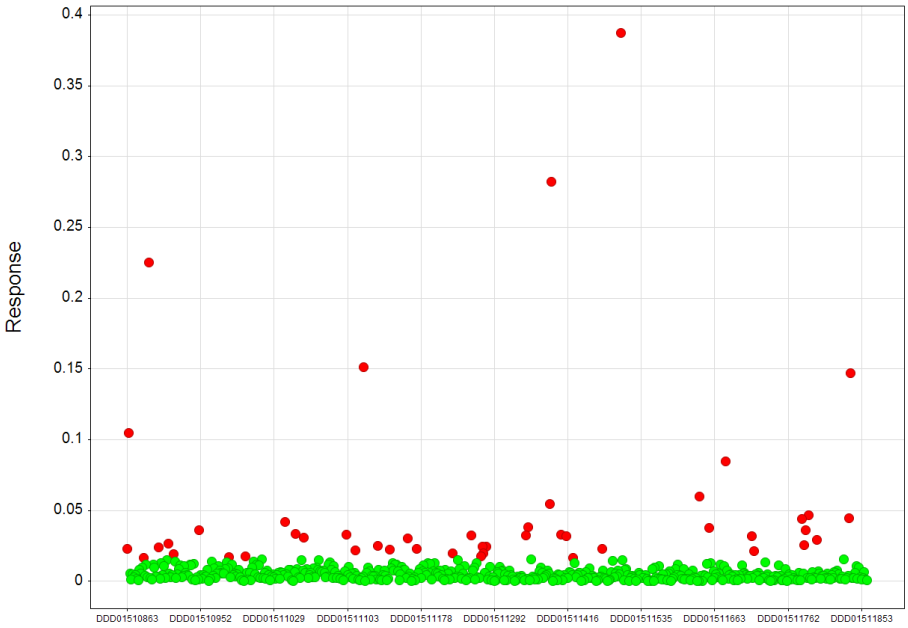

Figure 2.5: Primary screen hits of AfRho1 using BLI.

44 out of 1000 fragment compounds from the Maybridge library were identified as the hit molecules bound to *Af*Rho1. The Green blots represent the background signals of the Maybridge fragment library compounds bound to *Af*Rho1. The Red blots represent fragment compounds from the Maybridge library gave significant signals when bound to *Af*Rho1.

Table 2.3: Compound structures from the fragment screening

ID	STRUCTURE	K_d (μM)
DDD01510890	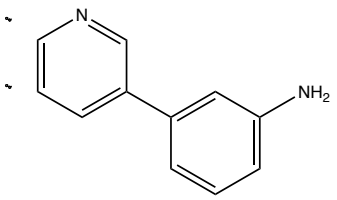	17.5
DDD01511052	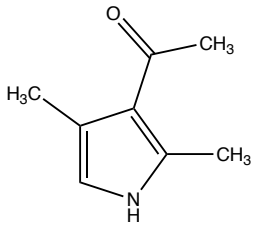	200
DDD01511101	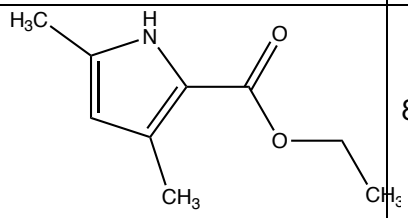	82.9
DDD01511162	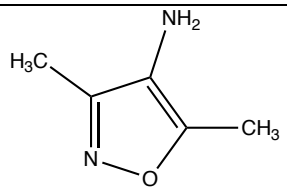	378

2.3.3 A complex structure of *Af*Rho1 with fragment DDD01511162 reveals the binding mode at the atomic level

To understand binding mode of *Af*Rho1 bound to the hit fragments, I attempted to use X-ray crystallography to solve the structure of *Af*Rho1 in complex with one

of the fragments. After iterative efforts to soak the *Af*Rho1 crystals with the fragment screen hit compounds and collect multiple X-ray diffraction data sets from the synchrotron, I succeeded in obtaining the structure of *Af*Rho1 in complex with the fragment hit (DDD01511162) at 1.4 Å resolution (Structural statistics are listed in Table 2.3). And since I couldn't get the complex structures of *Af*Rho1 with other fragment hits I found from the BLI screen, these fragments are not further investigated and discussed in this thesis.

The chemical structure of the fragment hit DDD01511162 is composed of a core isoxazole ring, with two methyl side chains at position 3 and position 5, and an amine group at position 5 (Fig 2.6A). In the complex structure, the fragment DDD01511162 was clearly visible in the unbiased F_o-F_c electron density map calculated from the molecular replacement solution using the solved *Af*Rho1 structure as a model. Since the fragment DDD01511162 is a chiral molecule that has a symmetric structure (Fig 2.6A), and the electron density between the N_{ring} and O_{ring} atoms are quite similar, it would be difficult to judge the orientation of the fragment based on the signal of the electron density map. However, the O_{ring} atom is more electron negative and is more favourable for forming hydrogen bonds with water molecules than the N_{ring} atom, therefore I was using that properties to determine the orientation of the fragment DDD01511162 in the electron density map. From the complex structure, we can see the fragment DDD01511162 bound to the surface pocket of *Af*Rho1 in a 2:1 molar ratio (Fig 2.6B). The binding pocket is located between the switch I and switch II regions, and it's away from the GDP binding pocket (Fig 2.6B).

To distinguish the binding of two identical fragments, I named the fragment that sits in the deep pocket as fragment-1, and the fragment that sits in the outer pocket as fragment-2 (Fig. 2.6B). The two fragments are bound adjacent to each

other, the distance between the fragment-1 position 4 amine group is only 4 Å away from the fragment-2 position 5 methyl group (Fig 2.6C). Binding of the fragment won't induce any significant conformational changes when compared to the native GDP bound state of *Af*Rho1 (Fig 2.6B), the overall R.M.S.D. is only 0.4 Å. However, there are two residue side chains in the fragment binding pocket that shifted significantly after the binding (Fig 2.6C). The Glu40 residue shifted from its original position towards the fragment binding pocket after the binding, and the Asn41 residue that originally occupied the binding pocket, shifted away from its original position to create space for the fragment-2 binding (Fig 2.6C).

The complex structure also reveals the key residues and water molecules in the *Af*Rho1 structure that contribute to the binding of the fragment in great details. For fragment-1, the O_{ring} atom in position 1 is forming the hydrogen bond interaction with water1, and water1 is also coordinated with the carboxyl group in Tyr66. The N_{ring} atom in position 2 is forming the hydrogen bond with the carboxyl group of the protein residue Leu69. The amine group in position 4 as a hydrogen donor are forming the hydrogen bonds with both the side chain of Glu40 residue and with water2, and water2 is also forming hydrogen bonds with the side chains of Glu40 and Tyr66.

The fragment-2 is inserted between Asn41 and Trp58, and the isoxazole ring of the fragment-2 is forming the π–π stacking interaction with the aromatic side chain of Trp58. The O_{ring} atom in position 1 from fragment-2 is both forming the hydrogen bond with water4, and coordinating the binding to Asn41 and Trp58 by forming hydrogen bonds. The amine group in position 4 is forming hydrogen bonds with the side chain of Glu40 and water3, water3 is also coordinating with the carboxyl group of Asp59 through hydrogen bond (Fig. 2.6C).

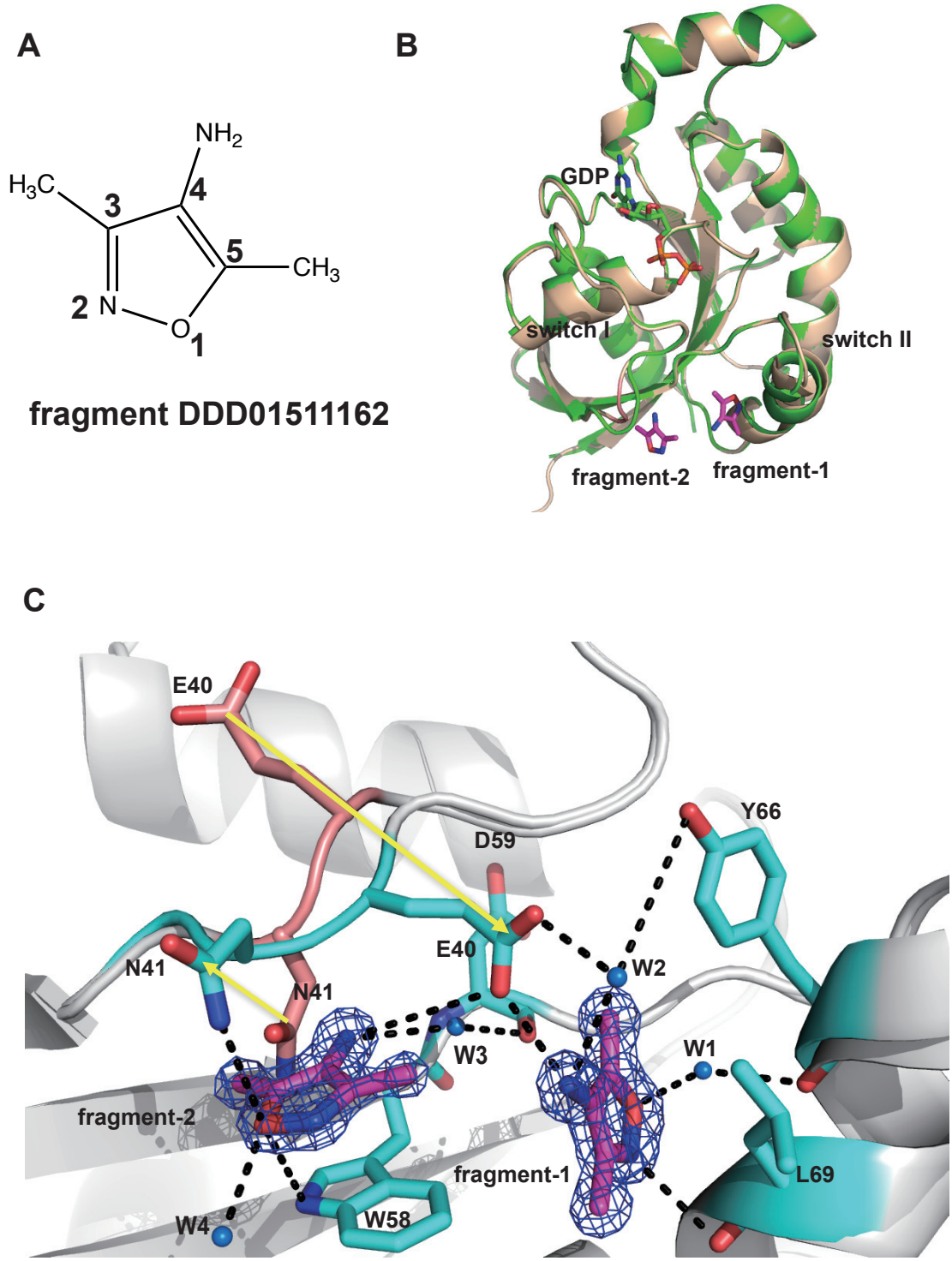

Figure 2.6*:* Chemical structure of the fragment hit DDD01511162 and the complex structure it bound to *Af*Rho1

(A) The chemical structure of the fragment hit DDD01511162

(B) Cartoon representation of *Af*Rho1 in complex with DDD01511162 (green) and superimposed with the *Af*Rho1 structure in the native GDP binding state (wheat).

(C) The crystal structure of *Af*Rho1 in complex with DDD01511162 (gray). The interaction residues to the fragment are shown as sticks (cyan). The *Af*Rho1 structure in the native GDP binding state is superimposed to the complex (red). The F_o-F_c map is contoured at 1.5 σ. The starting coordinates and topologies for the fragment DDD01511162 were generated by PRODRG (Schuttelkopf and van Aalten, 2004).

The above observations suggest that the side chain of the Glu40 residue is very important for the fragment bound to *Af*Rho1, since it is directly forming hydrogen bonds with the position 4 amine groups from both fragment-1 and fragment-2 (Fig. 2.6C). To validate the importance of Glu40 for the fragment binding to *Af*Rho1, an *Af*Rho1 Glu40Ala mutant was made by side directed mutagenesis. By the BLI measurement, it was apparent that the Glu40Ala mutant protein shows no binding to the fragment (Fig 2.7), which confirmed the importance of the Glu40 residue contributes to the fragment binding.

The aromatic side chain of the Trp58 residue is forming the π–π stacking interaction with the isoxazole ring of the fragment-2 (Fig. 2.6C). To validate the importance of this residue, a Trp58Ala mutant was also made. For the BLI binding test, the mutant protein was still binding to the fragment, but with the binding affinity decreased from 300 μM to 400 μM, which suggests the aromatic side chain of the Trp58 residue may be only important for the binding of fragment-2, but won't affect the binding of fragment-1 (Fig 2.7). To conclude, the complex structure of *Af*Rho1 with the fragment hit DDD01511162 reveals the detailed binding mode at the atomic level.

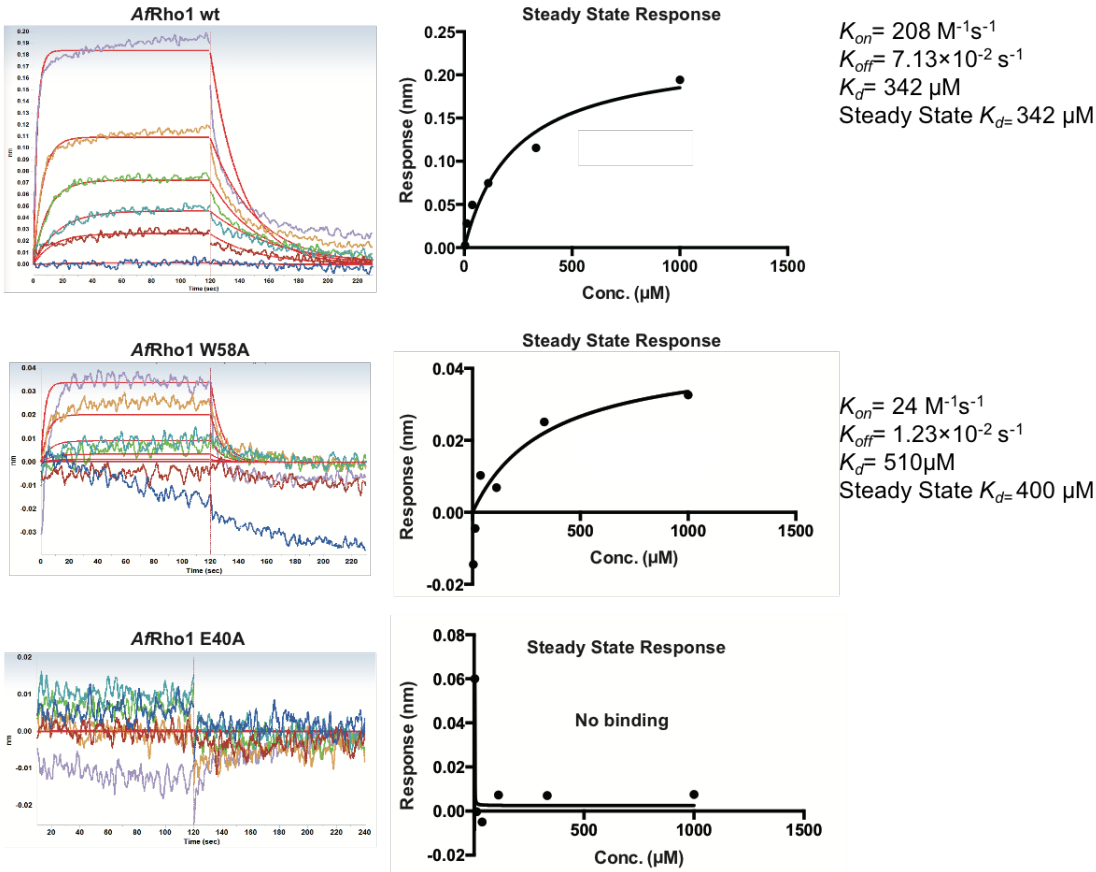

Figure 2.7*:* Biolayer interferometry (BLI) to test binding of the fragment DDD01511162 to AfRho1 and W58A, E40A mutants.

Binding profiles obtained and kinetic parameters calculated for interactions between DDD01511162 to *Af*Rho1 and the W58A, E40A mutants. Concentration series were started from a top concentration 1000 μM. Left hand panels: binding profiles and global curve fitting from which the kinetic parameters were calculated. The five coloured lines represent 3-fold dilutions from 1000 μM (control, blue base line). The abnormal decrease of the blue base line in *Af*Rho1 W58A represents the sensor failure. Right-hand panels: steady-state binding response from which the steady state K_d was calculated.

2.3.4 The fragment binding pocket is conserved in *Hs*RhoA and located at the Rho/Rho GEF interaction interface

By mapping all the identical residues between *Af*Rho1 and the human orthologue protein *Hs*RhoA on the surface of the *Af*Rho1 structure, I found the fragment binding pocket exists and is identical in the *Hs*RhoA protein (Fig. 2.8A). Therefore, I used BLI to test the binding of *Hs*RhoA to the fragment DDD01511162, revealing

that the fragment bound to *Hs*RhoA with the binding affinity (K_d =500 μM) (Fig. 2.8B). These results suggest that, the fragment DDD01511162 also bound to *Hs*RhoA and probably with a similar binding mode as we observed in the *Af*Rho1 fragment complex structure.

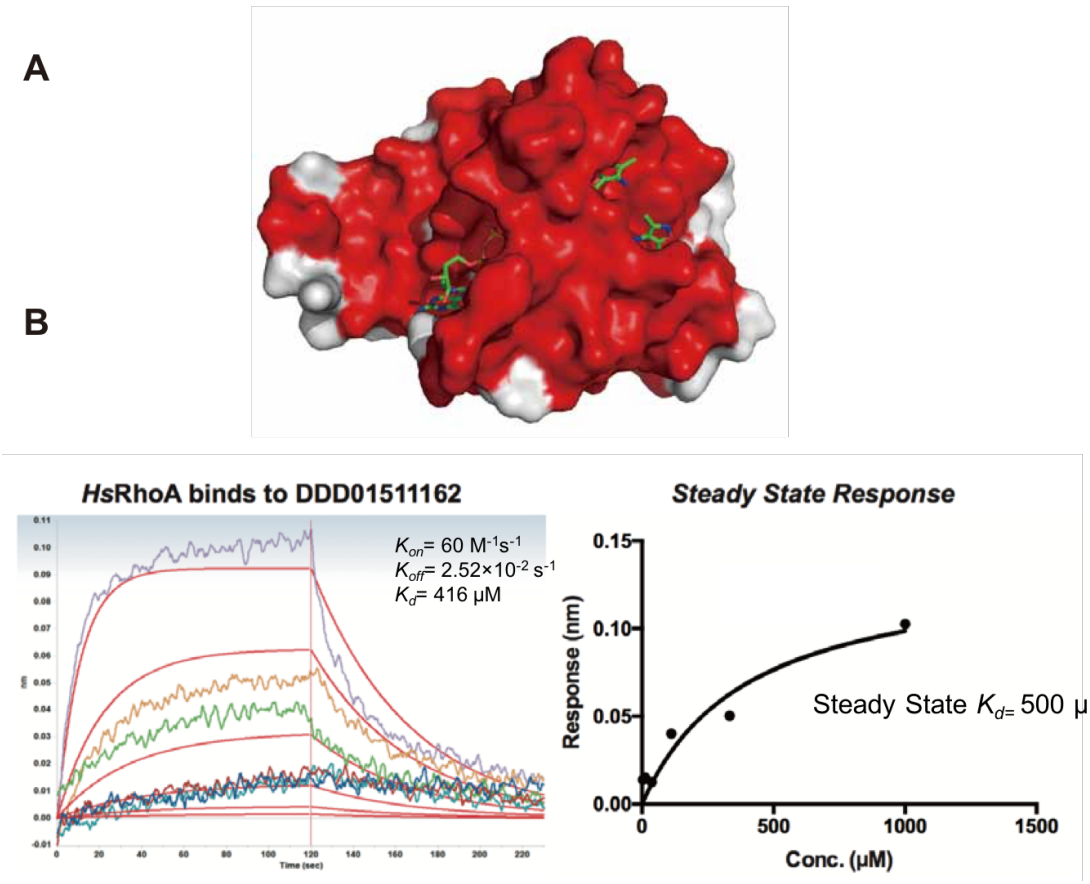

Figure 2.8: Surface comparison between *Af*Rho1 and *Hs*RhoA, and the BLI binding graphs of *Hs*RhoA to the fragment hit DDD01511162

(A) Surface diagram of *Af*Rho1 crystal structure bound with ligand GDP and DDD01511162, the identical residues between *Af*Rho1 and *Hs*RhoA are shown as red. The fragment hit DDD01511162 was shown as stick model.

(B) BLI Binding profiles obtained and kinetic parameters calculated for interactions between DDD01511162 to *Hs*RhoA. Concentration series of the fragments was started from a top concentration 1000 μM. The five coloured lines represent 3-fold dilutions from the top concentration (control, blue base line). Left- hand panels: binding profiles and global curve fitting from which the kinetic parameters were calculated. Right-hand panels: steady-state binding response from which the steady state K_d was calculated.

The structure of *Af*Rho1 in complex with the fragment DDD01511162 shows that the fragment binding pocket is distant from the GDP binding cleft (Fig 2.8A), but due to the versatile cellular functions of Rho GTPases, this pocket may be important for certain protein-protein interactions.

The structural biology of *Hs*RhoA with its interaction protein partners has already been well studied, and the fragment binding pocket was identical in the *Hs*RhoA (Fig. 2.8A). I therefore, searched all the structures of *Hs*RhoA in complexes with other effector or regulator proteins in the PDB. In the complex structure of *Hs*RhoA with its GEF (guanine nucleotide exchange factor) protein LARG (PDB: 1X86), I found that the fragment binding pocket I identified is right at the interaction interface between *Hs*RhoA and the DH (Dbl homology) domain of LARG (Fig 2.9A).

The DH an PH (pleckstrin homology) domains are the GEF catalytic domains of the *Hs*RhoA GEF protein LARG. From previous research and the solved complex structure (PDB: 1X86) (Kristelly et al., 2004), the DH and PH domains were both shown to interact with *Hs*RhoA (Fig 2.9A), and required for full *in vitro* GEF catalytic activity (Kristelly et al., 2004). When LARG DH-PH domains bound to *Hs*RhoA in the native GDP binding state, they will induce conformational changes in *Hs*RhoA by pushing the switch I and switch II regions away from the GDP binding pocket, that will lead to the release of GDP from the *Hs*RhoA active site and then facilitate the nucleotide exchange (Fig 2.9B) (Kristelly et al., 2004).

The fragment hit DDD01511162 was superimposed into the conserved fragment binding pocket in *Hs*RhoA when it is bound to LARG. I found the fragment binding pocket was located at the protein-protein interaction interface between *Hs*RhoA and the DH domain of LARG (Fig 2.9C). In the *Hs*RhoA and LARG DH domain complex structure (PDB: 1X86), the conserved Trp58 residue in *Hs*RhoA which is forming the π–π stacking interaction with fragment-2 was completely buried in the LARG DH domain interface and directly interacts with the Asp928 residue in LARG (Fig 2.9C). Recently published research also highlights the importance of the *Hs*RhoA Trp58 residue for interacting with the GEF protein DH domain

(Diviani et al., 2016). The *Hs*RhoA Trp58Ala mutant abolished protein-protein interaction with the DH domain from another *Hs*RhoA GEF protein Lbc in an *in vitro* pull-down experiment (Diviani et al., 2016). The fragment-1 sits in the protein-protein interaction interface where the Gln935 residue from LARG DH domain interacts with the *Hs*RhoA Glu40 residue, and pushes it away from its original position in the *Hs*RhoA native GDP binding state, the shift of the Glu40 is part of the conformational changes in the switch I region when bound to the GEF (Kristelly et al., 2004) (Fig 2.9C). Therefore, the binding of fragment 1 in this position could potentially interfere with this interaction.

The above observations suggest the fragment binding pocket I found in *Af*Rho1 and is identical in *Hs*RhoA, is involved in the protein-protein interaction between *Hs*RhoA with its up-stream GEF proteins. Based on that, I am hypothesizing the fragment hit DDD01511162 when bound to *Af*Rho1 and *Hs*RhoA, can potentially inhibit GEFs mediated nucleotide exchange of these two proteins.

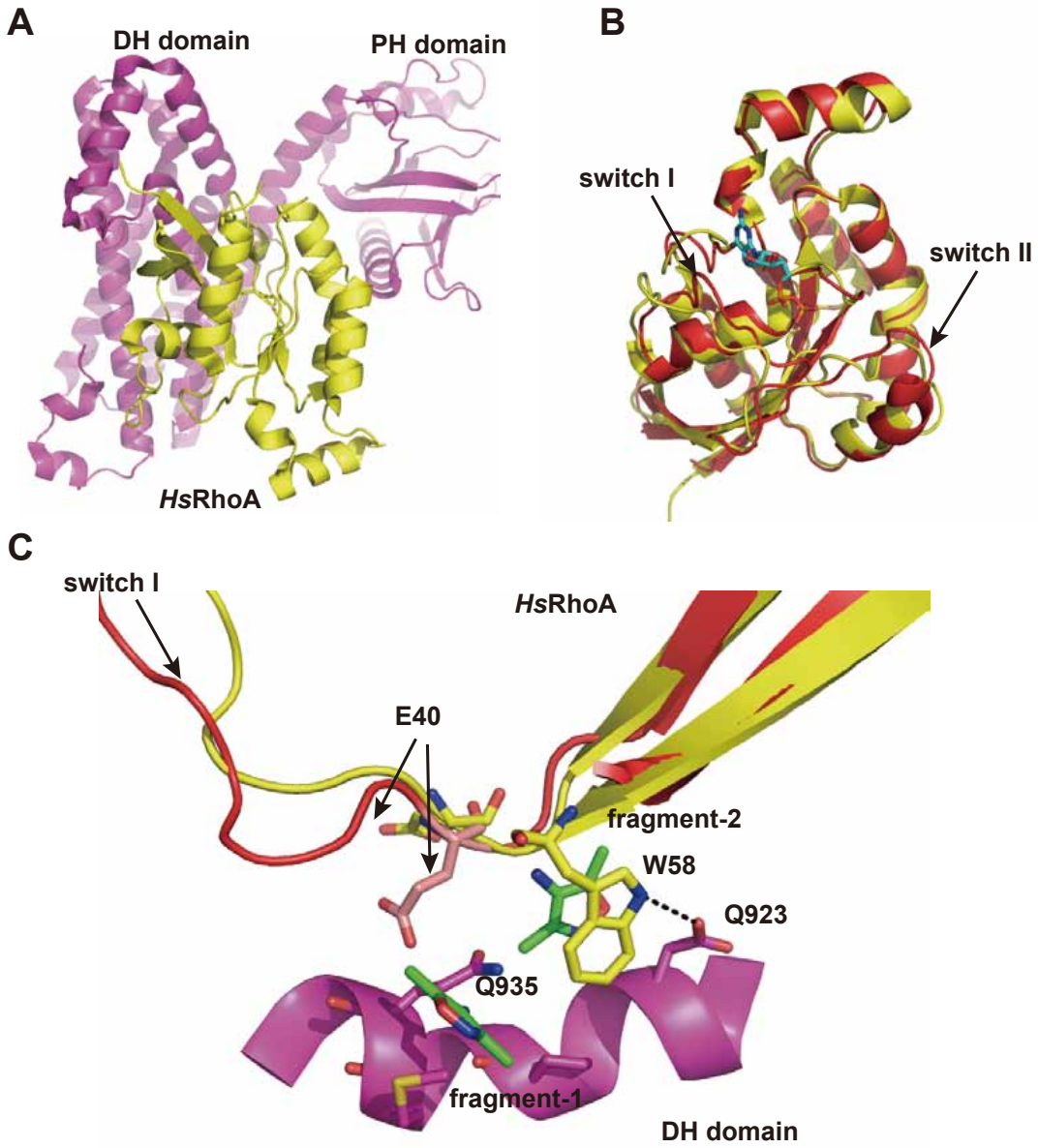

Figure 2.9: Structures of *Hs*RhoA in complex with LARG and superimposed with the fragment DDD01511162

(A) Cartoon representation to show the DH-PH domains (magenta) of LARG binding to *Hs*RhoA (yellow) (PDB: 1X86).

(B) Cartoon representation to show the superimposed structures of native GDP bound *Hs*RhoA (red) and *Hs*RhoA after binding with LARG (yellow).

(C) Cartoon representation to show that the conserved fragment binding pocket in *Af*Rho1 and *Hs*RhoA is located at the *Hs*RhoA and its GEF protein LARG interaction interface. Native GDP bound *Hs*RhoA (red) and DDD01511162 was superimposed to the complex structure of *Hs*RhoA (yellow) and LARG (magenta) (PDB: 1X86).

2.3.5 Fragment DDD01511162 inhibits the GEF mediated *Af*Rho1/ *Hs*RhoA nucleotide exchange

The biological functions of the DH-PH domains of GEF proteins are to facilitate the nucleotide exchange of Rho GTPases. To test whether the fragment hit DDD01511162 will inhibit this process, I applied the previously reported Rho GTPases mant-GDP assay in my research (Jank et al., 2013). Mant-GDP is a fluorescent analogue of GDP, and when bound to Rho GTPases will give a fluorescence signal (λ_{ex} 360 nm; λ_{em} 444 nm). However, the GEFs can facilitate the nucleotide exchange of mant-GDP in the presence of GDP, which will result in the decrease of fluorescence signal. In my research, *Af*Rho1 and *Hs*RhoA displayed increased fluorescence signal over time when incubated with mant-GDP (Fig. 2.10AB), the signals were then decreased when the corresponding DH-PH domains of GEF proteins (Rom2 and LARG) and GDP were added (Fig. 2.10CD). However, in the presence of 250 μm and 500 μM of DDD01511162, the GEFs mediated decrease in fluorescence signal was inhibited (Fig. 2.10CD), which suggested the GEFs activity was inhibited. These results suggest that fragment hit DDD01511162 can inhibit the GEFs mediated nucleotide exchanges of *Af*Rho1and *Hs*RhoA.

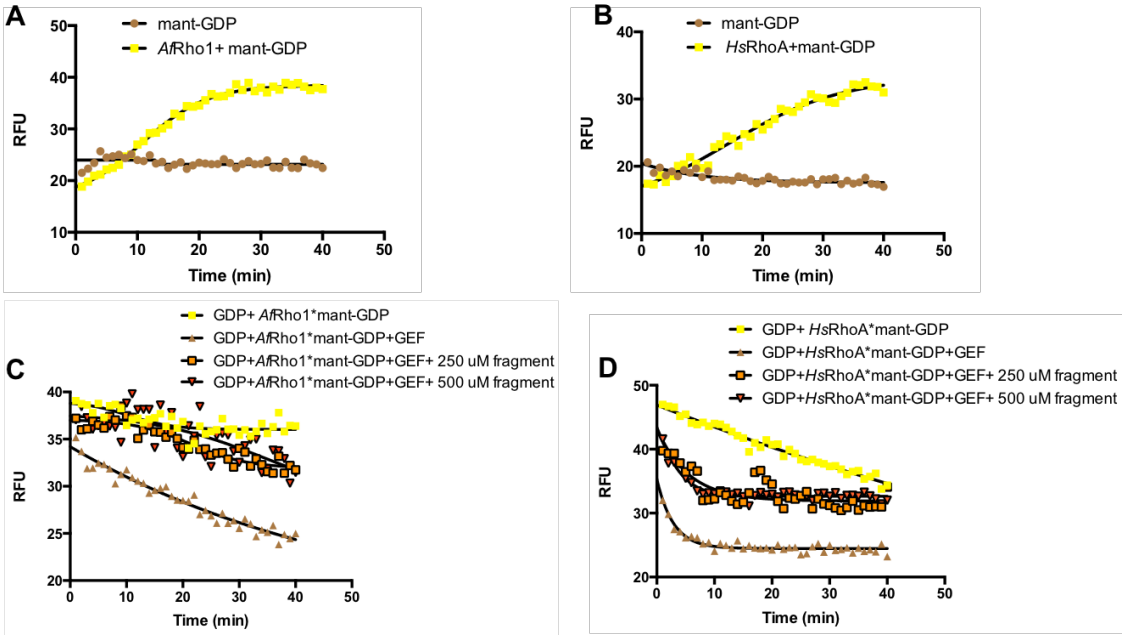

Figure 2.10*: mant-GDP assays to measure the nucleotide exchange of *Af*Rho1/*Hs*RhoA in the presence of their corresponding GEF proteins (LARG and Rom2), and in the presence of the fragment hit DDD01511162*

(A)(B) The fluorescence signals to show *Af*Rho1 and *Hs*RhoA binding to mant-GDP over the indicated time period, the control is mant-GDP alone.

(C)(D) The fluorescence signals to show mant-GDP bound *Af*Rho1 and *Hs*RhoA, after adding GDP and GEF proteins (Rom2 and LARG) and in the presence of the fragment hit DDD01511162 (250 µm and 500 µM).

2.3.6 The fragment-based ligand design

The fragment hit inhibited GEFs mediated nucleotide exchange of *Af*Rho1 and *Hs*RhoA which is important for their activation (Fig. 2.1). The use of this compound as a *Af*Rho1/*Hs*RhoA inhibitor in cells is limited by the low binding affinity (300- 500 µM). Therefore, it is necessary to design and synthesize a high affinity ($K_d \leq$ 100 nM) inhibitor from the initial fragment, guided by the complex structure of the fragment and protein, and with the help of medicinal chemistry. From the complex structure, the fragment DDD01511162 appears to be binding to *Af*Rho1 in a 2: 1 molar ratio and the two molecules are in close proximity, the distance between the two closest atoms is only 4 Å (fragment-1 position 4 amine

group to the fragment-2 position 5 methyl group) (Fig. 2.11A). One obvious strategy to develop the initial fragment hit into a high affinity binder is to link the two identical fragments together, since that will be thermodynamically more favourable for the binding. This fragment linking strategy has already been successfully applied in many drug discovery cases. For thrombin inhibitor discovery, the linking of two fragments with individual IC_{50} from 100- 300 μM resulted in a compound with an IC_{50} of 1.4 nM (Howard et al., 2006). And from a previous research in Daan van Aalten's lab, linking two caffeine molecules together created a highly potent chitinase inhibitor bisdionin C, which inhibits the enzyme activity at sub-micromolar range (Schuttelkopf et al., 2011).

There are currently two options of linking these two fragments together, based on the choice of linkage atoms from the fragment. Option one is to link the two fragments according to the orientation of the two fragments I observed from the complex structure, which is to link the position 4 amine group from fragment-1 to position 3 methyl group from fragment-2 (Fig. 2.11B). Option two provides a more direct way to link the two fragments together, which is to link the position 3 methyl groups from the two fragments (Fig. 2.11C).

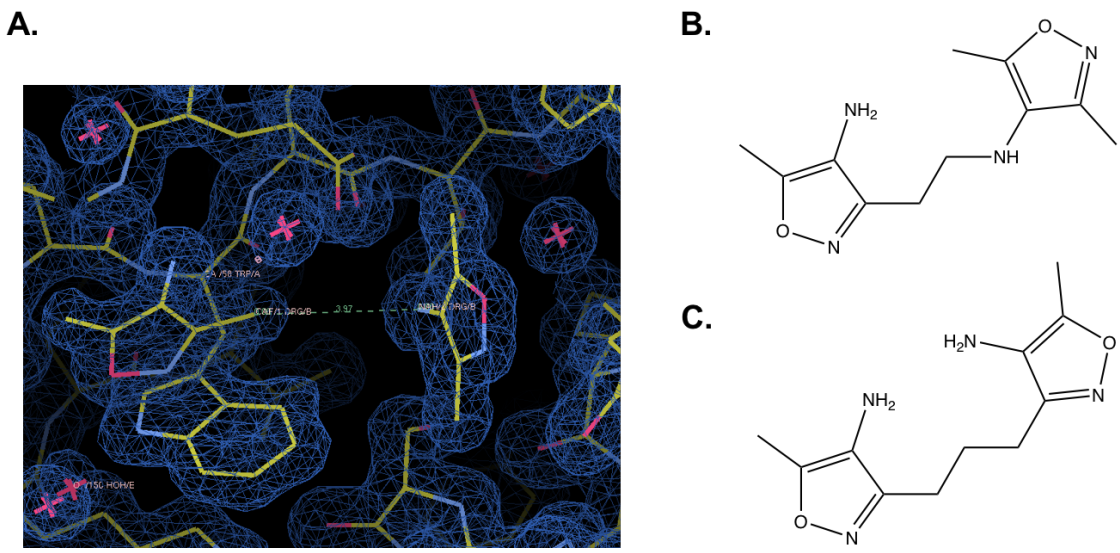

Figure 2.11*: Strategies for the fragment optimization based on the complex structure.* **(A)** The structure of fragment DDD01511162 in complex to *Af*Rho1, represented in COOT. The F_o-F_c map is contoured at 1.5 σ. **(B), (C)** two options to link the bound fragments together based on the observed complex structural conformation.

To prioritize which one of the two options is best suited for the next step optimization, a number of fragment derivatives were purchased to test the structure and activity relationships (SAR). Firstly, two fragment hit derivatives with additional methyl groups on either two directions of the methyl side chains from the fragment were tested for the binding to *Af*Rho1. Compared to the parental compound, these two derivatives didn't show binding to *Af*Rho1 (Fig. 2.12A). This implicates maybe option two is not our best choice, since the extension of the methyl side chain from the fragment will abolish the binding to *Af*Rho1. Option one was to link through the primer amine group from the fragment. However, I need to investigate whether the primer amine group is required for the binding. A number of fragment derivatives were purchased with different substitutions of the position 4 amine group which including direct deleting, changing it to hydrogen bond acceptor -NO_2, or by extending it (Fig. 2.12B), none of them showed binding

to *Af*Rho1, which suggests for option one, the existence of the position 4 amine group from the fragment must be reserved. This hypothesis was further confirmed by a fragment derivative which keeps the position 4 amine but with a carbon chain extended from it, this compound still showed binding to *Af*Rho1(Fig. 2.12B). To conclude, the above SAR study of the fragment derivatives suggest, linking the two bound fragments by option one (Fig. 2.12B) is our preferred choice to synthesize a highly potent *Af*Rho1/*Hs*RhoA inhibitor based on the fragment hit DDD01511162.

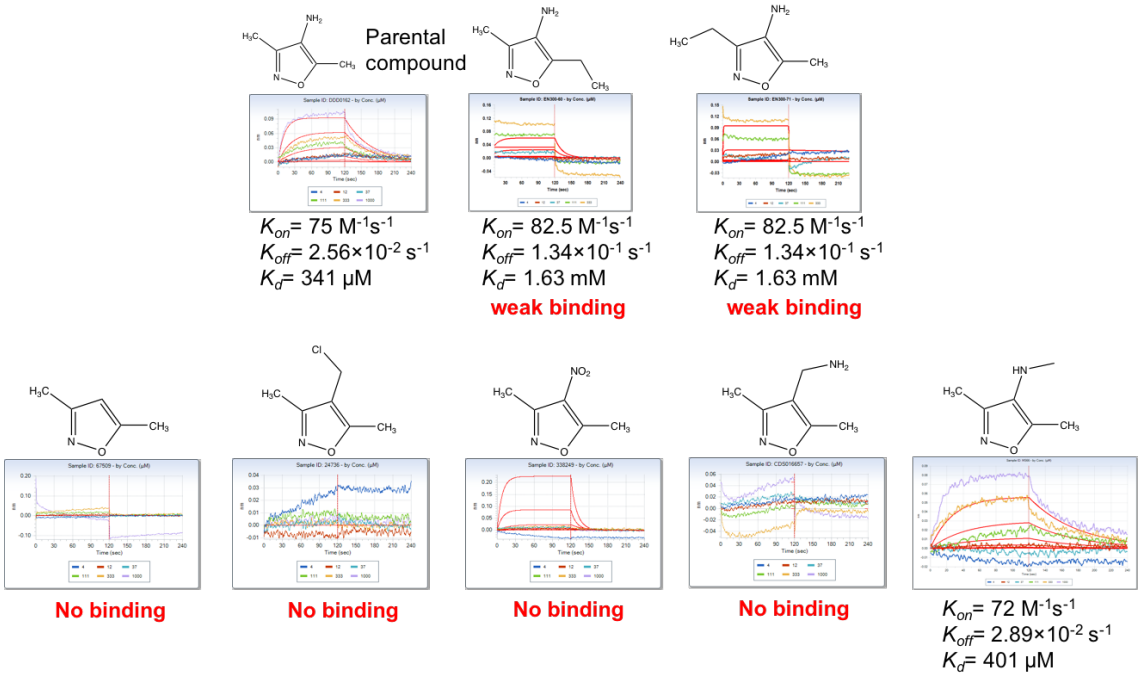

Figure 2.12: BLI binding graphs of the fragment hit DDD01511162 and derivatives compounds to *Af*Rho1.

(A) BLI binding graphs of two fragment derivative compounds with extended methyl group on position 3 and position 5 to *Af*Rho1, compared to the parental compound. **(B)** BLI binding graphs of fragment derivatives with different substitutions of the position 4 amine groups to *Af*Rho1. Concentration series were started from a top concentration 1000 μM. The five coloured lines represent 3-fold dilutions from the top concentration (control, blue base line).

2.4 Discussion

Rho1 GTPases in fungi belong to the small Rho family of GTPases and have been reported to play essential roles in fungal cell wall biosynthesis and organization due to the involvement in the CWI pathway (Dichtl et al., 2016) and as the regulatory subunit to the glucan synthase complex (Drgonova et al., 1996; Mazur and Baginsky, 1996). Therefore, Rho1 GTPases could be considered as potential anti-fungal targets to treat pathogenic fungal infections. However, Rho1 GTPases in fungi also have a close human orthologue *Hs*RhoA, and share over 70% sequence identity. *Hs*RhoA is a major molecular switch in human cells, which has been implicated to involve in many cellular events, such as gene transcription (Marinissen et al., 2001), cell proliferation (Provenzano and Keely, 2011), migration (Ridley, 2015) and cell division (Chircop, 2014). And over activation of *Hs*RhoA has been reported to induce several human cancers (Bellizzi et al., 2008; Faried et al., 2007). Therefore, *Hs*RhoA has been suggested as an anticancer target. However, due to the globular structure and with limited surface pockets that are suitable for small molecule binding (Wei et al., 1997), Rho family GTPases are usually considered as difficult targets for inhibitor development. Drug development based on small molecule fragment is now a widely-used technology both in industry and academia to generate initial hit compounds that bind to interesting targets. Fragment library which is composed of small molecules is an advantage to effectively identify initial binding hits, which could be optimized into leads or even drugs based on structure-activity relationship (SAR) (Hajduk et al., 1997; Harner et al., 2013).

In this research, I have expressed and purified a genetically validated essential protein *Af*Rho1 from the pathogenic fungus *A. fumigatus* (Fig. 2.2). Using X- ray crystallography, I have solved a high-resolution protein structure of *Af*Rho1 (1.4

Å) in complex with the ligand GDP and the cofactor magnesium (Fig. 2.2). The structure of *Af*Rho1 is highly identical to the human orthologue protein *Hs*RhoA in the same GDP binding state (Fig. 2.3B). There two loop regions and the insertion helix regions were found not conserved between *Af*Rho1 and *Hs*RhoA may imply the functional differences between *Af*Rho1 and *Hs*RhoA in two entirely different eukaryotic organisms (*A. fumigatus and H. sapiens*). However, it has never been addressed before, whether *Hs*RhoA can replace the cellular functions of *Af*Rho1 in *A. fumigatus* especially in the cell wall synthesis process.

To answer that, one should first investigate whether overexpression of *Hs*RhoA in the *A*fRho1 knockdown mutant can rescue the phenotype. In the previous research in *A. fumigatus*, it was shown that *Af*Rho1 co-precipitated with Fks1 (catalytic subunit of glucan synthase) in a product entrapment experiment (Beauvais et al., 2001). And in the research of the Rho1 glucan synthase complex in *C. albicans*, *in vitro* glucan synthesis reaction was reconstituted by separating the glucan synthase enzyme from the cell membrane, and the enzyme activity was shown to be increased when adding the GTP bound *Ca*Rho1 (Kondoh et al., 1997). It would be very interesting to test using the above-mentioned methods, whether *Hs*RhoA can also interact or activate the glucan synthase from *A. fumigatus*. Based on the result from that, we can form hypothesis whether the different structure regions I observed between *Af*Rho1 and *Hs*RhoA are playing functions in the glucan synthesis process, and by making mutants on those regions will test that hypothesis. The continuing research to reveal how *Af*Rho1 is regulating glucan synthase at the atomic level, will certainly help to provide new thoughts for anti-fungal development. And the high-resolution structure of *Af*Rho1 I solved in this research is definitely making a big step forward towards that end.

The enzyme active site is always the focus of research for inhibitor design and discovery. The *Af*Rho1 active site is the GDP and magnesium binding pocket which is highly conserved with the human orthologue protein *Hs*RhoA (Fig. 2.4C), thus to design and develop a selective substrate analogue inhibitor to target this area is very difficult to achieve. Therefore, the fragment screen approach was applied to identify small molecular weight binders to *Af*Rho1. A 1,000 Maybridge fragments library was used to screen against *Af*Rho1 by BLI (Biolayer interferometry), and 4 fragment hits were dentified to bind to *Af*Rho1 with micromolar binding affinity (Table 2.3). A complex structure of *Af*Rho1 with one of the hit fragments DDD01511162 was successfully obtained by crystal soaking and X-ray crystallography (Fig. 2.6AB). The binding mode of the fragment hit to the target protein was studied at the atomic level (Fig. 2.6C).

To address the binding selectivity of the fragment DDD01511162, the fragment binding pocket of *Af*Rho1 was compared with *Hs*RhoA, and it was found to be identical (Fig. 2.7A). The binding of fragment DDD01511162 to *Hs*RhoA was subsequently confirmed by the BLI binding test, with a binding affinity of K_d =500 μM (Fig. 2.7B). This conserved fragment binding pocket was also found to locate at the protein-protein interaction interface between *Hs*RhoA and the DH (Dbl homology) domain of its GEF (guanine nucleotide exchange factor) regulator LARG (Kristelly et al., 2004).

GEF proteins are the direct up-stream activators of the Rho family of GTPases. They usually contain the signature catalytic DH and PH (pleckstrin homology) domains. From the published *Hs*RhoA and LARG complex structure (PDB: 1x86) (Fig. 2.8A), the DH-PH domains both are interacting with the *Hs*RhoA switch I region, which will induce the conformational changes of *Hs*RhoA to a GDP excluding state (Fig. 2.9B) (Kristelly et al., 2004). The conserved fragment

binding pocket in *Hs*RhoA was buried inside the protein-protein interaction interface between the LARG domain and the *Hs*RhoA switch I region (Fig. 2.9C). A number of published *Hs*RhoA inhibitor development research also focuses on targeting this interaction interface. A compound named Rhosin was identified to bind to *Hs*RhoA using a virtual screen against the exact same conserved compound binding pocket I found in *Af*Rho1 (Shang et al., 2012). Rhosin was found to bind to *Hs*RhoA with submicromolar K_d , and shows inhibited LARG mediated nucleotide exchange in *Hs*RhoA and *Hs*RhoA related cellular functions (Shang et al., 2012). However, the detailed binding mode between RhoA and Rhosin is unknown and further chemical optimization of this compound cannot be performed, due to the lack of a complex crystal structure.

In my research, the fragment hit DDD01511162 displayed an inhibitory effect over the GEF (LARG and Rom2) mediated *Af*Rho1/*Hs*RhoA nucleotide exchange (Fig. 2.10). However, the inhibitory effect can only be observed using a very high concentration of compound, which is expected and caused by the low binding affinity of the fragment hit to the protein. Since the two fragments bound closely to each other (Fig. 2.11), the obvious strategy to develop a highly potent compound from the fragment hit is by linking these two fragments together with the help of medicinal chemistry. There are two options of achieving that, option one is to link the two fragments according to the orientation of the two fragments I observed from the complex structure, which is to link the position 4 amine group from fragment-1 to position 3 methyl group from fragment-2 (Fig. 2.11B). Option two provides a more direct way to link the two fragments together, which is to link through the position 3 methyl groups from the two fragments (Fig. 2.11C). The option 2 compound was shown the potential to still bind to the target protein

*Af*Rho1 by investigating the structure and activity relationships (SAR) of the parental fragment compound (Fig. 2.12).

To conclude, in this part of my research I have combined structural biology and fragment screen approaches, which identified a fragment hit DDD01511162 bound to a conserved pocket between *Af*Rho1 and *Hs*RhoA, and shows inhibitory effect over GEF protein mediated nucleotide exchange. Further medicinal chemistry work guided by the discovery of this research will provide the opportunity to develop a highly potent *Af*Rho1/*Hs*RhoA inhibitor.

Chapter 3 : Genetic and molecular characterization of Rom2 CNH domain in *Aspergillus fumigatus*

3.1 Introduction

The Rom2 orthologue protein was first identified in the budding yeast *Saccharomyces cerevisiae* as a guanine nucleotide exchange factor (GEF) to the Rho1 GTPase and as a key regulator of the CWI (cell wall integrity) pathway (Bickle et al., 1998; Vilella et al., 2005). The cellular functions of the Rom2 protein are to integrate signals from cell wall stress sensors such as Wsc1, Wsc2 and Mid2 then activate the downstream Rho1 GTPase to regulate cell wall synthesis by directly activating glucan synthase (Mazur and Baginsky, 1996), or by activating the downstream transcription factors through the CWI pathway (Bickle et al., 1998; Levin, 2011). The functions of a Rom2 orthologue protein (*Af*Rom2) have also been studied in the pathogenic fungus *Aspergillus fumigatus* (Samantaray et al., 2013). A genetic approach to knockdown the transcription of *rom2* gene in *A. fumigatus* results in a significantly reduced colony growth and increased sensitivity to cell wall stress chemicals such as Congo red and Calcofluor white, which suggesting a compromised cell wall phenotype (Samantaray et al., 2013). The GFP tagged *Af*Rom2 protein was shown to localize in the hyphal tips of *A. fumigatus* which shares a similar localization pattern with *Af*Rho1, and the C- terminal part of *Af*Rom2 (residue 733-1199) was found to interact with *Af*Rho1 in a co-immunoprecipitation experiment (Samantaray et al., 2013).

The Rom2 protein is a multi-domain protein, which contains a well conserved catalytic GEF domain (DH-PH domain) characteristic of all Rho GEF family proteins, and two additional domains that are not present in the human Rho GEF proteins: an N-terminal DEP (Dishevelled, Egl10 and Pleckstrin) domain and a C-terminal CNH (Citron homology) domain (Justa-Schuch et al., 2010; Samantaray et al., 2013). An important consideration, not addressed previously,

is whether (and how) each of the three domains present in Rom2 contributes to fungal viability? This forms the basis of my work to identify a Rom2 domain(s) unique to *A. fumigatus* but absent in the host since this is critical for target selectivity and minimising toxicity.

The DEP domain in a Rom2 orthologue protein *Nc*RGF1 from the filamentous fungus *Neurospora crassa*, has been shown to have an inhibitory function to negatively self-regulate the intrinsic GEF activity of *Nc*RGF1 (Richthammer et al., 2012). However, the function of the CNH domains from fungal Rom2 proteins has never been specifically addressed before.

Unique amongst fungal Rho GEF proteins, the C-terminal CNH domain is named after the signature C-terminal domain of Citron kinase. Citron kinase is a serine/threonine kinase and a RhoA effector protein important for cytokinesis in higher eukaryotic organisms such as *H. sapiens* and *Drosophila melanogaster* (Bassi et al., 2011; Gruneberg et al., 2006; Madaule et al., 1998). The molecular function and protein structure of the CNH domain in Citron kinase has never been fully investigated, however, in *D. melanogaster* the CNH domain was found to interact with *Dm*Rho1 by an *in cellullo* pull down experiment (Bassi et al., 2011).

In this part of my research, I tried to use a multidisciplinary approach (fungal genetics and X-ray crystallography) to investigate the biological functions and the protein structure of the *Af*Rom2 CNH domain. My results suggest that the *Af*Rom2 CNH domain plays essential roles in cell wall synthesis and interacts with key enzymes (*Af*Rho1 GTPase and Chitin Synthase G) that are involved in the cell wall synthesis process. The interaction between CNH domain and *Af*Rho1 was further confirmed by *in vitro* interaction assays, and the binding mode was revealed by X-ray crystallography and structure modelling.

3.2 Materials and Methods

3.2.1 Construction of *rom2Δcnh* mutant

Plasmid 434 (Vogt et al., 2005) was used as a backbone construct. A GFP and pyrG (selection marker) fusion cassette was amplified from the plasmid pHL83 (FGSC) with primers P1, containing a XbaI restriction site and P2, containing a SpeI restriction site. The *rom2 cnh* domain (2725-3792) N terminal flanking region (1674-2724) was amplified with primers P3 and P4. A downstream non-coding region of rom2 (1000 bp) was amplified with primers P5 and P6. The PCR product of *cnh* N terminal flanking region (1050 bp) and the *rom2* downstream non-coding region were cloned by a restrictionless method (Algire, 2013) into the upstream and downstream regions of the fusion cassette to create plasmid *rom2* (1674-2724) GFPpyrG+ (Figure 3.2A). The molecular cloning of this plasmid was done by Dr. Andrew Ferenbach from DVA lab.

Following DNA sequence verification, p-rom2(1674-2724) GFPpyrG+ was used to transform *A. fumigatus Ku80ΔpyrG-* strain derived from CEA17 by PEG-mediated fusion of protoplasts (Langfelder et al., 2002) and positive transformants were selected by uridine/uracil autotrophy. The transformants were confirmed by PCR and Western blot analysis. For PCR analysis, two pairs of primers (P7&P8, P7&P9) were utilized (Fig. 3.2). Primers P7 and P8 were used to amplify a 1093 bp fragment from the *rom2* gene. Primers P7 and P9 were used to amplify a 1563 bp fragment from the mutant gene (Table 3.1).

Table 3.1: Primers used to generate and verify the *rom2Δcnh* and *gfp-cnh* mutants

Primer	Sequence (5' to 3')
P1	AAATCTAGAATGAACAAGACAGTTTTGTGTTCAATTTTTTC
P2	CTGTCTGAGAGGAGGCACTGATG
P3	CATCACCGAATTCTGGCAATGTCTAGAGTGTTCGGAAATTGCTTGGAAGTTCTG
P4	GCTCCAGCGCCTGCACCAGCTCCAACAGGGACAAGGCAGTTCACGC)
P5	CGCATCAGTGCCTCCTCTCAGACAGGGCGCTTGAATGGCTGGTACAATCAAAAG
P6	CGGAGAGAGATTCTTCTGCTGCTGTACTAGTATGGTATCTGGCTGTTGCTTGCTCCCG
P7	TGTCACGGGTCAACACTGAGAG
P8	TATGTATCAGCTCGCTCGTCTC
P9	TGAAGGCTGTTCTGTCAGAGCG
P10	CATCACCGAATTCTGGCAATGTCTAGAatgAGTAAAGGAGAAGAACTTTTCACTGG
P11	GAGCATTGTTTGAGGCGACCGGTTTACTTGTTCCAGAAATCCAGACTGGC
P12	CGCCAAGGCTTTATCTATGTAG
P13	TCCCATGAGATCTTCCAATCCG

For Western blot confirmation of the *A. fumigatus rom2Δcnh* mutant, conidia from the mutant and the parental strain (negative control) were inoculated in 10 ml of YEPD (2% yeast extract, 2% glucose and 0.1 peptone) and cultured in a flask rotator at 37 °C for 48 h. Cell extracts were prepared by homogenizing the mycelia using liquid nitrogen in lysis buffer (50 mM Tris/HCl pH 7.5, 150 mM NaCl, 50 mM KCl, 0.01% Triton X-100, 1 mM PMSF, and 1:100 protease inhibitor cocktail). Total cell lysate was centrifuged at 5000 rpm to eliminate cell debris for 30 min before further centrifugation at 7000 rpm for 10 min at 4 °C. Cell lysate total protein was normalised to ~10 mg by Bradford method (Bradford, 1976) and separated using 10% SDS-PAGE followed by western blotting using a monoclonal anti-GFP antibody produced in mouse (Sigma). A control strain

expressing *gpd-gfp* was used as a control. The *A. fumigatus* strain *Ku80 pyrG+* strain derived from CEA17 was used as parental strain control for the phenotypic examination of the *rom2Δcnh* mutant.

3.2.2 Analysis of the *rom2Δcnh* mutant

100 of conidia from the *rom2Δcnh* mutant and the parental strain were inoculated onto the solid YEPD medium, and cultured in 37 °C incubator for 48 h, the plates were taken out and photographed. To test the sensitivity of the *rom2Δcnh* mutant to chemical reagents, serial dilutions of conidia from 10^7 to 10^4 were spotted on solid MM (minimum media) (Armitt et al., 1976) containing 50 μg/ml of Calcofluor white, 50 μg/ml Congo red, 50 μg/ml SDS, 2.5 μg/ml Caspofungin and 10 μg/ml Hygromycin B respectively. After incubation at 37 °C for 48 h, the plates were examined and images were captured. Three independent experiments were performed to confirm the results. To stimulate conidia formation for the *rom2Δcnh* mutant, the hyphae of the *rom2Δcnh* mutant were inoculated on the MM media supplemented with 1 M sorbitol (osmotic stabilizer) (Fortwendel et al., 2008).

To examine the ultra-structures of the cell wall, mycelia grown in solid MM medium were fixed and examined with an H-600 electron microscope as described by (Li et al., 2007). For the chemical analysis of the cell wall, conidia were inoculated into 100 ml MM liquid medium and incubated at 37 °C with shaking at 200 rpm for 48 h. The mycelia were harvested, washed with sterile water and stored at -80 °C.

The cell wall components were isolated and assayed as described previously (Fang et al., 2009). Briefly, 10 mg of dried mycelium from the parental strain and the mutant were homogenized in 1.5 ml 50 mM Tris-HCl pH 7.5 buffer, 6000 r.p.m. 1 min for four times in homogenizer (Thermo Fastprep) to fully disrupt cells, then centrifuged at 10,000 r.p.m. for 10 min. The pellets were washed and incubated

with 500 µl 1M NaOH 70°C for 30 min, then centrifuged at 10, 000 r.p.m. for 10 min, the supernatant (500 µl) is the alkali-soluble (AS) and the pellet is the alkali-insoluble (AI). The AS (500 µl) was acidified with acetic acid (25 µl) to pH 5.0, centrifuged at 10,000 r.p.m. for 10 min. The supernatant (450 µl) is separated from the pellet labbled as glycoprotein, and determined the concentration by Bradford assay (Bradford, 1976). The pellet is washed with water and labelled as α-glucan. The alkali-insoluble pellet and α-glucan were washed with water for three times, add 200 µl HCl into α-glucan and AI, then put in 100 °C for 2 hour to acid release glucose and glucosamine. After that add 200 ul water into AS and AI to dissolve the dry pellets. Glucan and chitin contents were estimated by determining the released glucose and N-acetylglucosamine after digestion. Glucose was measured by the phenol-sulfuric acid method by using glucose (Sigma) to make a standard curve (Dubois et al., 1951). N-Acetylglucosamine was measured by using GlcNAc (Sigma) to make a standard curve. Three samples of lyophilized mycelia were used for cell wall analysis from each strain and the experiment was performed three times (Lee et al., 2005).

3.2.3 Construction of *gfp-cnh* mutant

Plasmid p434 (Vogt et al., 2005) was used as a backbone construct. A *gfp* and *rom2 cnh* domain (2725-3792) fusion cassette was made and cloned into p434 after the *gpd* promoter (to induce expression) (Redkar et al., 1998) with primers P10 and P11, by using cross over PCR. The resulting plasmid *gpd-gfp-rom2* (2725-3792) was transformed into *A. fumigatus Ku80ΔpyrG-* strain derived from CEA17 by PEG-mediated fusion of protoplasts (Langfelder et al., 2002) and positive transformants were selected by uridine/uracil autotrophy. For PCR analysis, a pair of primers P12 and P13 was used to amplify 480 bp of the mutant.

Two mutants from 25 transformants were shown to have the *gpd-gfp-rom2* (2725-3792) insertions.

For Western Blot analysis of the mutants, conidia were inoculated in 10 ml YEPD (2% yeast extract, 2% glucose and 0.1 peptone) and cultured in a flask rotator at 37 °C for 48h. Protein extracts were lysed and run through a 10% SDS-PAGE. Cell lysate of total protein were normalised to ~10 mg by Bradford method (Bradford, 1976) and separated using 10% SDS-PAGE followed by Western Blotting using a GFP antibody. A strain expressing *gpd-gfp* was used as a control.

3.2.4 Protein extraction and GFP-Trap® affinity purification

The *A. fumigatus* strain expressing the *gpd-gfp-cnh* fusion construct and a control strain expressing *gpd-gfp* were grown in YEPD liquid medium with agitation for 24 h at 37 °C. The cells were collected by filtering through Miracloth (Millipore) and dried. Cell extracts were prepared by homogenizing the mycelia using liquid nitrogen in lysis buffer (50 mM Tris/HCl pH 7.5, 150 mM NaCl, 50 mM KCl, 0.01% Triton X-100, 1 mM PMSF, and 1:100 protease inhibitor cocktail). Total cell lysate was centrifuged at 5000 rpm to eliminate cell debris for 30 min before further centrifugation at 7000 rpm for 10 min at 4°C. The Bradford assay (Bradford, 1976) was used to determine the protein content of the resulting supernatant. Cell lysate total protein were normalised to ~10 mg before GFP-Trap affinity purification (Chromotek). GFP-Trap® resin (25 μl) were equilibrated in 400 µl of chilled dilution buffer (10 mM Tris-HCl pH 7.5, 150 mM NaCl, 0.5 mM EDTA, 1 mM PMSF, 1:100 Protease Inhibitory Cocktail) by washing three times according to the manufacturer's instructions. The GFP-Trap® resin were re-suspended in 100 µl of chilled dilution buffer, mixed with cell lysate and incubated for 2 h at 4 °C with gentle agitation. The suspension was centrifuged at 2000 rpm for 10 min at 4 °C and the pelleted GFP-Trap® resin were washed twice with 500 µl of wash

buffer (10 mM Tris-HCl pH 7.5, 350 mM NaCl, 0.5 mM EDTA, 1 mM PMSF, 1:100 Protease Inhibitory Cocktail). The bound proteins were eluted in 100 µl glycine pH 2.5, and centrifuged at 2000 rpm for 2 min at 4 °C. The eluted proteins were analysed by 10 % SDS page and mass spectrometry.

3.2.5 Mass spectrometry and data analysis

Protein samples were extracted from gel and dried in SpeedVac (Thermo Scientific) then submitted to overnight (16 h) trypsin digestion (Modified Sequencing Grade, Roche). Peptides released were resuspended in 50 µl 1% formic acid, centrifuged and transferred to HPLC vial. 15 µl of sample was injected for LC-MS, which was performed on an Ultimate 3000 RSLCnano System (Dionex- Thermo Scientific) coupled to a LTQ OrbiTrap Velos (Thermo Scientific). For data analysis, the extracted data were searched against *Aspergillus fumigatus* databases using Mascot Search Engine (Mascot Daemon Version 2.3.2). The MS experiment and the subsequent data analysis was done by Miss Samantha Kosto from Dundee FingerPrints Proteomics facility.

3.2.6 Protein expression and purification of the *Af*Rom2 CNH domain

For protein expression, an insert encoding His6-Rom2 CNH (862-1194) was cloned into a modified version of the expression vector pGEX6P1 (GE Healthcare) from which the GST tag and PreScission Protease cleavage site had been removed. The molecular cloning was done by using restriction enzymes BamI and NotI, and primers Hm2CT1_F and Hm2CT1_R (Table 2.1). The expression plasmid was made by Dr. Andrew Ferenbach from the DVA lab.

The expression construct was transformed into *E. coli* BL21 (non DE3) cells. When cells grew to an OD_{600} of 0.8 at 37 °C, 250 µM IPTG was added for induction at 25 °C for 16 h. Cells were harvested by centrifugation at 4000 rpm at 4 °C for 30 min in a J6-MI centrifuge (Beckman Coulter), and suspended in

TBD buffer with 0.5 mM TCEP, 5 mM $MgCl_2$,50 μM GDP plus a protease inhibitor cocktail (1 mM benzamidine, 0.2 mM PMSF, 5 μM leupeptin). Cells were lysed using pressure homogenization with an EmulsiFlex cell disruptor (15,000 kilopascals Avestin; Ottawa, Canada). Supernatant and inclusion bodies were separated by centrifugation at 16,000 rpm for 1 h using an Avanti J26S centrifuge (Beckman Coulter). The supernatant was incubated with pre-washed His-Nickel resin (GE Healthcare) at 4 °C on a rotating platform for 2 h. The resin with bound proteins was washed with five column volumes of resuspension buffer and the proteins were eluted using a 10- 250 mM imidazole gradient. The eluted proteins were concentrated to 5 ml and loaded onto a Superdex 200 column (Amersham Bioscience) previously equilibrated with purification buffer and eluted at a flow rate of 1 ml/min in the same buffer. The fractions were verified by SDS-PAGE. Pure fractions were pooled and concentrated to 2 mg/ml using a 10 kDa cut-off Vivaspin concentrator (GE Healthcare) before snap freezing and storing at -80 °C. The expression and purification of seleonomethionine labelled *Af*Rom2 CNH domain was done using the commercial kit (Cat. MD12-500) from Molecular Dimensions and according to the manufacture's protocol. Briefly, the expression construct was transformed into a methionine auxotroph DE3 *E. coli* expression strain (*E. coli* 834). The cells were first inoculated into 100 ml M9 minimal medium added with L-methionine, and was grown overnight at 37 °C. The cells were then pelleted by centrifugation at 4000 rpm at 4 °C for 10 min in a J6-MI centrifuge (Beckman Coulter) and washed 3 times in 100 ml of sterile water, resuspended in 1 ml of water and inoculated into 1 L of prewarmed (30 °C) M9 medium containing L-Semet. When cells grew to an OD_{600} of 0.8 at 37 °C, 1 mM IPTG was added for induction at 25 °C for 16 h. The cell lysis and protein purification steps are the same as native *A*fRom2 CNH protein.

3.2.7 *In vitro* interaction assay

Interaction between the *Af*Rom2 CNH domain and *Af*Rho1 was examined by a Nickel resin mediated pull-down assay. Briefly, *Af*Rho1 protein was incubated with 1 mM GppNHp (non-hydrolysable GTP analogue) (Sigma) or GDP (Sigma) for 90 min in 10 mM Tris-Cl buffer (pH 7.4) containing 10 mM EDTA, 150 mM NaCl, 1% (v/v) Triton X-100 and 1 mM DTT at room temperature. Then, 10 mM $MgCl_2$ was added and further incubated for 30 min at room temperature. His_6-*Af*Rom2CNH (20 μM) protein was bound to Nickel resin by incubating at 4 °C for 2 h and incubated with excess Rho1-GTP (40 μM) and Rho1-GDP (40 μM) at room temperature for 1 h. After extensive washing in buffer to elute the unbound protein (25 mM Tris pH 8.0, 100 mM NaCl, 3.0 mM DTT), the resin was then analysed by 12% SDS-PAGE, 100 μM BSA was used as negative control. The construct expressing *Af*Rho1 (E64A, R68A, R70A, D76A) was made by site directed mutagenesis, expressed and purified as the wild type protein. The mutant protein was tested to the binding the His_6-*Af*Rom2CNH using the above-mentioned method under the same condition.

3.2.8 Crystallization, data collection and structure determination of *Af*Rom2 CNH domain

*Af*Rom2 CNH native crystals were obtained in the Morpheus H10 condition (Molecular dimension), were flash-cooled in liquid nitrogen and the diffraction data were collected at the Diamond Light Source (Harwell, UK) I03 beamline, with the maximum diffraction up to 2.0 Å. The crystals contained one molecule per asymmetric unit with a space group of $P2_1 2_1 2$ and unit cell parameters: a = 77.9 Å, b = 93.7 Å, c = 52.6 Å; α = β = γ = 90.00°. The data were processed using XDS (Kabsch, 2010), merged and scaled in CCP4 (Collaborative Computational Project, 1994). Molecular replacement failed, as there was no suitable search

model in the protein databank. Se-met derivative *Af*Rom2 CNH protein was produced as described previously and crystallized in the same conditions as the native crystals. The diffraction data for the Se-met crystal was collected at the ESRF (Grenoble, France) BM-30A with the maximum diffraction up to 2. 4 Å. The space group of the Se-met crystal is identical to that of the native which is also $P2_1\,2_12$, with the unit cell parameters: a = 77.1 Å, b = 92.3 Å, c = 52.3 Å; α = β = γ = 90.00°. and was processed using XDS (Kabsch, 2010), merged and scaled in CCP4 (Collaborative Computational Project, 1994). The phases were solved using PHENIX, by Se-SAD phasing with AutoSol (Echols et al., 2012), five Semet atoms were giving apparent anomalous signals. Phases were improved by iterative cycles of manual model building using Coot (Emsley and Cowtan, 2004) and Refmac (Murshudov et al., 2011). The native structure was solved using molecular replacement by MOLREP (Murshudov et al., 1997; Vagin and Teplyakov, 1997). REFMAC (Murshudov et al., 1997) was used for further refinement and iterative model building using COOT (Emsley and Cowtan, 2004). Data collection and refinement statistics are presented in Table 3.2. Figures depicting the protein structure were generated using PyMOL (DeLano, 2004).

3.2.9 Differential scanning fluorimetry (DSF)

DSF experiments were carried out using a CFX96 real-time PCR detection system (Bio-Rad). 50 µl solution was added into the 96-well PCR plates, include 5 µM AfRho1 or *Af*Rho1 (E64A, R68A, R70A, D76A), 2.5× SYPRO orange in 25 mM HEPES, 150 mM NaCl, 0.25 mM TCEP. The samples were heated from 25 °C to 95 °C with increments of 0.5 °C/minute, and fluorescence was measured at each step. The d(RFU)/dT graph was plotted using Prims6.

3.3 Results

3.3.1 *Af*Rom2 possesses a C-terminal CNH domain of unknown function

The Rom2 protein from *Aspergillus fumigatus* (*Af*Rom2) is a Rho1 GEF protein that plays important roles in fungal cell wall organisation (Samantaray et al., 2013). An NCBI conserved domain search suggests that apart from the conserved Rho GEF catalytic domains (DH and PH), *Af*Rom2 also possesses a C-terminal CNH domain (amino acid residues 881-1170 aa) (Fig. 1.11). Interestingly, this domain is conserved in other fungi with 60-90% protein sequence identity (Fig.3.1A), but is absent from Rho GEF proteins in other eukaryotic organisms in metazoa (Fig. 1.11). However, the CNH domain as a citron homology domain is widely present in citron kinases from higher eukaryotic organisms, such as in *H. sapiens* and *D. melanogaster* (Madaule et al., 1998). Although citron kinases have been implicated as a Rho GTPase interacting kinase and play important roles in cytokinesis, the exact molecular functions of the CNH domain in citron kinases has not yet been investigated (Bassi et al., 2011; Gai et al., 2011).

Although all are named as CNH domains, the sequence identity between *Af*Rom2 CNH domain and the CNH domains from *H. sapiens* and *D. melanogaster* citron kinases is only 20% (Fig. 3.1). Based on the above observations, I hypothesized that the CNH domain in *Af*Rom2 may have some unique functions in fungal cell development.

A

```
AfRom2_CNH   N K T V L C S N F F T S A N R V N C L V P V D G G R K L V Y G T   894
AnRom2_CNH   N K N I I C E K F F N S V N R V N C L V P I D G G R K L V Y G T   893
ScRom2_CNH   N V T K M S D R F F D Y T N K I N S V T S C D G G R K L L I A T   1052
SpRom2_CNH   . . . T I C S N F F V G D N K V N A I G V Y D S G R R L L Y G T   1014
CaRom2_CNH   . . . . . . . . . F T G N N K I N C A V P C Y G G K K L L Y G T   1084
CnRom2_CNH   . . . T I T E G I L N G V R K V N C S S P Y D Q G N R M I F G T   878

AfRom2_CNH   D S G I F I S E R W . . . . . P K D K S . . . . A K P R R V L   916
AnRom2_CNH   D S G I Y V S D R N . . . . . P R D Q S . . . . A K P R K V L   915
ScRom2_CNH   N S G L Y M S N I K R Q Q N K D H R H K S S S A F F S T P I Q L V   1084
SpRom2_CNH   D T G V Y V S L R K . . . . . A N S P L Q . . . . F K P V R A L   1037
CaRom2_CNH   D S G V W V S T V R S I S A T S N E K I C . . . . S D P T M V I   1112
CnRom2_CNH   D E G V Y F A N L R . . . . . D E K L R . . . . . E P V K V I   899

AfRom2_CNH   D A S Q V T Q I D T L E E Y Q L L L V L A N K T L S S Y P M E A   948
AnRom2_CNH   D V S Q V T Q I D T L E E Y Q L L L V L A N K T L Y S Y P M D A   947
ScRom2_CNH   Q R N N I T Q I A V L E E F K S I I L L I D K K L Y S C P L S L   1116
SpRom2_CNH   N I P N I S Q L E V I E E Y S L L L L S D K V L Y S Y P L E M   1069
CaRom2_CNH   S K T Y V T Q I E V I V E Y S K L L V L S D K S L Y E F D L S C   1144
CnRom2_CNH   N L I D V T Q L D V I E E F Q L L I V L H E R C V T T F P L D S   931

AfRom2_CNH   L E L A . E G Q N S V A K R P K K I Q G H A N F F K A G I G L G   979
AnRom2_CNH   L E V T . E G Q N P A A K R P K K I Q G H A N F F K S G I G L G   978
ScRom2_CNH   I E A E G N G T S F F K K H H K E L I N H V S F F A E G D C N G   1148
SpRom2_CNH   I D A D . T T Q A P . . K K A R K V S G H T T F F R V G I C L G   1098
CaRom2_CNH   T D S L . D H V K N T . K S G K L L L S H V S F F K V G V C D G   1174
CnRom2_CNH   L D P S . D P N A A L . K R G K R I S S H T S F I K S G V C L G   961

AfRom2_CNH   R H L V C S V K T S A L S S T I K V Y E P M D . N L A K G K K K   1010
AnRom2_CNH   R H L V C S V K T S A L S T T I K V Y E P M D . N L A K G K K K   1009
ScRom2_CNH   K R L I V T A H S S . . S H S I K Y F E H E H . P L L A E K N G   1177
SpRom2_CNH   K V L V C A V K S S V L S A T I K V F E P V T . N Y S K T R N M   1129
CaRom2_CNH   K L L V I G A R T G S . S H S I C I F E P V N . P F D K S N K N   1204
CnRom2_CNH   K T L V A I V K S S T L S S T I K V M E P V D L S Q N R K K T Q   993

AfRom2_CNH   S A V S K M F Q S G Q D T L K P F K E Y Y I P A E S S S I H F L   1042
AnRom2_CNH   S T V S K M F Q S G Q D T L K P F K E F Y I P A E S S S I H Y L   1041
ScRom2_CNH   S G S G N K K S L K . . . . K K I T E V I F D S E P V S I S F L   1205
SpRom2_CNH   P S L K K F L T V N Q D P L R I V K E L Y I P T E S T S V H F L   1161
CaRom2_CNH   K N . . K R L E . . . . . I Q E I N F S S D P I S I S F L   1226
CnRom2_CNH   A G F M R R L N G K D D A L K L F K E F Y I P T E S S S V H F L   1025

AfRom2_CNH   R S T L C V G C A R G F E V V S L E T T E T Q S L L D Q A D T S   1074
AnRom2_CNH   R S T L C V G C A R G F E V V S L E T T E T Q S L L D Q A D T S   1073
ScRom2_CNH   K A N L C I G C K K G F Q I V S I S Q N A H E S L L D P A D T S   1237
SpRom2_CNH   K N K L C V G C T R G F E V V S L D N L E T Q S L L D P A D T S   1193
CaRom2_CNH   K T K L C I G C A K G F E I L S S Q T G T K E S I L D E A D P S   1258
CnRom2_CNH   K T K L C V G C T K G F E I V D L E T L D M Q G L L D P S D G S   1057

AfRom2_CNH   L D F V A R K E N V K P I H I E R M . N G E F L L N Y S D F S F   1105
AnRom2_CNH   L D F V A R K E N V K P I H I E R L . N G E F L L N Y S D F S F   1104
ScRom2_CNH   L E F A L . R D T L K P M A I Y R V . G N M F L L C Y T E F A F   1267
SpRom2_CNH   L E F V E K K E N V K P I A I Y R M N G G E F L L C Y S Q F A F   1225
CaRom2_CNH   L D F A T Q R E S V T P L A I H R L . G R D F L L C Y S E F V F   1289
CnRom2_CNH   L D F V L K R D N V R P I A I Y R I . E E D F L L C Y D E F A F   1088

AfRom2_CNH   F V N R N G W R A R P D W K I S W E G N P N A F A L S Y P Y I L   1137
AnRom2_CNH   F V N R N G W R A R A D W K I S W E G N P N S F A L S L P Y I L   1136
ScRom2_CNH   F V N N Q G W R K K E S H I I H W E G E P Q K F A I W Y P Y I L   1299
SpRom2_CNH   Y V N R D G W R S R P T W F V V W E G S P Q N F A L S Y P Y I L   1257
CaRom2_CNH   L I N R N G W R T N H D W G I F W E G N P Q N V A I F F P Y L L   1321
CnRom2_CNH   Y V N K N G W R S R P K W A I V W E G I P T S F A L Q Y P Y V I   1120

AfRom2_CNH   A F E P N F I E I R H I E T S E L I H I M T G K N I R M L . . .   1166
AnRom2_CNH   A F E P N F I E F R H I D T S E L I H I M T G K N I R M L . . .   1165
ScRom2_CNH   A F D S N F I E I R K I E T G E L I R C V L A D K I R L L . . .   1328
SpRom2_CNH   A F E P T F I E I R H V E T S E L I H V I S G R N I R L L A D G   1289
CaRom2_CNH   S F E P G F V E I R D L H T T N L L R A L T G E N I R F L . . .   1350
CnRom2_CNH   A F E P T F I E V H H V E T G H L V Q I I P G N N I Q C L . . .   1149

AfRom2_CNH   . . . H S S T R E I L Y A Y E D E G G E D V V A S L D F W N K   1194
AnRom2_CNH   . . . H S S T R E I L Y A Y E D D S G E D V V A S L D F W . .   1191
ScRom2_CNH   . . . Q T S T Q E I L Y C Y E D Y R G Y D T V A S L D F W . .   1354
SpRom2_CNH   R G K L G D G G E I F Y A C . D Q R G E N C E T S V . . . .   1314
CaRom2_CNH   . . . H S N E H E A M F A C . E E N G Y D I I I S I D F L N .   1376
CnRom2_CNH   . . . F A D T . . . . . .   1153
```

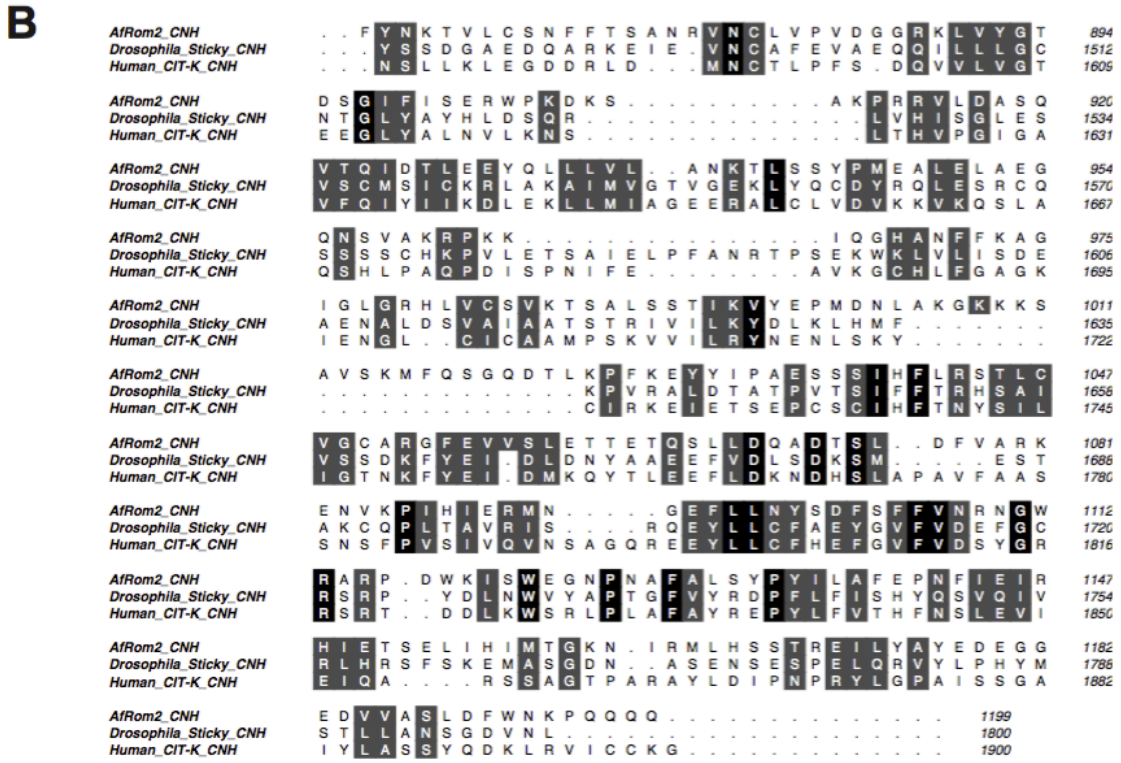

Figure 3.1: Sequence conservation of Rom2 CNH domain from fungal organisms and to citron kinases CNH domain from *Drosophila* and Human

(A) (B) Multiple protein sequence alignment of Rom2 CNH domain among different fungal species (*A. fumigatus*, *A. nidulans*, *C. albicans*, *C. neoformans*, *S. cerevisiae*, *S. pombe*) and the alignment of *Af*Rom2 CNH domain to the CNH domain from Human and *Drosophila* Citron kinases. The alignment was performed using ClustalW2 from EMBL-EBI server. The aligned sequences are displayed according to the secondary structure using Aline (Bond and Schuttelkopf, 2009). Black represents identical and grey represents conserved.

3.3.2 The *Af*Rom2 CNH domain is required for cell growth and cell wall integrity

To investigate the *in vitro* growth of an *A. fumigatus* strain unable to transcribe the *Af*Rom2 CNH domain, a *rom2Δcnh* mutant was constructed using a GFP tag and *pyrG* selection marker to replace the DNA coding sequence (*rom2 2725-3792*) that is transcribed and translated into the CNH domain (Fig. 3.2A). After homologous recombination, the marker insertion and replacement of the native CNH domain was verified by PCR (Fig. 3.2B). From the PCR analysis, a pair of

primers P7 and P8 amplifies a region (1096 bp) of the *rom2* gene including the *cnh* coding region from the parental strain, however such region cannot be amplified from the mutant, suggesting the successful deletion of *cnh* coding region in the *rom2* gene (Fig. 3.2AB). The primers P7 and P9 can amplify a corresponding region (1563 bp) that includes the N-terminal of the *cnh* coding region and the replacing *gfp-pyrG* cassette from the mutant, however not from the parental strain, suggesting in the mutant, original *cnh* coding region is replaced by the *gfp-pyrG* cassette through homologous recombination.

The gene functionality with associated expression of a truncated *Af*Rom2 protein was confirmed by Western blot using a GFP antibody (Fig. 3.2C). The GFP antibody was shown to detect a protein band from the cell lysate of *rom2Δcnh* mutant with the molecular weight around 70 kDa, which is corresponding to the similar protein size with Rom2ΔCNH protein (46 kDa) but attach to a GFP tag (26 kDa). The cell lysate from the parental strain and the strain to overexpress GFP protein was used as controls (Fig. 3.2C).

To investigate the colony phenotypes of the *rom2Δcnh* mutant, the same amount of conidia (10^2) from the wild type strain and the *rom2Δcnh* mutant were inoculated onto the solid rich medium YEPD (Fig. 3.2D). After growth at 37 °C for 48 h, the *rom2Δcnh* mutant was shown to grow very slowly, lacking the radial growth at the edge of the colony, and formed almost no conidia on the surface of the colony (Fig. 3.2D). This observation suggested that the *Af*Rom2 CNH has important functions in terms of colony growth and conidia production in *A. fumigatus* (Fig. 3.2D). The colony phenotypes of the *rom2Δcnh* mutant is also very similar to the published research (Samantaray et al., 2013) describing the knock down mutant of the full length *rom2* gene in *A. fumigatus*, which suggests

the C-terminal CNH domain is required for the biological functions of the *Af*Rom2 protein.

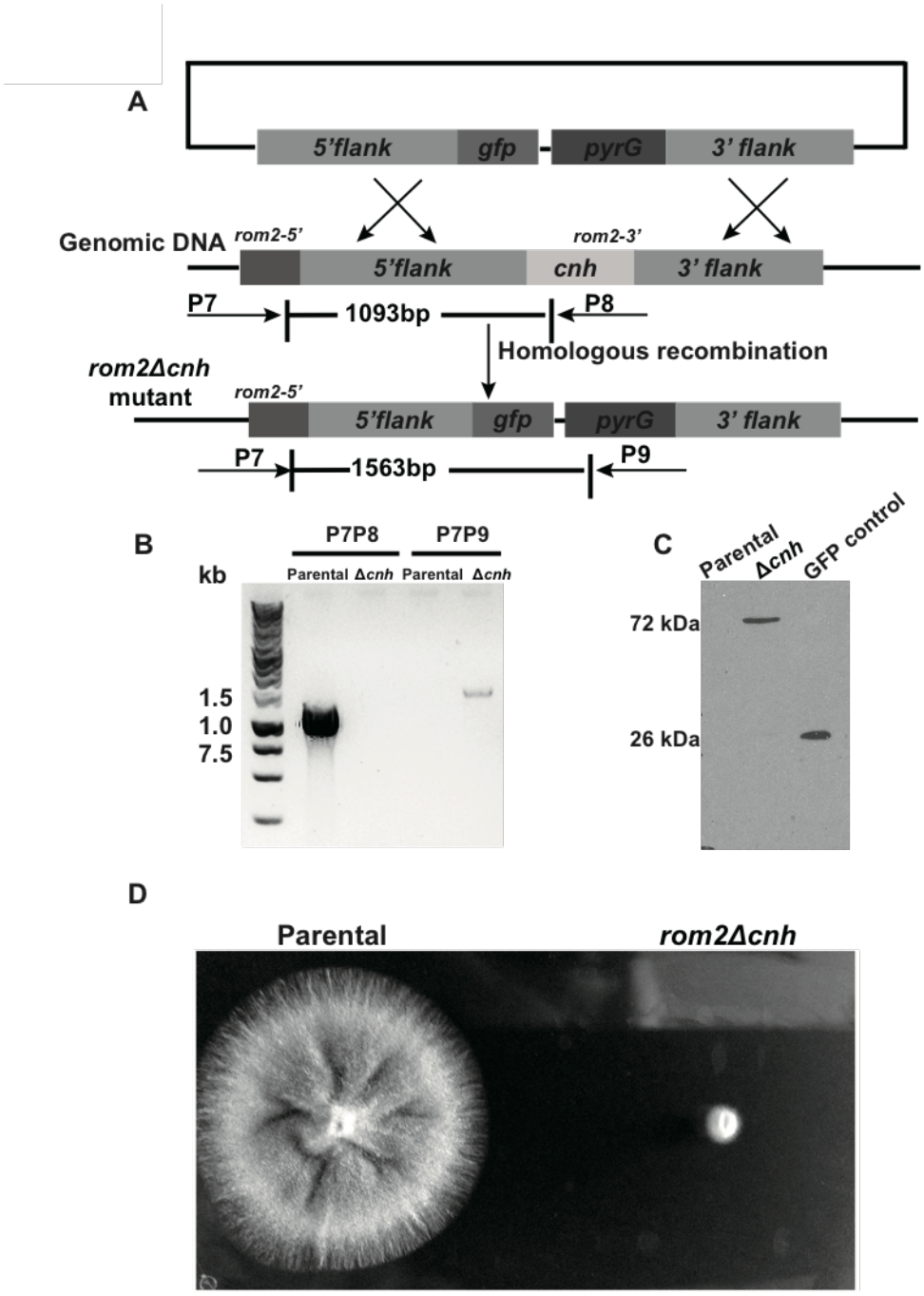

Figure 3.2: Generation of *rom2Δcnh* mutant

(A) Schematic diagram of the strategy towards generating the *rom2Δcnh* mutant

(B) PCR confirmation of the *rom2Δcnh* mutant using primers P7&P8, P7&P9 to amplify the N-terminal *rom2* gene with the *cnh* domain and the N-terminal *rom2* gene with the *pyrG* marker respectively.

(C) Western blot using the *rom2Δcnh* mutant cell lysate and GFP antibody, recombinant GFP

protein as a positive control. The band size from the *rom2Δcnh* (72 kDa) strain represents the correct molecular weight of the *Af*Rom2ΔCNH which is 46 kDa, attached to a GFP tag (26 kDa) . **(D)** Growth of the *rom2Δcnh* mutant in comparison with the parental strain on the solid YEPD medium. 10^2 of conidia from the *rom2Δcnh* mutant and the parental strain were inoculated in the solid YEPD medium at 37°C for 48 h.

As previously reported, knockdown expression of the full length *rom2* gene in *A. fumigatus* leads to increased susceptibility to cell wall perturbing agents (Samantaray et al., 2013), suggesting that *Af*Rom2 play important roles in cell wall organisation, and knockdown of the *rom2* gene will induce a cell wall defective phenotype. To investigate whether the *Af*Rom2 CNH domain also functions in cell wall organisation, a serial conidia dilution of the *rom2Δcnh* mutant and the wild type strain were inoculated onto solid MM medium supplemented with cell wall perturbing chemicals such as Congo red, Calcofluor White and Caspofungin (Fig. 3.3). Congo red and Calcofluor White are dyes that have been shown before to affect chitin and β-1,3-glucan synthesis in fungal organisms (Roncero and Duran, 1985), and were used as cell wall stresses to test the cell wall defective phenotypes of *rom2* gene knockdown mutant (Samantaray et al., 2013). Caspofungin is a clinically used antifungal drug that inhibits β-1,3-glucan synthesis in the fungal cell wall (Deresinski and Stevens, 2003). After growth at 37 °C for 48 h, the *rom2Δcnh* mutant showed increased sensitivity to all the cell wall perturbing agents (Congo red, Calcofluor White and Caspofungin), but not the in media with the detergent SDS and the peptide synthesis inhibitor Hygromycin B when compared to the wild type (Fig 3.3). This result indicates that the cellular function of *Af*Rom2 as a cell wall integrity regulator is largely dependent on its *C*-terminal CNH domain. Thus, the above observations to compare the colony phenotypes of the *rom2Δcnh* mutant and the wild type strain

show that the *Af*Rom2 CNH domain is required for colony growth and cell wall integrity.

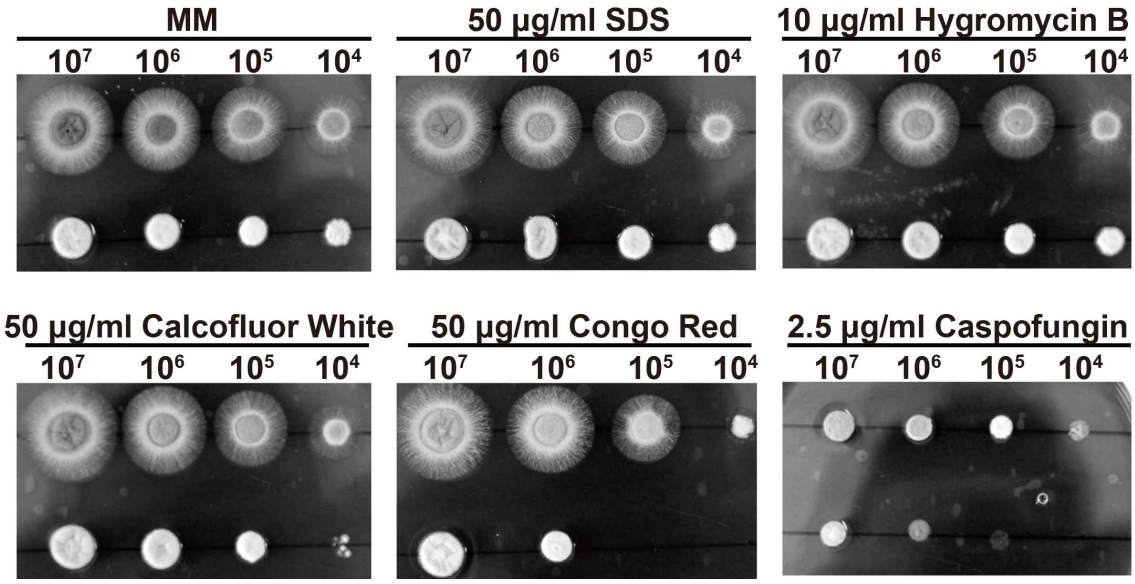

Figure 3.3: Sensitivity of the *rom2Δcnh* mutant to chemical reagents

Serial dilutions of conidia from 10^7 to 10^4 were spotted on solid MM medium containing 50 µg/ml SDS, 10 µg/ml Hygromycin B, 50 µg/ml Calcofluor White, 50 µg/ml Congo Red, 2.5 µg/ml Caspofungin. Colonies in the upper rows of the plates are parental strain and the lower rows are the *rom2Δcnh* mutant strain. The colonies were grown at 37°C for 48 h. The concentrations of the chemicals were chosen according to (Fang et al., 2013).

3.3.3 The CNH domain is required for cell wall synthesis and ultrastructure

The sensitivity of the *rom2Δcnh* mutant to the cell wall perturbing agents (Fig. 3.3) suggests a compromised cell wall. Thus, I examined the ultra-structure of the cell wall using transmission electron microscopy (TEM). Compared to the wild type, the *rom2Δcnh* mutant had an approximately 20-fold reduction in the diameter of the middle layer of the cell wall which is β-glucan, [15 ± 4 nm versus 290±30 nm (n≥12)] (Fig 3.4A), with associated detachment of the outermost glycoproteins layer (Fig. 3.4A). Next I separated and quantified the different carbohydrate components in the cell wall of the wild type and *rom2Δcnh* mutant cell walls

chemically (Fang et al., 2009). In agreement with my TEM findings, the β-glucan level is drastically decreased from 2100 μg/10 mg in the wild type to only 530 μg/10 mg in the *rom2Δcnh* mutant (Fig. 3.4B). The chitin level is also decreased significantly from 620 μg/10 mg in the wild type to 210 μg/10 mg in the mutant (Fig. 3.4B). However, for the glycoprotein and α-glucan levels, there were no significant differences between the parental and the *rom2Δcnh* mutant (Fig. 3.4B). In combination, these data suggest that the *Af*Rom2CNH domain is involved in the synthesis of the key components of fungal cell wall, β-glucan and chitin. Thus, the *Af*Rom2 CNH domain contributes to regulation of cell wall synthesis and organization in *A. fumigatus.*

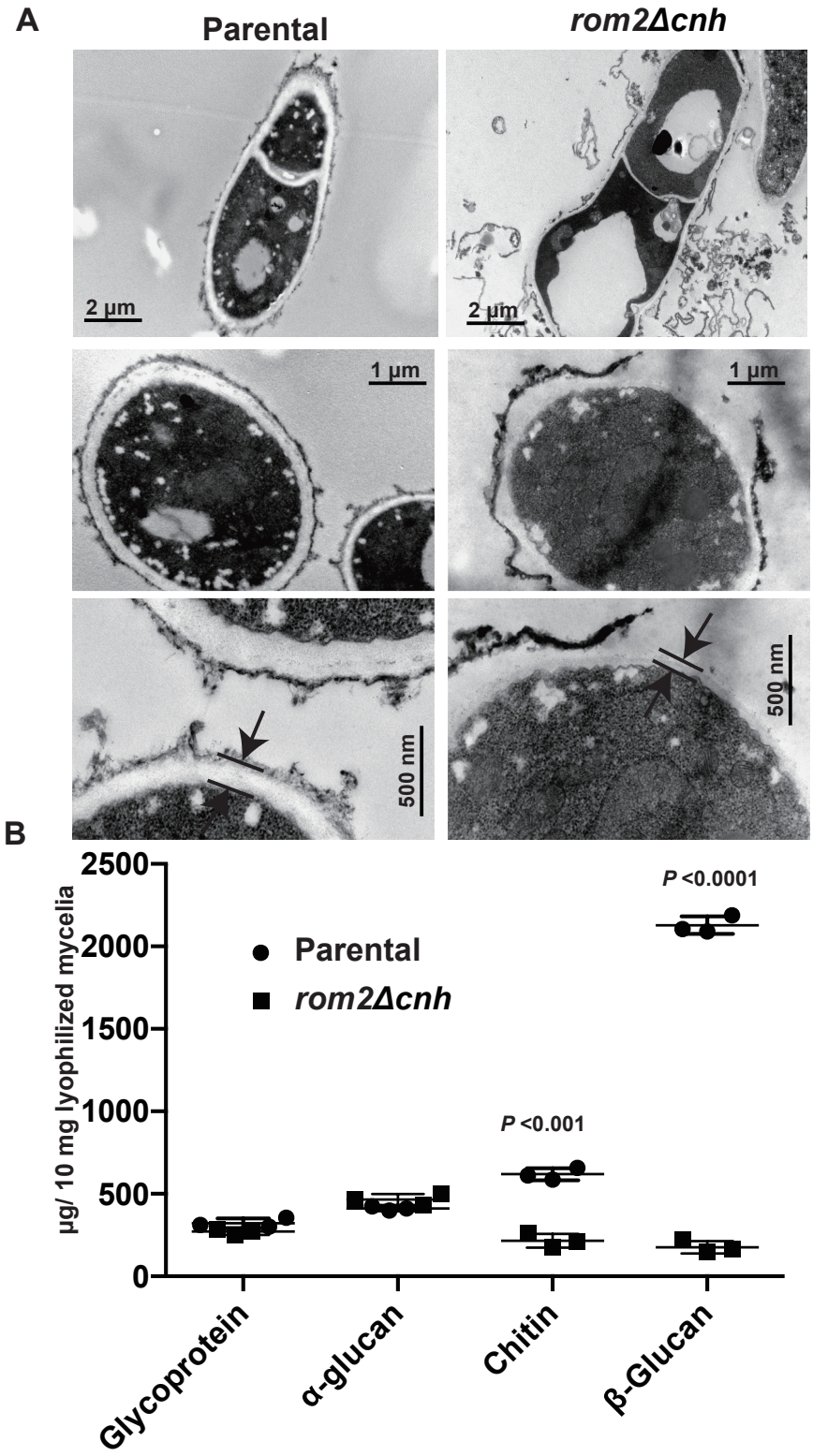

Figure 3.4: Cell wall analysis of the *rom2Δcnh* mutant

(A) TEM images of representative parental (left) and *rom2Δcnh* (right) mutant hypha cells.

(B) Cell wall composition of the *rom2Δcnh* mutant compared to the wild type strain by chemical analysis (Fang et al., 2009). The plot of the data and the P value by the multiple t tests were calculated using Prism 6 (GraphPad software).

3.3.4 The *Af*Rom2 CNH domain bound to the major cell wall synthesizing protein *Af*Rho1

To gain insight into whether the *A. fumigatus* Rom2 CNH acts alone or by forming a complex that is responsible for the altered cell wall phenotype, I aimed to identify potential binding partners of the Rom2 CNH domain using GFP pull down methodology. In brief, an N-terminal *gfp* labelled *Afrom2 cnh* fused to an overexpression *gpd* promoter (Redkar et al., 1998) was integrated into the *A. fumigatus* genome (fig. 3.5A) and verified by PCR and Western blotting (fig. 3.5BC).

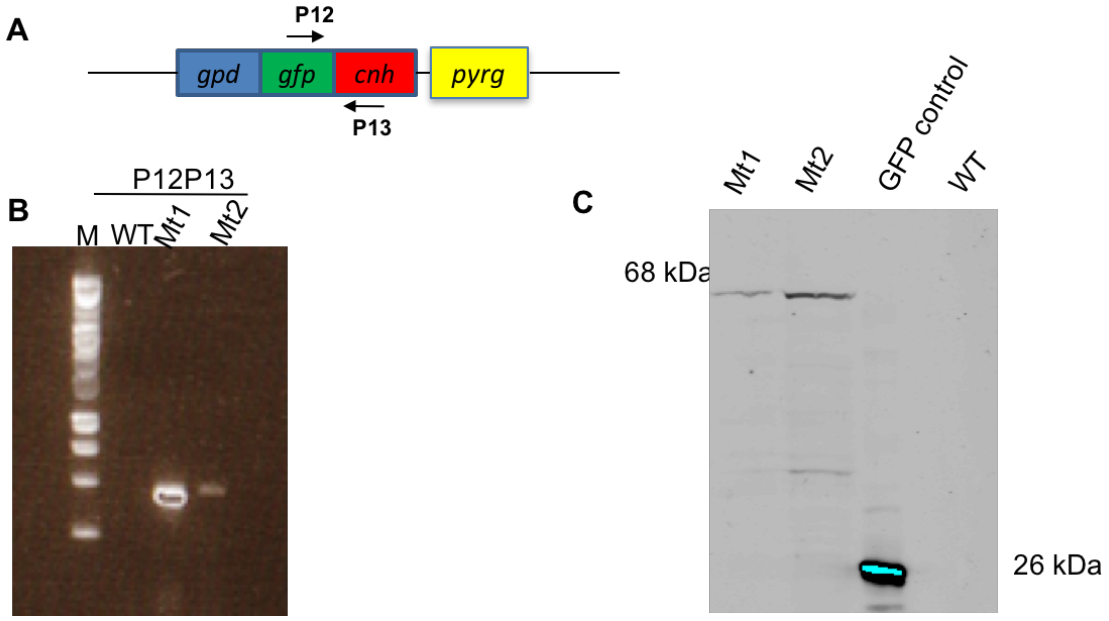

Figure 3.5: Generation of *gfp-cnh* mutant

(A) Schematic diagram towards the *gfp-cnh* mutant. The *gfp-cnh* fusion cassette was randomly integrated into the *A. fumigatus* genome.

(B) PCR confirmation of two transformants as *gfp-cnh* mutants. Two mutants (Mt1 and Mt2) were shown the correct size of the band (420 bp),

(C) Western blot using the *gfp-cnh* mutant cell lysate and GFP antibody, with a *gfp* control strain as a positive control, and the parental wild type strain as negative control. The size difference

between the Mt1 and Mt2 to the *gfp* control strain represents the correct molecular weight of the CNH protein which is 40 kDa.

The GFP tagged AfRom2 CNH along with the protein binding partners were then isolated from the *A. fumigatus* cell lysates using GFP trap beads (GFP-Trap (ChromoTek), cell lysate expressing *gfp* alone was used as negative control (Fig. 3.6AB). Eluates from the GFP pull down experiment were then processed and subjected to Mass spectrometry. A total of 175 unique protein hits (subtract the non-specific binding to GFP alone) were identified from the eluates that co-eluted with the *Af*Rom2 CNH domain. The protein hits span a variety of cellular locations although most (107 of 175) are congregated in the cytosol (Fig. 3.6C). Among the binding partners identified, two proteins (*Af*Rho1 and Chitin synthase G) have previous been reported to be directly involved in the cell wall synthesis (Fig. 3.6C, Table 3.2). *Af*Rho1 was previously reported as a regulatory subunit of glucan synthase and the downstream GTPase protein of *Af*Rom2 in *A. fumigatus* (Beauvais et al., 2001; Samantaray et al., 2013). And Chitin synthase G belongs to the class 3 chitin synthase family, that plays important roles in cell wall chitin synthesis and is required for fungal development (Borgia et al., 1996). The reported functions of these two interacting proteins, *Af*Rho1 and Chitin synthase G, support our findings that loss of the coding region for the CNH domain in *A. fumigatus* Rom2 manifests as a reduction in crucial cell wall components such a chitin and β-glucan. In conclusion, the identification of these potential binding partners of the Rom2 CNH domain, offer insight into the potential molecular mechanisms of how this domain regulates cell wall synthesis in *A. fumigatus*.

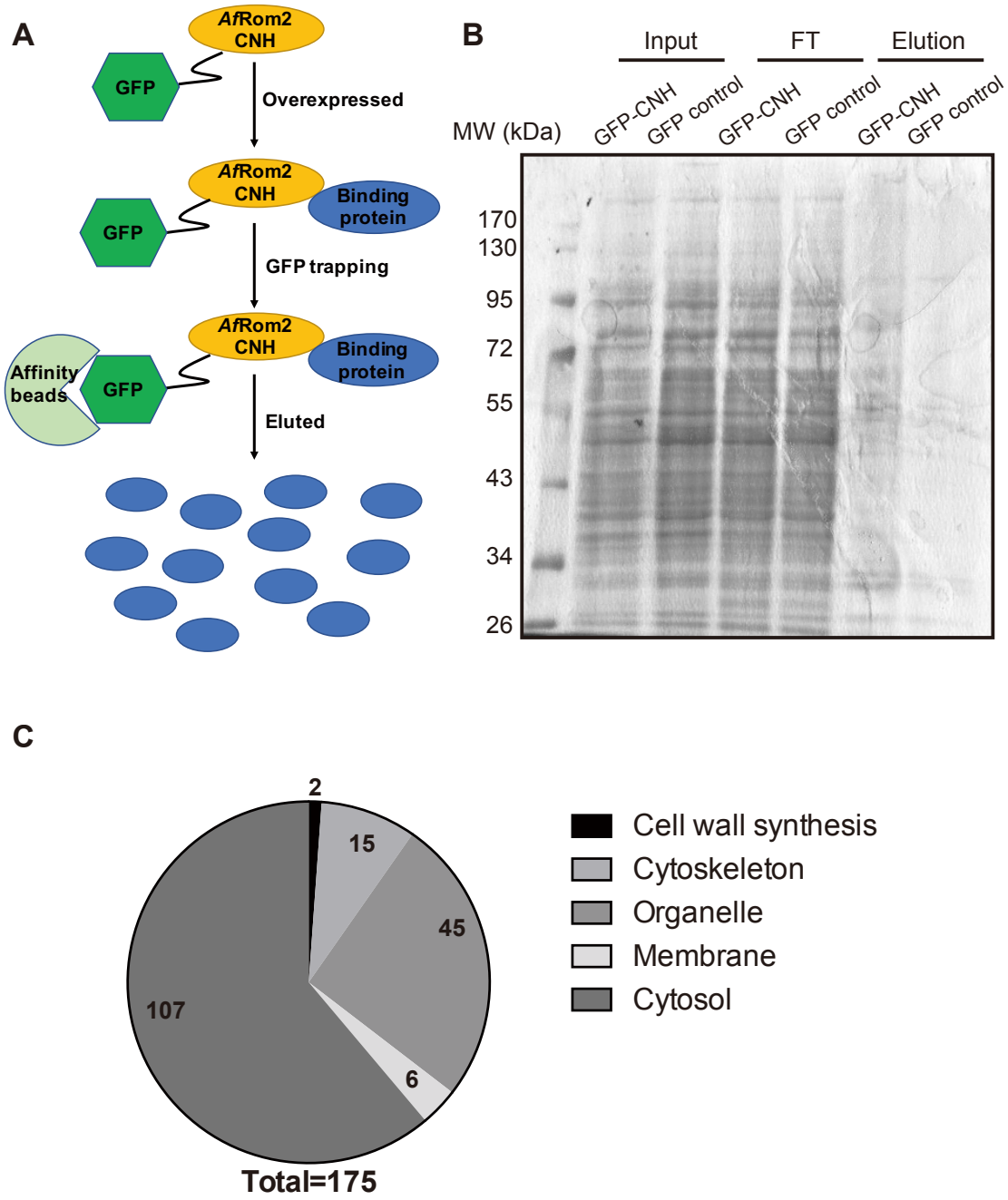

Figure 3.6: Pull down of *Af*Rom2 CNH interacting proteins by GFP-CNH

(A) Schematic representation of the GFP-CNH pull-down experiment. Eluted proteins from the GFP affinity beads were then processed for MS.

(B) 10% SDS gel of the GFP-CNH pull down results, mutant that expresses GFP alone was used

as a control strain.

(C) Cellular component analyses of proteins identified by GFP-CNH pull down MS.

*Af*Rho1 has been reported before as an important regulator protein of glucan synthase and the direct downstream Rho GTPase of *Af*Rom2 (Beauvais et al., 2001; Samantaray et al., 2013) . In the previous research, *Af*Rho1 was found to bind to the C-terminal region of *Af*Rom2 (733-1199) in a co-immunoprecipitation experiment (Samantaray et al., 2013). In addition to that, the CNH domain from *Drosophila* citron kinase was also reported to interact with a Rho GTPase orthologue protein in both the GDP and GTP binding conformation (Bassi et al., 2011). Therefore, I decided to further investigate the binding between the *Af*Rho1 to the *Af*Rom2 CNH domain by biophysical and structural biology methods.

Table 3.2: Protein hits from the GFP pull down experiment that are involved in cell wall synthesis

Protein accessions	Protein name	Unique peptides	Previous reported
Q9C3YC	*Af*Rho1	2	(Beauvais et al., 2001)
P54267	Chitin synthase G	1	(Borgia et al., 1996)

I expressed and purified His6-*Af*Rom2CNH and *Af*Rho1, for an *in vitro* binding assay. The His6-*Af*Rom2CNH protein was first incubated with the Nickel resin, and then incubated with either GDP and GTP loaded *Af*Rho1. After extensive washing of the resin with buffer, the resin was then run on an SDS page. As shown in Fig. 3.7, both GDP and GTP loaded *Af*Rho1 co-precipitated with *Af*Rom2CNH, suggesting *Af*Rho1 bound to *Af*Rom2CNH *in vitro*, independent of the nucleotide bound.

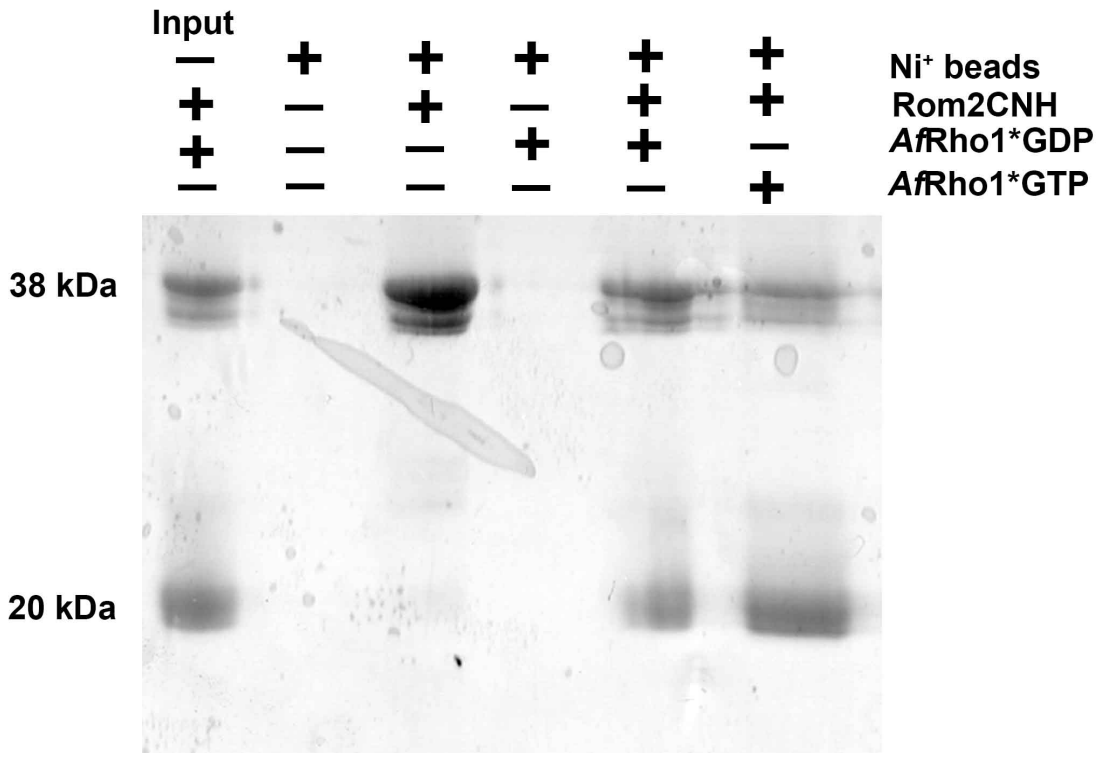

Figure 3.7: *In vitro* binding analysis of Rom2 CNH domain and *Af*Rho1

The SDS page gel results to show the His tag pull- down assay to determine the *in vitro* interaction between Rom2 CNH domain and *Af*Rho1.

3.3.5 The *Af*Rom2 CNH structure adopts a seven bladed WD40 fold

To understand the molecular basis of how the *Af*Rom2 CNH domain bound to *Af*Rho1, I decided to solve the protein structure of this protein domain by using

X-ray crystallography. The *Af*Rom2 CNH domain (aa 862–1194) was expressed and purified using an *E. coli* (BL21) expression system. The native crystal and the selenomethionine derivative crystals were grown from conditions determined in a screen using the commercial Morpheus kit (Molecular Dimensions). Phases were obtained from a single anomalous data (SAD) data-collection experiment (Table 3.2). The model was refined to R and R_{free} values of 20.7% and 24.7%, respectively, at a final resolution of 2.0 Å.

Table 3.3: X-ray crystallographic data collection and refinement statistics of *Af*Rom2 CNH domain

Data collection statistics	Se-met Rom2CNH	Rom2CNH_native
Wavelength (Å)	0.97961	0.92818
Resolution range (Å)*	92.33- 2.39	45.87- 2.01
Space group	$P2_12_12$	$P2_12_12$
Unit cell (Å)	77.0 92.3 52.3	78.0 93.7 52.6
	90.0 90.0 90.0	90.0 90.0 90.0
Total reflections	213616 (21388)	174698 (13083)
Unique reflections	15368 (1565)	26362 (1909)
Multiplicity	13.9 (13.7)	6.6 (6.9)
Completeness (%)	100 (100)	99.9 (100)
Mean I/σ(I)	16.7 (2.2)	17.4 (1.3)
R-merge	0.1 (1.4)	0.1 (1.3)
Refinement Statistics		
Resolution range (Å)	92.33- 2.391	45.87- 2.01
R-factor	0.31	0.20708
R-free (5%)	0.36	0.2478
Protein residues		310
Solvent molecules		61
RMSD (bonds, Å)		2.02
RMSD (angles, °)		0.13
Ramachandran favoured (%)		95.0
Ramachandran allowed (%)		3.6
Ramachandran disallowed (%)		1.4

The *Af*Rom2 CNH domain structure comprises residues 863 to 1194, with one region (loop residues 1001 to 1023) not defined in the electron density map. The *Af*Rom2 CNH domain folds into a seven-bladed WD40 structure. The WD40 proteins were first described in the GTPase binding protein bovine β-transducin (Fong et al., 1986; Sondek et al., 1996), which showed that the repeats formed a seven-bladed circular β-propeller fold, with each blade comprising a four-stranded anti-parallel β-sheets (Fig. 3.8A). The *Af*Rom2 CNH domain also formed a seven- bladed β-propeller fold, with a height (28 Å) similar to that of the reported β- transducin protein (25 Å) (Fig. 3.8AB). The overall shape of the *Af*Rom2 CNH domain is oval rather than circular, with the length (Cα - Cα) of the X-axis 1.5 times longer than that of the Y-axis. This is caused by the two-extended insertion loop-helix-loop regions between β8 β9 and between β17 β18 (Fig. 3.8AC). The insertion of α-helices into the blade region has never been observed in β-transducin or any other WD40 proteins, the functional implications of these two-extended regions are not yet known. From the structure based sequence alignment between the *Af*Rom2CNH domain and the WD40 domain from β-transducin (1GOT) (Fig. 3.8C), we can see that although the general sequence identity between *Af*Rom2 CNH and β-transducin is low (20%), the residues in the β sheet region are mostly conserved. This suggests that the conserved residues determine the general folding of the *Af*Rom2 CNH domain as a WD40 fold. The above observations show that the *Af*Rom2 CNH structure shares the similar seven bladed WD40 fold compared to the GTPase binding β-transducin, however with two additional insertion α-helices regions.

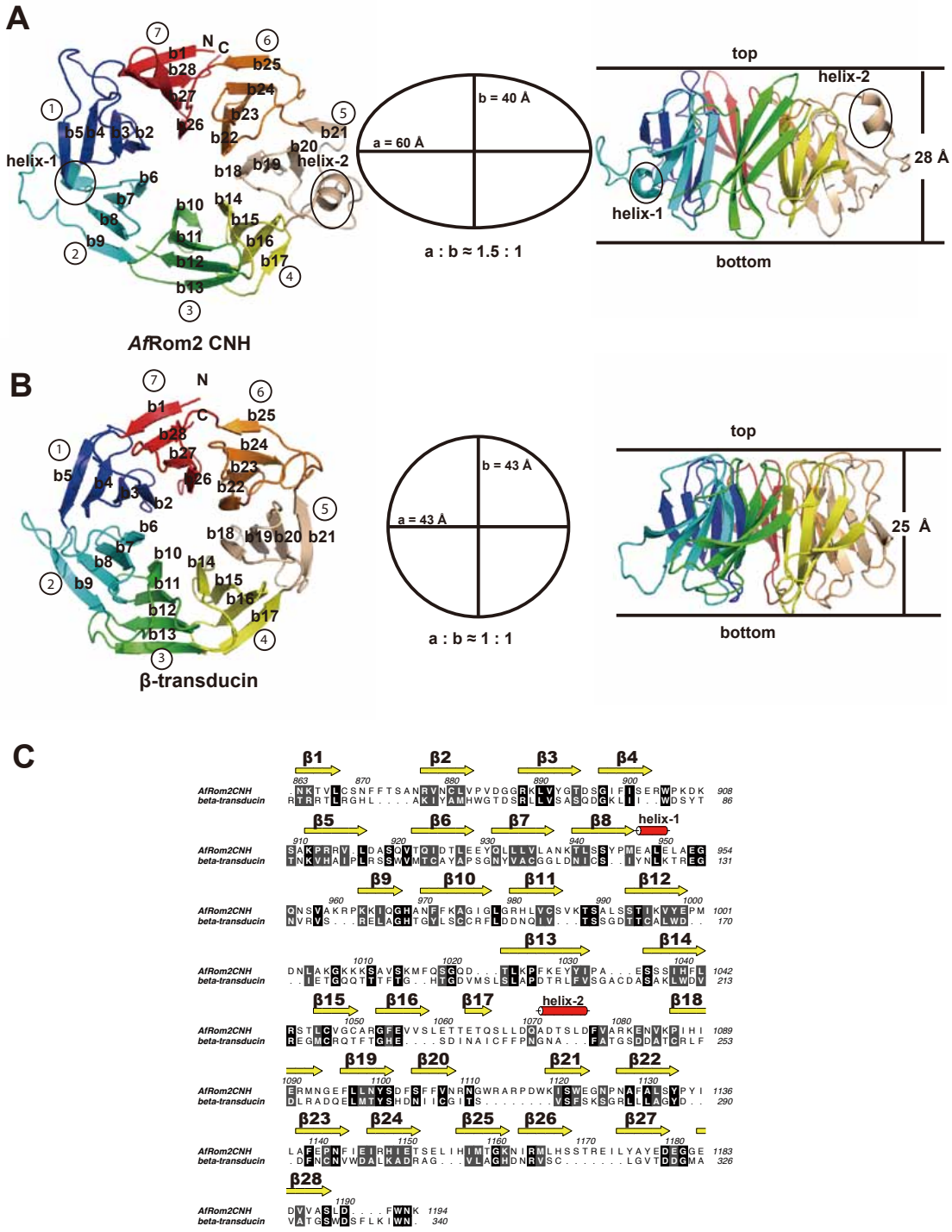

Figure 3.8: Overall structure of *Af*Rom2 CNH and comparison with bovine β-transducin

(A)(B) Cartoon representation of Rom2 CNH domain structure compared with the WD40 domain of bovine β-transducin (PDB:1tbg) (Lambright et al., 1996). The different blades of the seven-bladed β-propeller are coloured and labelled. The diameter and the height of the protein were

measured using COOT (Emsley and Cowtan, 2004). This and all subsequent structural figures were generated with PyMOL (DeLano, 2004).

(C) The structure based sequence alignment between the Rom2 CNH domain from *Aspergillus fumigatus* and bovine β-transducin (1tbg) was performed using ClustalW2 from the EMBL–EBI server. The aligned sequences are displayed according to the secondary structure using Aline (Bond and Schuttelkopf, 2009). Black represents identical, and grey represents conserved.

Another interesting observation is from the structure based sequence alignment, these two insertion α-helices were also found to be conserved in other CNH domain containing proteins, including the *Drosophila* and Human citron kinases (Fig. 3.9). This observation suggests that the two extended α-helices maybe the signature features of all CNH domain containing proteins.

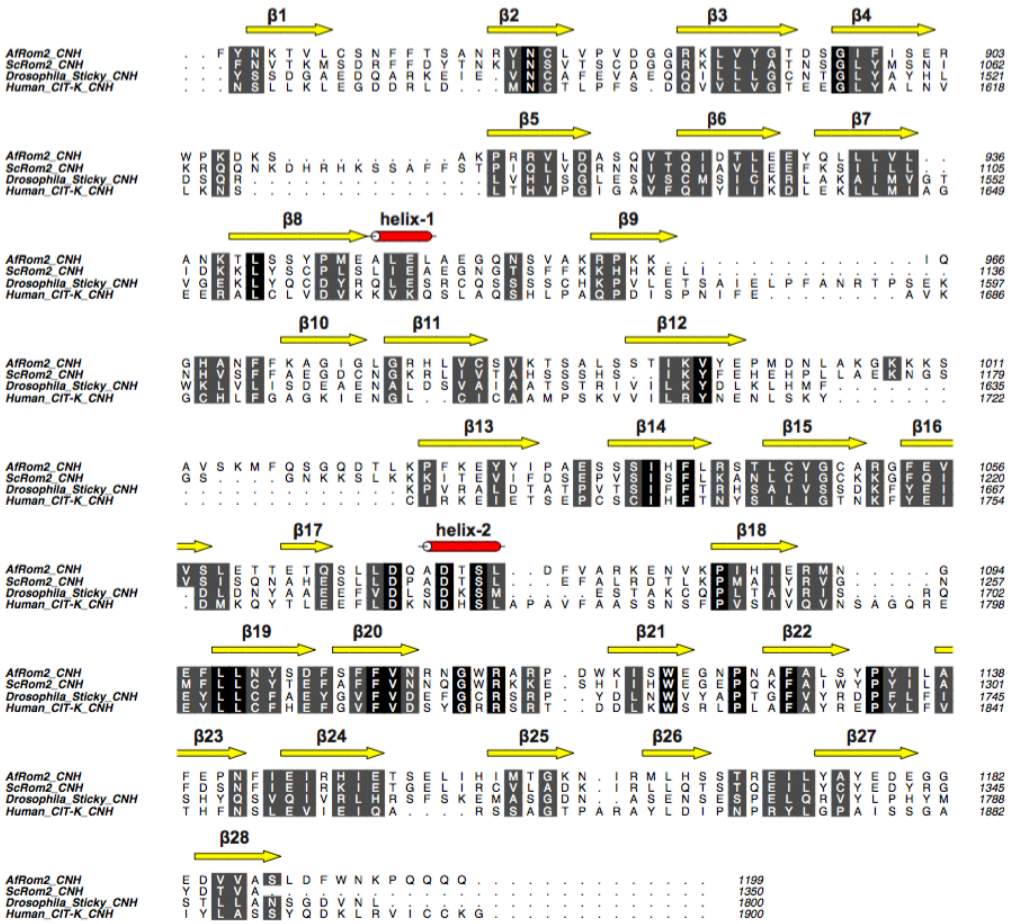

Figure 3.9*:* The sequence alignment of CNH domain containing proteins based on the AfRom2 CNH domain structure

The alignment of CNH domain among fungi Rom2 (*Aspergillus fumigatus* and *Saccharomyces cerevisiae)*, Human and *Drosophila* Citron kinases was performed using ClustalW2 from EMBL-EBI server. The aligned sequences are displayed according to the secondary structure using Aline (Bond and Schuttelkopf, 2009). Black represents identical and grey represents conserved. Secondary structures are annotated as observed from the *Af*Rom2 CNH domain structure.

3.3.6 An interaction mode of *Af*Rom2 CNH domain with *Af*Rho1 GTPase suggested by the transducin complex

The complex structure of the WD40 domain of β-transducin bound to the GTPase domain of α-transducin has already been described in the heterotrimeric bovine transducin complex (PDB code: 1GOT) (Lambright et al., 1996).

The transducin complex consists of three subunits which are α, β and γ (Fig 3.10A). The α-transducin has a GTPase core domain and an N-terminal extended helix region. The β-transducin has a seven bladed WD40 domain and also a N-terminal extended helix region. The γ-transducin contains two helix regions linked by a loop. The transducin complex belongs to the heterotrimeric G protein family, which is activated by the G protein-coupled receptor (GPCR), once activated the α-transducin changes the conformation from GDP bound to the GTP bound state and dissociates from the transducin complex, then activates the downstream effector proteins (Lambright et al., 1996). The β-transducin WD40 domain is essential for the organisation of the heterotrimeric transducin complex by forming multiple interactions with both the α and γ transducin through its versatile protein binding surface (Lambright et al., 1996). In the complex structure, the β-transducin WD40 domain uses the top surface to interact with the switch II helix from the α-transducin GTPase domain, two opposite side surfaces to interact with

both the N-terminal helix from α-transducin and the N-terminal helix from γ-transducin, and the bottom surface to interact with the C-terminal helix from γ-transducin (Fig 3.10A).

Since the structure of the *Af*Rom2 CNH domain is similar to that of the β-transducin WD40 domain (Fig. 3.8) and *Af*Rom2 CNH domain also interacts with a GTPase protein *Af*Rho1, I hypothesized that the *Af*Rom2 CNH domain interacts with *Af*Rho1 through a similar binding mode when compared to the structure of α β-transducin complex. To test that hypothesis, I decided to use the transducin complex structure as a guide to model the protein-protein interaction between *Af*Rom2 CNH domain and *Af*Rho1. The *Af*Rom2 CNH domain was superimposed to the β-transducin WD40 domain, with the core R.M.S.D. 3.2 Å, and the structure of *Af*Rho1 was superimposed to the GTPase domain of the α-transducin, with core R.M.S.D. 2.6 Å (Fig. 3.10AB).

From the superimposed structure model, an α-helix in the switch II region of *Af*Rho1 is overlapping with the corresponding α-helix from the GTPase domain in α-transducin that interacts with the β-transducin WD40 domain, the R.M.S.D. in this region is only 0.7 Å (Fig 3.10EF). The potential amino acid interactions between this switch II α-helix of *Af*Rho1 to the top surface of the CNH domain was also found to be conserved in the transducin complex (Fig. 3.10CD). In the transducin complex, the β-transducin Lys57 is forming a salt bridge interaction with Glu212 from the switch II α-helix in α-transducin, and in the superimposed model, this salt bridge interaction could be instead Arg877 from CNH domain to Asp76 from *Af*Rho1 at the exact same interaction position (Fig. 3.10BC). The conserved interactions have been observed at multiple sites at the superimposed CNH domain *Af*Rho1 complex model, for example, the hydrogen bond interaction between β-transducin Asn119 to α-transducin Gln200 is instead the hydrogen

bond between CNH domain His968 to *Af*Rho1 Tyr66, the hydrogen bond between β-transducin Thr143 to α-transducin Arg201 is instead a salt bridge interaction between CNH domain Lys987 to *Af*Rho1 Glu64, and the salt bridge interaction between β-transducin Asp228 to α-transducin Lys206 is instead a salt bridge interaction between CNH domain Glu1035 to *Af*Rho1 Arg68 (Fig. 3.10CD). The above observations led the interacting mode of *Af*Rom2 CNH domain with *Af*Rho1 to be proposed, which is mainly via the top surface of CNH domain and the α-helix in the switch II region of *Af*Rho1. Another interesting observation is the switch II helix is identical among the *Af*Rho1, *H. sapiens* RhoA and *Drosophila* Rho1 (Fig. 3.10E), which are all reported to interact with CNH domain or citron kinases, and the conserved CNH residues among *A. fumigatus, H. sapiens* and *Drosophila* are mainly on the top surface of CNH domain and are mostly charged or polar residues (Fig. 3.10F), which suggest our Rom2 CNH domain and *Af*Rho1 interacting model could also suggest the binding between the citron kinases CNH domains to their interacting Rho GTPases.

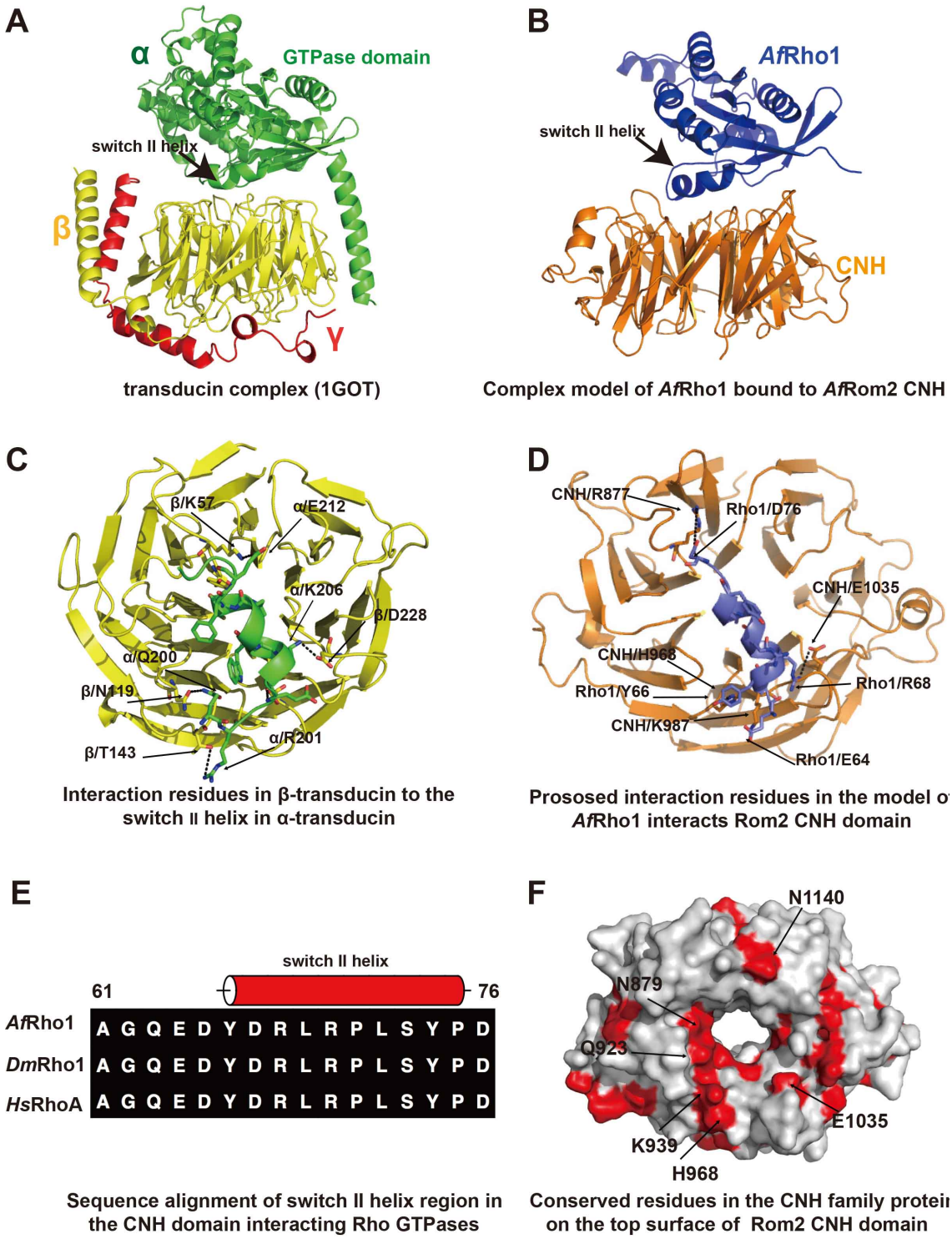

Figure 3.10: Binding surface comparison of *Af*Rom2 CNH domain with the bovine transducin complex

A) Cartoon illustration of transducin complex (PDB: 1GOT)

(B) Cartoon illustration of *Af*Rom2 CNH bound to *Af*Rho1 based on the transducin cpmplex

(C) Cartoon representation of reported interacting residues in the top surface of β-transducin to α-transducin (Lambright et al., 1996).

(**D)** Cartoon representation of conserved residues from the top surface of Rom2 CNH domain

interacts with Rho1 GTPase switch II helix region.

(E) Conserved residues in the Rho GTPase switch II helix from *Aspergillus fumigatus*, *Drosophila* and *H. sapiens*. The aligned sequences are displayed according to the secondary structure using Aline (Bond and Schuttelkopf, 2009). Black represents identical.

This binding mode is further confirmed in the *in vitro* binding assay, As shown in Fig 3.11A, both GDP- and GTP- binding *Af*Rho1 co-precipitated with *Af*Rom2CNH, suggesting *Af*Rom2 CNH domain bound to *Af*Rho1 irrespective of the nucleotide binding form, and this result is consistent with the previous observation of the binding between Rho GTPase and the citron kinase CNH domain in Drosophila (Bassi et al., 2011). However, for the *Af*Rho1 mutant protein to mutate the potential interacting charged residues (E64A, R68A, R70A, D76A) from the switch II helix into Alanine, the mutant protein showed diminished binding to the CNH domain (Fig 3.11B). The mutant *Af*Rho1 protein did not show increased instability from the Thermoshift experiment (Fig. 3.11C). We were also trying to express a CNH domain mutant, which to mutate the top surface charged potential interacting residues into Alanine, however the resulting protein was found insoluble. To conclude, the transducin complex suggests how Rho GTPaes and the CNH domain interact.

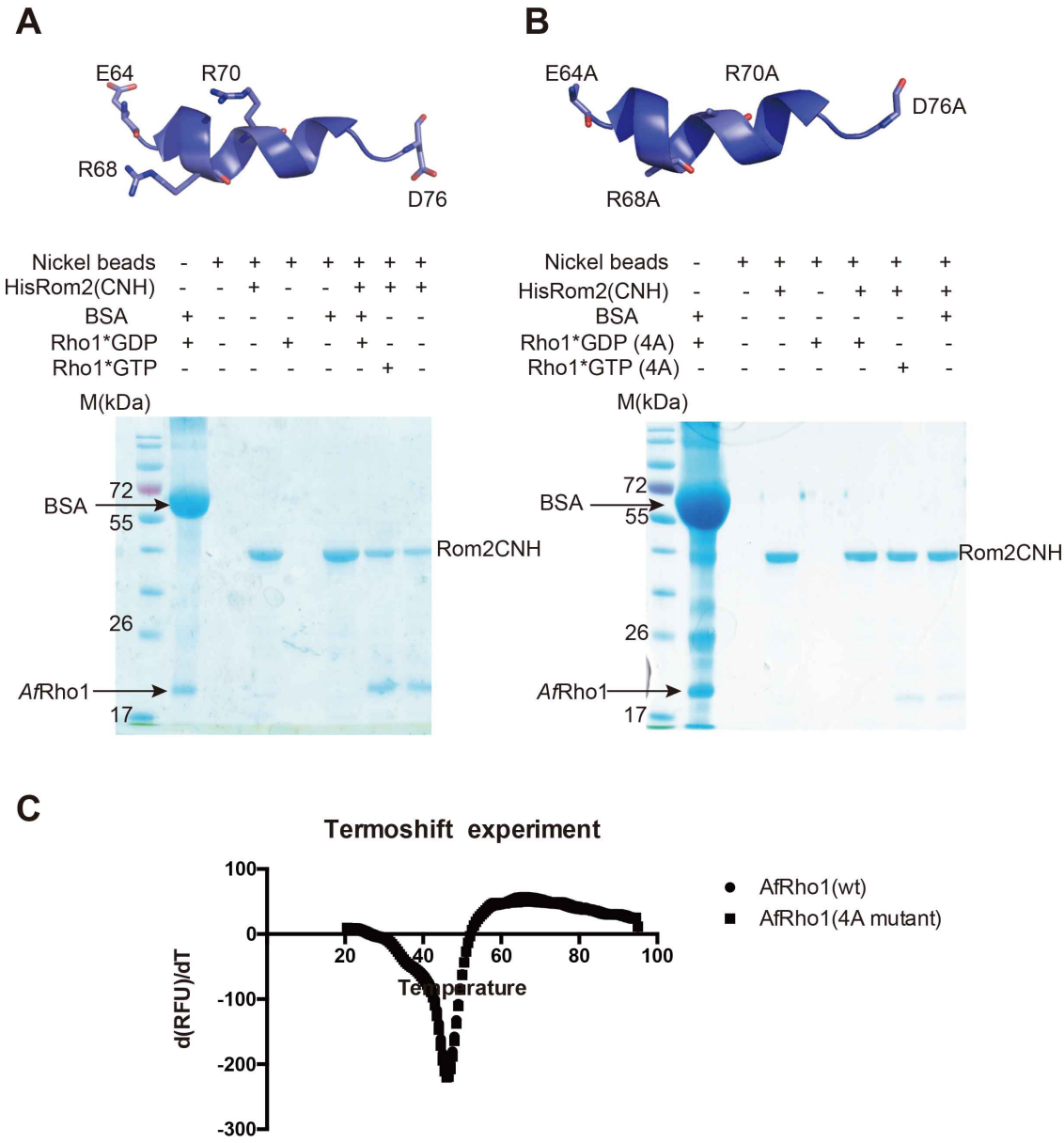

Figure 3.11: *In vitro* binding analysis of Rom2 CNH domain to *Af*Rho1, and to the *Af*Rho1 switch II helix mutant

(A)(B) The SDS page gel results to show the His tag pull- down assay to determine the *in vitro* interaction between Rom2 CNH domain to *Af*Rho1, and to the *Af*Rho1 switch II helix mutant (E64A, R68A, R70A, D76A). + means with, - means without.

(C) Differential scanning fluorimetry (DSF) to show the melting temperature of *Af*Rho1 compared to the *Af*Rho1 (E64A, R68A, R70A, D76A) mutant. The d(RFU)/dT graph was plotted using Prims6.

3.4 Discussion

The CNH domain is the signature C-terminal domain from the fungal Rho GEF Rom2 orthologue proteins, and the *H. sapiens* and *Drosophila* conserved citron kinases. However, it is unknown yet the exact cellular functions of the CNH domain and whether it is conserved among Rom2 and citron kinases. Our studies not only investigated the cellular functions of Rom2 CNH domain in the pathogenic fungus *A. fumigatus* by making *rom2Δcnh* mutant, but also proposed a binding mechanism between CNH domain and the important cell wall regulator protein Rho1 through structure modelling.

In our genetics research to investigate the functions of CNH domain in Rom2, we found *rom2Δcnh* mutant shares several cell wall defective phenotypes with the full length *rom2* knockdown mutant (Figure 3.3 and Figure 3.4). Interestingly, in *Drosophila* melanogaster the CNH domain containing citron kinase Sticky plays important cellular functions in the process of cytokinesis, and the StickyΔCNH could not fully rescue the cytokinesis defects caused by the RNAi depletion of Sticky (Bassi et al., 2011). Collectively, our results and the work in *Drosophila* citron kinase suggest, the C-terminal CNH domain is required for the cellular functions of fungal Rom2 protein and citron kinases.

In *Aspergillus fumigatus*, Rom2 regulates the cell wall synthesis mainly through the downstream Rho1 GTPase. In this research, Rho1 was found to interact with the Rom2 CNH domain by the pull-down Mass spec experiment (Fig. 3.5), and from the *in vitro* binding assay *Af*Rho1 was found to bound to the CNH domain independent of GTP or GDP binding state (Fig. 3.6), which suggests the Rom2 CNH domain is a bona fide *Af*Rho1 binding partner. Coincidentally, the CNH domain containing citron kinase was initially identified as a RhoA effector from the *H. sapiens* cell line, and the subsequent research in *Drosophila* and *H.*

sapiens cells has shown that the citron kinase is required for the cellular localization of RhoA (Bassi et al., 2011; Gai et al., 2011; Madaule et al., 1998). In *Drosophila*, the citron kinase CNH domain was found to interact with both wild type and constitutively active Rho1 mutant by yeast two-hybrid assay and the pull-down experiment, which is consistent with our *in vitro* findings (Bassi et al., 2011). However, in *Drosophila* the CNH domain is not required for the cellular localization of Rho1, since Sticky∆CNH can still rescue the Rho1 localization after the depletion of the endogenous Sticky (Bassi et al., 2011). In *Aspergillus fumigatus*, *Af*Rom2 protein shares the similar cellular localization pattern with *Af*Rho1 to the fungal hyphal tips (Samantaray et al., 2013), however it is not further investigated whether the localization of *Af*Rho1 is dependent on *Af*Rom2 or the Rom2 CNH domain.

The structure of *Af*Rom2 CNH domain was solved in this research as a seven bladed β-propeller (Fig. 3.8), which belongs to the WD40 family proteins. In nature, the WD40 protein is known to function as protein-protein interaction platform due to its versatile binding surface (Stirnimann et al., 2010; Xu and Min, 2011). In the CNH domain pull-down MS experiment, we have identified the potential protein binding partners of the *Af*Rom2 CNH domain *in cellulo* (Figure 5). Among all in total 175 protein binding hits identified, there are two proteins (*Af*Rho1 and Chitin Synthase G), were previously reported to regulate the synthesis of two major components of the cell wall, glucan and chitin individually (Table 3.2) (Beauvais et al., 2001; Borgia et al., 1996). A hypothesis which has not been tested yet, is the important cell wall regulating function of the Rom2 CNH domain is through mediating the interaction of Rho1 GTPase with the cell wall synthesizing enzymes such as Chitin synthase G. The rest of the potential protein binding hits are also need to be further confirmed and investigated, and

the research from that will help to reveal other cellular functions of the *Af*Rom2 CNH domain and the underlying molecular mechanisms.

The structure of *Af*Rho1 was also solved in this research to further investigate the interaction of Rho GTPase to the CNH domain at the atomic level (Fig. 2.2). Based on the WD40 domain interacts with GTPase domain transducin complex (Wall et al., 1995), we proposed a model to show the interaction of Rho GTPase and the CNH domain is mainly though the top surface of the CNH domain and an α-helix in the switch II region of Rho GTPases (Fig. 3.10). The importance of the Rho switch II α-helix in mediating the binding is confirmed by making mutants and tested in the *in vitro* binding assay (Fig. 3.11). Interestingly, the Rho switch II α-helix is found to be identical among *Af*Rho1, *Drosophila* Rho1 and *H. sapiens* RhoA, which all have been reported to interact with the CNH domain containing proteins, the top surface of CNH domain was also found to be conserved among these three organisms, which suggest the binding mode we proposed in this study could be a conserved binding mechanism of Rho GTPases bind to CNH domain containing proteins （Fig. 3.11）. However, to final confirm the proposed binding mode of *Af*Rom2 CNH bound to *Af*Rho1 observed from the superimposed model, it is still necessary to solve the actual crystal structure of this complex.

As the first solved CNH domain structure, the structure of *Af*Rom2 CNH domain could also be used as a model to study the structure function relationship of the CNH domain containing citron kinases. For example, our superimposed model to show the interaction between the *Af*Rom2 CNH domain and *Af*Rho1 could also be used to speculate the binding model of CNH domain from citron kinase to the Rho orthologue GTPases. In recent research, it has also shown that the CNH domain bound strongly to the important cytokinesis regulators, INCENP,

Borealine and Aurora B (McKenzie et al., 2016). Our CNH domain structure will be helpful to understand the binding in a much more detail.

4.1 Fragment based inhibitor discovery of *Af*Rho1

*Af*Rho1 from the pathogenic fungus *A. fumigatus* is an essential protein and regulates the synthesis of one major component of the cell wall β-1,3-glucan (Beauvais et al., 2001; Dichtl et al., 2012). Therefore, *Af*Rho1 is a potential therapeutic target against fungal infections. *Af*Rho1 is a GDP/GTP binding protein, belongs to the small Rho GTPase family, and shares 70% sequence identity with a human orthologue protein *Hs*RhoA. Rho GTPase inhibitor discovery has been attracting a lot of attentions, because the Rho GTPase upregulation in human cells has been related to many cancer types (Bellizzi et al., 2008; Faried et al., 2007; Kamai et al., 2003). However, the Rho GTPases have been considered as difficult targets, because of the globular structure and the lack of apparent pockets at the surface. In this research, I have combined x-ray crystallography and a fragment-based approach to develop a novel inhibitor against *Af*Rho1. A fragment compound DDD01511162 was found from a BLI based fragment screen against *Af*Rho1 with a binding affinity around 300 μM (Fig 2.4). A complex structure of *Af*Rho1 and the fragment DDD01511162 was obtained by x-ray crystallography which revealed the binding mode at the atomic level (Fig 2.5). From the complex structure, the fragment DDD01511162 was shown binding with *Af*Rho1 in a 2: 1 molar ratio, with two fragments bound adjacently to a surface pocket (Fig 2.6). From the structural comparison of *Af*Rho1 with the published *Hs*RhoA complex structures, the fragments binding pocket was found to be conserved with *Hs*RhoA and at the interface between *Hs*RhoA and the upstream GEF protein LARG (Kristelly et al., 2004). Based on these observations, the fragment DDD01511162 was then shown to inhibit the protein-protein interaction of *Af*Rho1/*Hs*RhoA with their corresponding GEF proteins, and the GEF mediated Rho activation (Fig 2.7). However, with the low

binding affinity of the initial fragment compound to the target protein (300 μM to *Af*Rho1 and 500 μM to *Hs*RhoA), the cellular effects of the inhibition cannot be tested yet, therefore a further optimisation of the fragment hit is needed.

There are three main approaches for optimising the initial fragment hit into high potency compounds, which are: fragment merging, linking and growing (Scott et al., 2012). Fragment merging is to incorporate the overlapping structural components into the fragment hit from other chemical entities bound to the same pockets, which can be other fragment hits, substrates or known ligands (Erlanson et al., 2004). The known application of this approach is the fragment screen against Hsp90, the merged molecule increased the IC_{50} from the initial 350 μM to the final 0.9 μM (Brough et al., 2009). Fragment linking is theoretically the most efficient way for fragment elaboration. It means to efficiently link two fragments binding at non-overlapping sites but with close proximity. This is because in theory, the linking compound will significantly reduce the Gibbs free energy from the sum of the two individual fragments. For example, for the thrombin inhibitor discovery, the linking of two fragments with individual IC_{50} from 100- 300 μM resulted in a compound with an IC_{50} of 1.4 nM (Howard et al., 2006). Fragment growing is the most widely used and the most time-consuming approach for fragment optimisation. It needs step by step chemical modifications of the initial fragment hit to fully explore the binding environment. An example of such approach is the FBDD against Pin1, the IC_{50} of the initial fragment is 180 μM, the potency was increased to 2.0 μM when adding a chlorine atom and a benzylic amide group to the phenyl ring of the fragment (Potter et al., 2010).

For my *Af*Rho1 FBDD project, the preferred approach for the fragment optimisation is without doubt by fragment linking as I found two identical fragments bound to *Af*Rho1 with proximity. A compound by linking the two bound

fragments together is predicted to significantly increase the potency based on the previous examples (Howard et al., 2006; Schuttelkopf et al., 2011). There are currently two options of linking these two fragments together. Option one is to link the two fragments according to the orientation of the two fragments we observed from the complex structure, which is to link the primer amine group from one of the fragments to one of the methyl arms from the other fragment (Fig. 2.10 B). And option two is to link the two fragments together, by linking the two methyl arms of the two fragments (Fig. 2.10 C). We are now choosing option one for the further fragment optimisation, because of intermediate molecules for the option two has been found decreased binding to *Af*Rho1 (Fig. 2.11). The optimised compound will first be tested by measuring the IC_{50} for the *in vitro* GEF inhibition activity and then the *A. fumigatus* cells, in the hope to create a phenotype that is similar to the *Af*Rho1 knockout mutants (Dichtl et al., 2012).

Another great potential of the final fragment-optimised compound from this project is to use against cancer cells. Since the initial fragment also bound to *Hs*RhoA (Fig 2.7), which is a known anti-cancer target (Bellizzi et al., 2008). The previous virtual screen against *Hs*RhoA has identified a compound named Rhosin, which bound to *Hs*RhoA with K_d around 300 nM (Shang et al., 2012). However, this compound has never entered into clinical trials, as no structural information is available, and the further optimisation of the compound is therefore limited. Interestingly to notice, the predicted binding pocket of Rhosin to *Hs*RhoA is the exact same binding pocket I found in *Af*Rho1 which is centred by the key conserved residue Try58 (Shang et al., 2012). These observations gave us great confidence that our fragment-lead molecule will also bind to *Hs*RhoA, and has the potential to be used as an anti-cancer treatment by inhibiting the *Hs*RhoA activity.

4.2 The potential of using *Af*Rom2 CNH domain as a selective anti-fungal target

In my *Af*Rho1 structural biology and fragment screen research, I have identified a fragment bound pocket in *Af*Rho1. The bound fragment has a great potential to be developed into a high affinity inhibitor against the protein-protein interaction between *Af*Rho1 and the upstream GEF protein. However, this fragment bound pocket was found to be identical in the human orthologue protein *Hs*RhoA (Fig 2.7). Thus, when considering target selectivity for the anti-fungal treatment, this fragment bound pocket I found is still not an optimal drug target, although *Hs*RhoA was also considered as an anti-cancer target (Shang et al., 2012). And this is due to the high sequence identity between these two proteins, which caused the surface binding properties of these two orthologues to be highly similar.

Therefore, I was very keen to identify a fungal specific target in the hope to achieve selectivity. The Rom2 orthologue protein as the upstream GEF to Rho1 GTPase has been shown as essential in several pathogenic fungi, including *A. fumigatus, C. glabrata and C. albicans* (Kanno et al., 2015; Samantaray et al., 2013). Rom2 protein was also found to be highly conserved in fungi but less homologous to that of *H. sapiens* Rho GEF proteins (Kanno et al., 2015). The reason for that is in addition to the conserved GEF activity (DH-PH) domains, there are also two protein domains (N-terminal DEP domain and C-terminal CNH domain) only found in fungal Rom2 orthologues but not in the human orthologue Rho GEF proteins (Fig 1.11). The N-terminal DEP domain was studied in a Rom2 orthologue in the filamentous fungus *N. crassa* (Richthammer et al., 2012), which proposed the function of this domain as a self-inhibitory regulator to the intrinsic

GEF activity. The C-terminal CNH domain, however, has never been studied before in fungal Rom2 proteins.

In my research, I have created a *rom2Δcnh* mutant, to show that the CNH domain is not only unique, but also important for the colony growth and cell wall organization in *A. fumigatus* (Fig. 3.3 3.4). The colony growth and cell wall defective phenotypes of the *rom2Δcnh* mutant was also very similar to that of the *rom2* knockdown mutant (Samantaray et al., 2013), which suggests the full cellular functions of the Rom2 protein is largely dependent on the existence of the C-terminal CNH domain. These results have already suggested that the *Af*Rom2 CNH domain could be considered as a potential selective target for the anti-fungal development. However, the exact molecular functions of this domain still need to be investigated.

In my CNH domain pull-down MS experiment, I have identified the potential protein binding partners of the *Af*Rom2 CNH domain *in cellulo* (Fig. 3.5). Among the total 175 protein binding hits identified, there are two proteins (*Af*Rho1 and Chitin Synthase G), were previously reported to be involved in regulating the synthesis of two major components of the cell wall, glucan and chitin individually (Table 3.2) (Beauvais et al., 2001; Borgia et al., 1996). A hypothesis which has not been tested yet, is the important cell wall regulating function of the *Af*Rom2 CNH domain is through the interaction to the two protein binding hits (*Af*Rho1 and Chitin Synthase G). The rest of the potential protein binding hits are also need to be further confirmed and investigated, and the research from that will help to reveal other cellular functions of the *Af*Rom2 CNH domain and the underlying molecular mechanisms.

To understand the molecular basis of the *Af*Rom2 CNH domain bound to important cellular components, the structure of this domain was solved by X-ray

crystallography. The structure of the *Af*Rom2 CNH domain was shown as a seven bladed β-propeller (Fig 3.10), which belongs to the WD40 family proteins. In nature, the WD40 protein is known to function as a protein-protein interaction platform due to its versatile binding surface (Stirnimann et al., 2010; Xu and Min, 2011). Among all the WD40 family proteins, the β-subunit of transducin was known to interact with a GTPase domain and also a seven-bladed propeller (Wall et al., 1995), therefore the β-transducin was used to predict the binding mode of the *Af*Rom2 CNH domain to *Af*Rho1. From the superimposed structure model, I proposed the potential binding mode of the *Af*Rom2 CNH domain to *Af*Rho1 is mainly through the top surface of the CNH domain and an α-helix in the switch II region of Rho GTPases (Fig 3.11). Although there is no clear evidence so far, the protein-protein interaction between *Af*Rho1 and *Af*Rom2 CNH is very likely to be important in *A. fumigatus*. Therefore, a chemical compound to interrupt this interaction could potentially become a therapeutic approach for treatment of the *A. fumigatus* invasive fungal conditions. Although the CNH domain can also be found in human citron kinases, the sequence identity between the *Af*Rom2 CNH domain to the closest human orthologue protein is only around 20% (Fig. 3.1B), which means the chance of finding a selective compound binding pocket is high. Therefore, in this research I have identified the *Af*Rom2 CNH domain as a potential selective target for the anti-fungal development, my structural biology study of this domain also provides the molecular basis for the future drug discovery.

List of References:

(2008). Molecular replacement. Proceedings of the CCP4 study weekend, University of Reading, United Kingdom. Acta Crystallogr D Biol Crystallogr *64*, 1-140.
Abad, A., Fernandez-Molina, J.V., Bikandi, J., Ramirez, A., Margareto, J., Sendino, J., Hernando, F.L., Ponton, J., Garaizar, J., and Rementeria, A. (2010). What makes Aspergillus fumigatus a successful pathogen? Genes and molecules involved in invasive aspergillosis. Rev Iberoam Micol *27*, 155-182.
Agarwal, R., Chakrabarti, A., Shah, A., Gupta, D., Meis, J.F., Guleria, R., Moss, R., Denning, D.W., and group, A.c.a.I.w. (2013). Allergic bronchopulmonary aspergillosis: review of literature and proposal of new diagnostic and classification criteria. Clin Exp Allergy *43*, 850-873.
Al-Shboul, O., Nalli, A.D., Kumar, D.P., Zhou, R., Mahavadi, S., Kuemmerle, J.F., Grider, J.R., and Murthy, K.S. (2014). Jun kinase-induced overexpression of leukemia-associated Rho GEF (LARG) mediates sustained hypercontraction of longitudinal smooth muscle in inflammation. Am J Physiol Cell Physiol *306*, C1129-1141.
Algire, M.A. (2013). Restrictionless cloning. Methods Enzymol *529*, 125-134.
Arellano, M., Duran, A., and Perez, P. (1996). Rho 1 GTPase activates the (1-3)beta-D-glucan synthase and is involved in Schizosaccharomyces pombe morphogenesis. EMBO J *15*, 4584-4591.
Armitt, S., McCullough, W., and Roberts, C.F. (1976). Analysis of acetate non-utilizing (acu) mutants in Aspergillus nidulans. J Gen Microbiol *92*, 263-282.
Bains, S.N., and Judson, M.A. (2012). Allergic bronchopulmonary aspergillosis. Clin Chest Med *33*, 265-281.
Balakrishnan, A.R., and Easwaran, K.R. (1993). CD and NMR studies on the aggregation of amphotericin-B in solution. Biochim Biophys Acta *1148*, 269-277.
Bassi, Z.I., Verbrugghe, K.J., Capalbo, L., Gregory, S., Montembault, E., Glover, D.M., and D'Avino, P.P. (2011). Sticky/Citron kinase maintains proper RhoA localization at the cleavage site during cytokinesis. J Cell Biol *195*, 595-603.
Beauvais, A., Bruneau, J.M., Mol, P.C., Buitrago, M.J., Legrand, R., and Latge, J.P. (2001). Glucan synthase complex of Aspergillus fumigatus. J Bacteriol *183*, 2273-2279.
Beauvais, A., Drake, R., Ng, K., Diaquin, M., and Latge, J.P. (1993). Characterization of the 1,3-beta-glucan synthase of Aspergillus fumigatus. J Gen Microbiol *139*, 3071-3078.
Bellizzi, A., Mangia, A., Chiriatti, A., Petroni, S., Quaranta, M., Schittulli, F., Malfettone, A., Cardone, R.A., Paradiso, A., and Reshkin, S.J. (2008). RhoA protein expression in primary breast cancers and matched lymphocytes is associated with progression of the disease. Int J Mol Med *22*, 25-31.
Bennett, J.W. (2010). An Overview of the Genus Aspergillus. Aspergillus: Molecular Biology and Genomics, 1-17.
Bickle, M., Delley, P.A., Schmidt, A., and Hall, M.N. (1998). Cell wall integrity modulates RHO1 activity via the exchange factor ROM2. EMBO J *17*, 2235-2245.
Bond, C.S., and Schuttelkopf, A.W. (2009). ALINE: a WYSIWYG protein-sequence alignment editor for publication-quality alignments. Acta Crystallogr D Biol Crystallogr *65*, 510-512.
Borgia, P.T., Iartchouk, N., Riggle, P.J., Winter, K.R., Koltin, Y., and Bulawa, C.E. (1996). The chsB gene of Aspergillus nidulans is necessary for normal hyphal growth and development. Fungal Genet Biol *20*, 193-203.

Bowman, S.M., and Free, S.J. (2006). The structure and synthesis of the fungal cell wall. Bioessays *28*, 799-808.
Bradford, M.M. (1976). A rapid and sensitive method for the quantitation of microgram quantities of protein utilizing the principle of protein-dye binding. Anal Biochem *72*, 248-254.
Brough, P.A., Barril, X., Borgognoni, J., Chene, P., Davies, N.G., Davis, B., Drysdale, M.J., Dymock, B., Eccles, S.A., Garcia-Echeverria, C.*, et al.* (2009). Combining hit identification strategies: fragment-based and in silico approaches to orally active 2-aminothieno[2,3-d]pyrimidine inhibitors of the Hsp90 molecular chaperone. J Med Chem *52*, 4794-4809.
Brown, G.D., Denning, D.W., Gow, N.A., Levitz, S.M., Netea, M.G., and White, T.C. (2012). Hidden killers: human fungal infections. Sci Transl Med *4*, 165rv113.
Cabib, E., Roh, D.H., Schmidt, M., Crotti, L.B., and Varma, A. (2001). The yeast cell wall and septum as paradigms of cell growth and morphogenesis. J Biol Chem *276*, 19679-19682.
Chen, S.C., Slavin, M.A., and Sorrell, T.C. (2011). Echinocandin antifungal drugs in fungal infections: a comparison. Drugs *71*, 11-41.
Chircop, M. (2014). Rho GTPases as regulators of mitosis and cytokinesis in mammalian cells. Small GTPases *5*.
Collaborative Computational Project, N. (1994). The CCP4 suite: programs for protein crystallography. Acta Crystallogr D Biol Crystallogr *50*, 760-763.
Congreve, M., Carr, R., Murray, C., and Jhoti, H. (2003). A 'rule of three' for fragment-based lead discovery? Drug Discov Today *8*, 876-877.
Cowen, L.E. (2008). The evolution of fungal drug resistance: modulating the trajectory from genotype to phenotype. Nat Rev Microbiol *6*, 187-198.
Cowtan, K., Emsley, P., and Wilson, K.S. (2011). From crystal to structure with CCP4. Acta Crystallogr D Biol Crystallogr *67*, 233-234.
Dagenais, T.R., and Keller, N.P. (2009). Pathogenesis of Aspergillus fumigatus in Invasive Aspergillosis. Clin Microbiol Rev *22*, 447-465.
Dean, S.O., and Spudich, J.A. (2006). Rho kinase's role in myosin recruitment to the equatorial cortex of mitotic Drosophila S2 cells is for myosin regulatory light chain phosphorylation. PLoS One *1*, e131.
DeLano, W.L. (2004). Use of PYMOL as a communications tool for molecular science. Abstr Pap Am Chem S *228*, U313-U314.
Denning, D.W., Pleuvry, A., and Cole, D.C. (2013). Global burden of allergic bronchopulmonary aspergillosis with asthma and its complication chronic pulmonary aspergillosis in adults. Med Mycol *51*, 361-370.
Deresinski, S.C., and Stevens, D.A. (2003). Caspofungin. Clin Infect Dis *36*, 1445-1457.
Dichtl, K., Ebel, F., Dirr, F., Routier, F.H., Heesemann, J., and Wagener, J. (2010). Farnesol misplaces tip-localized Rho proteins and inhibits cell wall integrity signalling in Aspergillus fumigatus. Mol Microbiol *76*, 1191-1204.
Dichtl, K., Helmschrott, C., Dirr, F., and Wagener, J. (2012). Deciphering cell wall integrity signalling in Aspergillus fumigatus: identification and functional characterization of cell wall stress sensors and relevant Rho GTPases. Mol Microbiol *83*, 506-519.
Dichtl, K., Samantaray, S., Aimanianda, V., Zhu, Z., Prevost, M.C., Latge, J.P., Ebel, F., and Wagener, J. (2015). Aspergillus fumigatus devoid of cell wall beta-1,3-glucan is viable, massively sheds galactomannan and is killed by septum formation inhibitors. Mol Microbiol *95*, 458-471.

Dichtl, K., Samantaray, S., and Wagener, J. (2016). Cell wall integrity signalling in human pathogenic fungi. Cell Microbiol *18*, 1228-1238.
Diviani, D., Raimondi, F., Del Vescovo, C.D., Dreyer, E., Reggi, E., Osman, H., Ruggieri, L., Gonano, C., Cavin, S., Box, C.L.*, et al.* (2016). Small-Molecule Protein-Protein Interaction Inhibitor of Oncogenic Rho Signaling. Cell Chem Biol *23*, 1135-1146.
Dotis, J., Simitsopoulou, M., Dalakiouridou, M., Konstantinou, T., Panteliadis, C., Walsh, T.J., and Roilides, E. (2008). Amphotericin B formulations variably enhance antifungal activity of human neutrophils and monocytes against Fusarium solani: comparison with Aspergillus fumigatus. J Antimicrob Chemother *61*, 810-817.
Douglas, C.M. (2001). Fungal beta(1,3)-D-glucan synthesis. Med Mycol *39 Suppl 1*, 55-66.
Douglas, C.M., Foor, F., Marrinan, J.A., Morin, N., Nielsen, J.B., Dahl, A.M., Mazur, P., Baginsky, W., Li, W., el-Sherbeini, M.*, et al.* (1994). The Saccharomyces cerevisiae FKS1 (ETG1) gene encodes an integral membrane protein which is a subunit of 1,3-beta-D-glucan synthase. Proceedings of the National Academy of Sciences of the United States of America *91*, 12907-12911.
Dransart, E., Olofsson, B., and Cherfils, J. (2005). RhoGDIs revisited: novel roles in Rho regulation. Traffic *6*, 957-966.
Drgonova, J., Drgon, T., Tanaka, K., Kollar, R., Chen, G.C., Ford, R.A., Chan, C.S., Takai, Y., and Cabib, E. (1996). Rho1p, a yeast protein at the interface between cell polarization and morphogenesis. Science *272*, 277-279.
Dubois, M., Gilles, K., Hamilton, J.K., Rebers, P.A., and Smith, F. (1951). A colorimetric method for the determination of sugars. Nature *168*, 167.
Echols, N., Grosse-Kunstleve, R.W., Afonine, P.V., Bunkoczi, G., Chen, V.B., Headd, J.J., McCoy, A.J., Moriarty, N.W., Read, R.J., Richardson, D.C.*, et al.* (2012). Graphical tools for macromolecular crystallography in PHENIX. J Appl Crystallogr *45*, 581-586.
Emsley, P., and Cowtan, K. (2004). Coot: model-building tools for molecular graphics. Acta Crystallogr D Biol Crystallogr *60*, 2126-2132.
Erlanson, D.A., Fesik, S.W., Hubbard, R.E., Jahnke, W., and Jhoti, H. (2016). Twenty years on: the impact of fragments on drug discovery. Nat Rev Drug Discov *15*, 605-619.
Erlanson, D.A., McDowell, R.S., and O'Brien, T. (2004). Fragment-based drug discovery. J Med Chem *47*, 3463-3482.
Fang, W., Du, T., Raimi, O.G., Hurtado-Guerrero, R., Urbaniak, M.D., Ibrahim, A.F., Ferguson, M.A., Jin, C., and van Aalten, D.M. (2013). Genetic and structural validation of Aspergillus fumigatus UDP-N-acetylglucosamine pyrophosphorylase as an antifungal target. Mol Microbiol *89*, 479-493.
Fang, W., Yu, X., Wang, B., Zhou, H., Ouyang, H., Ming, J., and Jin, C. (2009). Characterization of the Aspergillus fumigatus phosphomannose isomerase Pmi1 and its impact on cell wall synthesis and morphogenesis. Microbiology *155*, 3281-3293.
Faried, A., Faried, L.S., Usman, N., Kato, H., and Kuwano, H. (2007). Clinical and prognostic significance of RhoA and RhoC gene expression in esophageal squamous cell carcinoma. Ann Surg Oncol *14*, 3593-3601.
Fernandez-Garcia, R., de Pablo, E., Ballesteros, M.P., and Serrano, D.R. (2017). Unmet clinical needs in the treatment of systemic fungal infections: the role of amphotericin B and drug targeting. Int J Pharm.
Fong, H.K., Hurley, J.B., Hopkins, R.S., Miake-Lye, R., Johnson, M.S., Doolittle, R.F., and Simon, M.I. (1986). Repetitive segmental structure of the transducin beta subunit: homology with the CDC4 gene and identification of related mRNAs. Proc Natl Acad Sci U S A *83*, 2162-2166.

Fontaine, T., Simenel, C., Dubreucq, G., Adam, O., Delepierre, M., Lemoine, J., Vorgias, C.E., Diaquin, M., and Latge, J.P. (2000). Molecular organization of the alkali-insoluble fraction of Aspergillus fumigatus cell wall. J Biol Chem *275*, 27594-27607.
Fortwendel, J.R., Fuller, K.K., Stephens, T.J., Bacon, W.C., Askew, D.S., and Rhodes, J.C. (2008). Aspergillus fumigatus RasA regulates asexual development and cell wall integrity. Eukaryot Cell *7*, 1530-1539.
Free, S.J. (2013). Fungal cell wall organization and biosynthesis. Adv Genet *81*, 33-82.
Fritz, G., Brachetti, C., Bahlmann, F., Schmidt, M., and Kaina, B. (2002). Rho GTPases in human breast tumours: expression and mutation analyses and correlation with clinical parameters. Br J Cancer *87*, 635-644.
Gai, M., Camera, P., Dema, A., Bianchi, F., Berto, G., Scarpa, E., Germena, G., and Di Cunto, F. (2011). Citron kinase controls abscission through RhoA and anillin. Mol Biol Cell *22*, 3768-3778.
Gao, Y., Dickerson, J.B., Guo, F., Zheng, J., and Zheng, Y. (2004). Rational design and characterization of a Rac GTPase-specific small molecule inhibitor. Proc Natl Acad Sci U S A *101*, 7618-7623.
Gastebois, A., Clavaud, C., Aimanianda, V., and Latge, J.P. (2009). Aspergillus fumigatus: cell wall polysaccharides, their biosynthesis and organization. Future microbiology *4*, 583-595.
Gomez del Pulgar, T., Benitah, S.A., Valeron, P.F., Espina, C., and Lacal, J.C. (2005). Rho GTPase expression in tumourigenesis: evidence for a significant link. Bioessays *27*, 602-613.
Gruneberg, U., Neef, R., Li, X., Chan, E.H., Chalamalasetty, R.B., Nigg, E.A., and Barr, F.A. (2006). KIF14 and citron kinase act together to promote efficient cytokinesis. J Cell Biol *172*, 363-372.
Guilluy, C., Sauzeau, V., Rolli-Derkinderen, M., Guerin, P., Sagan, C., Pacaud, P., and Loirand, G. (2005). Inhibition of RhoA/Rho kinase pathway is involved in the beneficial effect of sildenafil on pulmonary hypertension. Br J Pharmacol *146*, 1010-1018.
Hajduk, P.J., Meadows, R.P., and Fesik, S.W. (1997). Discovering high-affinity ligands for proteins. Science *278*, 497,499.
Harner, M.J., Frank, A.O., and Fesik, S.W. (2013). Fragment-based drug discovery using NMR spectroscopy. Journal of biomolecular NMR *56*, 65-75.
Hopkins, A.L., and Groom, C.R. (2002). The druggable genome. Nature reviews. Drug discovery *1*, 727-730.
Hopkins, A.L., and Groom, C.R. (2003). Target analysis: a priori assessment of druggability. Ernst Schering Research Foundation workshop, 11-17.
Howard, N., Abell, C., Blakemore, W., Chessari, G., Congreve, M., Howard, S., Jhoti, H., Murray, C.W., Seavers, L.C., and van Montfort, R.L. (2006). Application of fragment screening and fragment linking to the discovery of novel thrombin inhibitors. J Med Chem *49*, 1346-1355.
Jank, T., Bogdanovic, X., Wirth, C., Haaf, E., Spoerner, M., Bohmer, K.E., Steinemann, M., Orth, J.H., Kalbitzer, H.R., Warscheid, B.*, et al.* (2013). A bacterial toxin catalyzing tyrosine glycosylation of Rho and deamidation of Gq and Gi proteins. Nat Struct Mol Biol *20*, 1273-1280.
Joly, V., Saint-Pierre-Chazalet, M., Saint-Julien, L., Bolard, J., Carbon, C., and Yeni, P. (1992). Inhibiting cholesterol synthesis reduces the binding and toxicity of amphotericin B against rabbit renal tubular cells in primary culture. J Infect Dis *165*, 337-343.

Justa-Schuch, D., Heilig, Y., Richthammer, C., and Seiler, S. (2010). Septum formation is regulated by the RHO4-specific exchange factors BUD3 and RGF3 and by the landmark protein BUD4 in Neurospora crassa. Mol Microbiol *76*, 220-235.
Kabsch, W. (2010). Xds. Acta Crystallogr D Biol Crystallogr *66*, 125-132.
Kamai, T., Tsujii, T., Arai, K., Takagi, K., Asami, H., Ito, Y., and Oshima, H. (2003). Significant association of Rho/ROCK pathway with invasion and metastasis of bladder cancer. Clin Cancer Res *9*, 2632-2641.
Kamai, T., Yamanishi, T., Shirataki, H., Takagi, K., Asami, H., Ito, Y., and Yoshida, K. (2004). Overexpression of RhoA, Rac1, and Cdc42 GTPases is associated with progression in testicular cancer. Clin Cancer Res *10*, 4799-4805.
Kanno, T., Takekawa, D., and Miyakawa, Y. (2015). Analysis of the essentiality of ROM2 genes in the pathogenic yeasts Candida glabrata and Candida albicans using temperature-sensitive mutants. J Appl Microbiol *118*, 851-863.
Kawano, Y., Kaneko-Kawano, T., and Shimamoto, K. (2014). Rho family GTPase-dependent immunity in plants and animals. Front Plant Sci *5*, 522.
Kondoh, O., Tachibana, Y., Ohya, Y., Arisawa, M., and Watanabe, T. (1997). Cloning of the RHO1 gene from Candida albicans and its regulation of beta-1,3-glucan synthesis. J Bacteriol *179*, 7734-7741.
Kristelly, R., Gao, G., and Tesmer, J.J. (2004). Structural determinants of RhoA binding and nucleotide exchange in leukemia-associated Rho guanine-nucleotide exchange factor. J Biol Chem *279*, 47352-47362.
Kuntz, I.D., Chen, K., Sharp, K.A., and Kollman, P.A. (1999). The maximal affinity of ligands. Proc Natl Acad Sci U S A *96*, 9997-10002.
Lambright, D.G., Sondek, J., Bohm, A., Skiba, N.P., Hamm, H.E., and Sigler, P.B. (1996). The 2.0 A crystal structure of a heterotrimeric G protein. Nature *379*, 311-319.
Lane, J.W., Rehak, N.N., Hortin, G.L., Zaoutis, T., Krause, P.R., and Walsh, T.J. (2008). Pseudohyperphosphatemia associated with high-dose liposomal amphotericin B therapy. Clin Chim Acta *387*, 145-149.
Langfelder, K., Gattung, S., and Brakhage, A.A. (2002). A novel method used to delete a new Aspergillus fumigatus ABC transporter-encoding gene. Curr Genet *41*, 268-274.
Latge, J.P. (1999). Aspergillus fumigatus and aspergillosis. Clin Microbiol Rev *12*, 310-350.
Latge, J.P. (2007). The cell wall: a carbohydrate armour for the fungal cell. Mol Microbiol *66*, 279-290.
Latge, J.P. (2010). Tasting the fungal cell wall. Cell Microbiol *12*, 863-872.
Lee, J.I., Yu, Y.M., Rho, Y.M., Park, B.C., Choi, J.H., Park, H.M., and Maeng, P.J. (2005). Differential expression of the chsE gene encoding a chitin synthase of Aspergillus nidulans in response to developmental status and growth conditions. FEMS Microbiol Lett *249*, 121-129.
Levin, D.E. (2005). Cell wall integrity signaling in Saccharomyces cerevisiae. Microbiol Mol Biol Rev *69*, 262-291.
Levin, D.E. (2011). Regulation of cell wall biogenesis in Saccharomyces cerevisiae: the cell wall integrity signaling pathway. Genetics *189*, 1145-1175.
Li, H., Zhou, H., Luo, Y., Ouyang, H., Hu, H., and Jin, C. (2007). Glycosylphosphatidylinositol (GPI) anchor is required in Aspergillus fumigatus for morphogenesis and virulence. Mol Microbiol *64*, 1014-1027.
Liu, W., Xie, Y., Ma, J., Luo, X., Nie, P., Zuo, Z., Lahrmann, U., Zhao, Q., Zheng, Y., Zhao, Y.*, et al.* (2015). IBS: an illustrator for the presentation and visualization of biological sequences. Bioinformatics *31*, 3359-3361.

Losada, L., Sugui, J.A., Eckhaus, M.A., Chang, Y.C., Mounaud, S., Figat, A., Joardar, V., Pakala, S.B., Pakala, S., Venepally, P.*, et al.* (2015). Genetic Analysis Using an Isogenic Mating Pair of Aspergillus fumigatus Identifies Azole Resistance Genes and Lack of MAT Locus's Role in Virulence. PLoS Pathog *11*, e1004834.
Madaule, P., Axel, R., and Myers, A.M. (1987). Characterization of two members of the rho gene family from the yeast Saccharomyces cerevisiae. Proc Natl Acad Sci U S A *84*, 779-783.
Madaule, P., Eda, M., Watanabe, N., Fujisawa, K., Matsuoka, T., Bito, H., Ishizaki, T., and Narumiya, S. (1998). Role of citron kinase as a target of the small GTPase Rho in cytokinesis. Nature *394*, 491-494.
Marinissen, M.J., Chiariello, M., and Gutkind, J.S. (2001). Regulation of gene expression by the small GTPase Rho through the ERK6 (p38 gamma) MAP kinase pathway. Genes Dev *15*, 535-553.
Mazur, P., and Baginsky, W. (1996). In vitro activity of 1,3-beta-D-glucan synthase requires the GTP-binding protein Rho1. J Biol Chem *271*, 14604-14609.
Mazur, P., Morin, N., Baginsky, W., el-Sherbeini, M., Clemas, J.A., Nielsen, J.B., and Foor, F. (1995). Differential expression and function of two homologous subunits of yeast 1,3-beta-D-glucan synthase. Molecular and cellular biology *15*, 5671-5681.
McGrail, D.J., Kieu, Q.M., and Dawson, M.R. (2014). The malignancy of metastatic ovarian cancer cells is increased on soft matrices through a mechanosensitive Rho-ROCK pathway. J Cell Sci *127*, 2621-2626.
McKenzie, C., Bassi, Z.I., Debski, J., Gottardo, M., Callaini, G., Dadlez, M., and D'Avino, P.P. (2016). Cross-regulation between Aurora B and Citron kinase controls midbody architecture in cytokinesis. Open Biol *6*.
Mohr, J., Johnson, M., Cooper, T., Lewis, J.S., and Ostrosky-Zeichner, L. (2008). Current options in antifungal pharmacotherapy. Pharmacotherapy *28*, 614-645.
Mondal, M.S., Wang, Z., Seeds, A.M., and Rando, R.R. (2000). The specific binding of small molecule isoprenoids to rhoGDP dissociation inhibitor (rhoGDI). Biochemistry *39*, 406-412.
Munro, C.A., Winter, K., Buchan, A., Henry, K., Becker, J.M., Brown, A.J., Bulawa, C.E., and Gow, N.A. (2001). Chs1 of Candida albicans is an essential chitin synthase required for synthesis of the septum and for cell integrity. Molecular microbiology *39*, 1414-1426.
Murshudov, G.N., Skubak, P., Lebedev, A.A., Pannu, N.S., Steiner, R.A., Nicholls, R.A., Winn, M.D., Long, F., and Vagin, A.A. (2011). REFMAC5 for the refinement of macromolecular crystal structures. Acta Crystallogr D Biol Crystallogr *67*, 355-367.
Murshudov, G.N., Vagin, A.A., and Dodson, E.J. (1997). Refinement of macromolecular structures by the maximum-likelihood method. Acta Crystallogr D Biol Crystallogr *53*, 240-255.
Newcomer, V.D., Sternberg, T.H., Wright, E.T., and Reisner, R.M. (1959). Current status of amphotericin B in the treatment of the systemic fungus infections. J Chronic Dis *9*, 353-374.
Nicholls, R.A., Long, F., and Murshudov, G.N. (2012). Low-resolution refinement tools in REFMAC5. Acta Crystallogr D Biol Crystallogr *68*, 404-417.
Nobes, C.D., Hawkins, P., Stephens, L., and Hall, A. (1995). Activation of the small GTP-binding proteins rho and rac by growth factor receptors. J Cell Sci *108 (Pt 1)*, 225-233.
Nubel, T., Dippold, W., Kleinert, H., Kaina, B., and Fritz, G. (2004). Lovastatin inhibits Rho-regulated expression of E-selectin by TNFalpha and attenuates tumor cell adhesion. FASEB J *18*, 140-142.

O'Gorman, C.M., Fuller, H., and Dyer, P.S. (2009). Discovery of a sexual cycle in the opportunistic fungal pathogen Aspergillus fumigatus. Nature *457*, 471-474.
Ostrem, J.M., Peters, U., Sos, M.L., Wells, J.A., and Shokat, K.M. (2013). K-Ras(G12C) inhibitors allosterically control GTP affinity and effector interactions. Nature *503*, 548-551.
Ostrosky-Zeichner, L., Casadevall, A., Galgiani, J.N., Odds, F.C., and Rex, J.H. (2010). An insight into the antifungal pipeline: selected new molecules and beyond. Nat Rev Drug Discov *9*, 719-727.
Palacios, D.S., Dailey, I., Siebert, D.M., Wilcock, B.C., and Burke, M.D. (2011). Synthesis-enabled functional group deletions reveal key underpinnings of amphotericin B ion channel and antifungal activities. Proc Natl Acad Sci U S A *108*, 6733-6738.
Pan, Y., Bi, F., Liu, N., Xue, Y., Yao, X., Zheng, Y., and Fan, D. (2004). Expression of seven main Rho family members in gastric carcinoma. Biochem Biophys Res Commun *315*, 686-691.
Petros, A.M., Swann, S.L., Song, D., Swinger, K., Park, C., Zhang, H., Wendt, M.D., Kunzer, A.R., Souers, A.J., and Sun, C. (2014). Fragment-based discovery of potent inhibitors of the anti-apoptotic MCL-1 protein. Bioorg Med Chem Lett *24*, 1484-1488.
Pochynyuk, O., Stockand, J.D., and Staruschenko, A. (2007). Ion channel regulation by Ras, Rho, and Rab small GTPases. Exp Biol Med (Maywood) *232*, 1258-1265.
Potter, A., Oldfield, V., Nunns, C., Fromont, C., Ray, S., Northfield, C.J., Bryant, C.J., Scrace, S.F., Robinson, D., Matossova, N.*, et al.* (2010). Discovery of cell-active phenyl-imidazole Pin1 inhibitors by structure-guided fragment evolution. Bioorg Med Chem Lett *20*, 6483-6488.
Provenzano, P.P., and Keely, P.J. (2011). Mechanical signaling through the cytoskeleton regulates cell proliferation by coordinated focal adhesion and Rho GTPase signaling. J Cell Sci *124*, 1195-1205.
Qadota, H., Python, C.P., Inoue, S.B., Arisawa, M., Anraku, Y., Zheng, Y., Watanabe, T., Levin, D.E., and Ohya, Y. (1996). Identification of yeast Rho1p GTPase as a regulatory subunit of 1,3-beta-glucan synthase. Science *272*, 279-281.
Redkar, R.J., Herzog, R.W., and Singh, N.K. (1998). Transcriptional activation of the Aspergillus nidulans gpdA promoter by osmotic signals. Appl Environ Microbiol *64*, 2229-2231.
Renshaw, M.W., Toksoz, D., and Schwartz, M.A. (1996). Involvement of the small GTPase rho in integrin-mediated activation of mitogen-activated protein kinase. J Biol Chem *271*, 21691-21694.
Richthammer, C., Enseleit, M., Sanchez-Leon, E., Marz, S., Heilig, Y., Riquelme, M., and Seiler, S. (2012). RHO1 and RHO2 share partially overlapping functions in the regulation of cell wall integrity and hyphal polarity in Neurospora crassa. Mol Microbiol *85*, 716-733.
Ridley, A.J. (2006). Rho GTPases and actin dynamics in membrane protrusions and vesicle trafficking. Trends Cell Biol *16*, 522-529.
Ridley, A.J. (2015). Rho GTPase signalling in cell migration. Curr Opin Cell Biol *36*, 103-112.
Roemer, T., and Krysan, D.J. (2014). Antifungal drug development: challenges, unmet clinical needs, and new approaches. Cold Spring Harb Perspect Med *4*.
Roncero, C., and Duran, A. (1985). Effect of Calcofluor white and Congo red on fungal cell wall morphogenesis: in vivo activation of chitin polymerization. J Bacteriol *163*, 1180-1185.

Rose, R., Wittinghofer, A., and Weyand, M. (2005). The purification and crystallization of mDia1 in complex with RhoC. Acta crystallographica. Section F, Structural biology and crystallization communications *61*, 225-227.
Rossman, K.L., Der, C.J., and Sondek, J. (2005). GEF means go: turning on RHO GTPases with guanine nucleotide-exchange factors. Nat Rev Mol Cell Biol *6*, 167-180.
Sah, V.P., Seasholtz, T.M., Sagi, S.A., and Brown, J.H. (2000). The role of Rho in G protein-coupled receptor signal transduction. Annu Rev Pharmacol Toxicol *40*, 459-489.
Samantaray, S., Neubauer, M., Helmschrott, C., and Wagener, J. (2013). Role of the guanine nucleotide exchange factor Rom2 in cell wall integrity maintenance of Aspergillus fumigatus. Eukaryot Cell *12*, 288-298.
Schuttelkopf, A.W., Andersen, O.A., Rao, F.V., Allwood, M., Rush, C.L., Eggleston, I.M., and van Aalten, D.M. (2011). Bisdionin C-a rationally designed, submicromolar inhibitor of family 18 chitinases. ACS Med Chem Lett *2*, 428-432.
Schuttelkopf, A.W., and van Aalten, D.M. (2004). PRODRG: a tool for high-throughput crystallography of protein-ligand complexes. Acta Crystallogr D Biol Crystallogr *60*, 1355-1363.
Scott, D.E., Coyne, A.G., Hudson, S.A., and Abell, C. (2012). Fragment-based approaches in drug discovery and chemical biology. Biochemistry *51*, 4990-5003.
Shang, X., Marchioni, F., Sipes, N., Evelyn, C.R., Jerabek-Willemsen, M., Duhr, S., Seibel, W., Wortman, M., and Zheng, Y. (2012). Rational design of small molecule inhibitors targeting RhoA subfamily Rho GTPases. Chem Biol *19*, 699-710.
Smithers, C.C., and Overduin, M. (2016). Structural Mechanisms and Drug Discovery Prospects of Rho GTPases. Cells *5*.
Somlyo, A.P., and Somlyo, A.V. (2003). Ca2+ sensitivity of smooth muscle and nonmuscle myosin II: modulated by G proteins, kinases, and myosin phosphatase. Physiol Rev *83*, 1325-1358.
Sondek, J., Bohm, A., Lambright, D.G., Hamm, H.E., and Sigler, P.B. (1996). Crystal structure of a G-protein beta gamma dimer at 2.1A resolution. Nature *379*, 369-374.
Stirnimann, C.U., Petsalaki, E., Russell, R.B., and Muller, C.W. (2010). WD40 proteins propel cellular networks. Trends Biochem Sci *35*, 565-574.
Tang, Y., Olufemi, L., Wang, M.T., and Nie, D. (2008). Role of Rho GTPases in breast cancer. Front Biosci *13*, 759-776.
Tkacz, J.S., and DiDomenico, B. (2001). Antifungals: what's in the pipeline. Current opinion in microbiology *4*, 540-545.
Todd, R.B., Davis, M.A., and Hynes, M.J. (2007). Genetic manipulation of Aspergillus nidulans: heterokaryons and diploids for dominance, complementation and haploidization analyses. Nat Protoc *2*, 822-830.
Touge, H., Chikumi, H., Igishi, T., Kurai, J., Makino, H., Tamura, Y., Takata, M., Yoneda, K., Nakamoto, M., Suyama, H.*, et al.* (2007). Diverse activation states of RhoA in human lung cancer cells: contribution of G protein coupled receptors. Int J Oncol *30*, 709-715.
Vagin, A., and Teplyakov, A. (1997). MOLREP: an automated program for molecular replacement. Journal of Applied Crystallography *30*, 1022-1025.
van der Linden, J.W., Camps, S.M., Kampinga, G.A., Arends, J.P., Debets-Ossenkopp, Y.J., Haas, P.J., Rijnders, B.J., Kuijper, E.J., van Tiel, F.H., Varga, J.*, et al.* (2013). Aspergillosis due to voriconazole highly resistant Aspergillus fumigatus and recovery of genetically related resistant isolates from domiciles. Clin Infect Dis *57*, 513-520.
Verdine, G.L., and Walensky, L.D. (2007). The challenge of drugging undruggable targets in cancer: lessons learned from targeting BCL-2 family members. Clinical cancer

research : an official journal of the American Association for Cancer Research *13*, 7264-7270.
Vilella, F., Herrero, E., Torres, J., and de la Torre-Ruiz, M.A. (2005). Pkc1 and the upstream elements of the cell integrity pathway in Saccharomyces cerevisiae, Rom2 and Mtl1, are required for cellular responses to oxidative stress. J Biol Chem *280*, 9149-9159.
Vogt, K., Bhabhra, R., Rhodes, J.C., and Askew, D.S. (2005). Doxycycline-regulated gene expression in the opportunistic fungal pathogen Aspergillus fumigatus. BMC Microbiol *5*, 1.
Wakefield, A.E., Peters, S.E., Banerji, S., Bridge, P.D., Hall, G.S., Hawksworth, D.L., Guiver, L.A., Allen, A.G., and Hopkin, J.M. (1992). Pneumocystis carinii shows DNA homology with the ustomycetous red yeast fungi. Mol Microbiol *6*, 1903-1911.
Wall, M.A., Coleman, D.E., Lee, E., Iniguez-Lluhi, J.A., Posner, B.A., Gilman, A.G., and Sprang, S.R. (1995). The structure of the G protein heterotrimer Gi alpha 1 beta 1 gamma 2. Cell *83*, 1047-1058.
Walsh, T.J., Anaissie, E.J., Denning, D.W., Herbrecht, R., Kontoyiannis, D.P., Marr, K.A., Morrison, V.A., Segal, B.H., Steinbach, W.J., Stevens, D.A.*, et al.* (2008). Treatment of aspergillosis: clinical practice guidelines of the Infectious Diseases Society of America. Clin Infect Dis *46*, 327-360.
Wang, Y.X., Martin-McNulty, B., da Cunha, V., Vincelette, J., Lu, X., Feng, Q., Halks-Miller, M., Mahmoudi, M., Schroeder, M., Subramanyam, B.*, et al.* (2005). Fasudil, a Rho-kinase inhibitor, attenuates angiotensin II-induced abdominal aortic aneurysm in apolipoprotein E-deficient mice by inhibiting apoptosis and proteolysis. Circulation *111*, 2219-2226.
Wei, Y., Zhang, Y., Derewenda, U., Liu, X., Minor, W., Nakamoto, R.K., Somlyo, A.V., Somlyo, A.P., and Derewenda, Z.S. (1997). Crystal structure of RhoA-GDP and its functional implications. Nat Struct Biol *4*, 699-703.
Winter, G., Lobley, C.M., and Prince, S.M. (2013). Decision making in xia2. Acta Crystallogr D Biol Crystallogr *69*, 1260-1273.
Xu, C., and Min, J.R. (2011). Structure and function of WD40 domain proteins. Protein Cell *2*, 202-214.
Yamashita, M., Kurokawa, K., Sato, Y., Yamagata, A., Mimura, H., Yoshikawa, A., Sato, K., Nakano, A., and Fukai, S. (2010). Structural basis for the Rho- and phosphoinositide-dependent localization of the exocyst subunit Sec3. Nat Struct Mol Biol *17*, 180-186.
Zmeili, O.S., and Soubani, A.O. (2007). Pulmonary aspergillosis: a clinical update. QJM *100*, 317-334.
Zong, H., Kaibuchi, K., and Quilliam, L.A. (2001). The insert region of RhoA is essential for Rho kinase activation and cellular transformation. Mol Cell Biol *21*, 5287-5298.